BIFURCATION PORTRAIT OF A HYBRID SPIKING NEURON MODEL

A Thesis
Submitted to the Graduate Faculty
of the
North Dakota State University
of Agriculture and Applied Science

By

Brandon Grae Goodell

In Partial Fulfillment of the Requirements
for the Degree of
MASTER OF SCIENCE

Major Department:
Mathematics

March 2012

Fargo, North Dakota

North Dakota State University
Graduate School

Title

Bifurcation Portrait of a Hybrid Spiking Neuron Model

By

Brandon Grae Goodell

The Supervisory Committee certifies that this ***disquisition*** complies with North Dakota State University's regulations and meets the accepted standards for the degree of

MASTER OF SCIENCE

SUPERVISORY COMMITTEE:

Davis Cope
Chair

Nikita Barabanov

Friedrich Littmann

Jim Coykendall

Mark McCourt

Approved:

14 May 2013
Date

Dogan Çömez
Department Chair

ABSTRACT

A bifurcation portrait classifies the behavior of a dynamical system and how it transitions between different behaviors. A hybrid dynamical system displays both continuous and discrete dynamics and may display nonsmooth bifurcations. Herein, we analyze a novel hybrid model of a spiking neuron proposed by E.M. Izhikevich [9] that is based on a previous hybrid model with a convex spike-activation function f(x), but modified with a conductance reversal potential term. We analyze the model proposed by Izhikevich and obtain a bifurcation portrait for the continuous dynamics for an arbitrary convex spike activation function f(x). Both subcritical and supercritical Andronov-Hopf bifurcations are possible, and we numerically confirm the presence of a Bautin bifurcation for a particular choice of spike activation function. The model is capable of simulating common cortical neuron types and presents several possibilities for generalizations that may be capable of more complicated behavior.

ACKNOWLEDGMENTS

I thank my wife and family for putting up with me while I wrote this. I would like to thank Nikita Barabanov for his thorough introduction to bifurcation theory, as well as Yuri Kuznetsov for the book upon which that introduction was based. Colleen Webb and Michael Kirby introduced me to applied mathematics and scientific research in general, and without them I would not have proceeded to graduate school. E.M. Izhikevich *Dynamical Systems in Neuroscience* is possibly the most readable introduction into dynamical systems in publication today, and his papers on hybrid spiking models make for an easy introduction into computational neuroscience. Richard Dawkins and Carl Sagan (the latter posthumously) unwittingly conspired to instill a sense of awe and wonder in the natural world without which I would not be a scientist.

Aaron Feickert, Jon Totushek, and Sean Sather-Wagstaff helped me with LaTeX commands. Thanks also to Jim Coykendall, Davis Cope, and Nikita Barabanov for the myriad useful conversations.

TABLE OF CONTENTS

LIST OF TABLES

LIST OF FIGURES

CHAPTER 1. INTRODUCTION

Any discussion of a model spiking neuron inevitably begins with the famous Hodgkin-Huxley model [5]. In terms of chemistry, ach ionic species in the extracellular medium flows into and out of the cell via passive and active processes. Passive "leak" currents tend to bring the cell toward electrochemical equilibrium while active ion pumps work against these passive processes. The flow of each distinct ionic species across the cell membrane contributes to the membrane current, which in turn contributes to membrane voltage. Hodgkin and Huxley developed a procedure to estimate the voltage-sensitive conductance in the neural membrane, and hence quantified the processes contributing to membrane electrodynamics. They developed a nonlinear system of ordinary differential equations as a continuous-time model to describe their results.

Denoting the Nernst equilibrium potential of the i^{th} ionic species as E_i, and the voltage-sensitive conductance $g_i(V)$, we have the generalized conductance-based model of a small patch of neural membrane

$$\begin{cases} C\dot{V} &= I - I_0(V) - \sum_i g_i\left(E_i - V\right) \\ \dot{g}_i &= h_i\left(g_i, V\right) \end{cases} \tag{1.1}$$

where V is membrane voltage, C is membrane capacitance, I is the DC input current, I_0 is the sum of currents with constant conductance. The particular form of each h_i is usually nonlinear and dependent on other dynamic variables not listed here. Indeed, this dependence on other dynamic variables leads the original Hodgkin-Huxley equations to be high dimensional; usually the state space is at least four dimensional.

The nonlinearity and high dimensionality of the system provides a strong incentive to reduce the model. However, without at least three dimensions, spike upstroke and downstroke behavior cannot both be simulated in a strictly smooth model [8].

Spike downstroke behavior can be simulated by introducing a discontinuous cutoff into an otherwise smooth, low-dimensional model; Izhikevich and others demonstrated two-dimensional models capable of recreating a wide range of biologically plausible behaviors. Izhikevich proposed the dimensionless hybrid model ([6],[8])

$$\begin{cases} \dot{v} = & f(v) - u + I \\ \dot{u} = & a(bv - u) \\ v \geqslant & v_{max} \Rightarrow v \leftarrow c, u \leftarrow u + d \end{cases} \tag{1.2}$$

in which f is usually a convex C^k function for some $k \geqslant 2$, $I \in \mathbb{R}$, and $a, b > 0$. The model phenomenologically describes dimensionless voltage v and some slow dimensionless conductance u with a spike activation function f, dimensionless current I, and dimensionless phenomenological parameters $a, b > 0$. When voltage exceeds a maximum value $v_{max} \in \mathbb{R}$, a spike is said to have occurred; a discontinuous reset in voltage and conductance with an additive gain in conductance occurs. With only two dimensions, this model is capable of a broad range of biologically plausible behavior and is computationally efficient. It has been extensively studied [7], [12], [13]. Izhikevich analyzed this model with $f(v) = v^2$ ([8], [7], [6]), Brette and Gerstner analyzed Izhikevich's model with $f(v) = e^v - v$ ([1]), and Touboul analyzed Izhikevich's model in the general case and with $f(v) = v^4 + 2av$ ([12]). Although model 1.2 typically appears in the literature in the dimensionless form stated here, it can be reduced by one parameter by the change of coordinates and time $v = \frac{1}{a}x, u = \frac{b}{a}y, t = \frac{1}{a}T$.

Izhikevich suggested investigating the effects of voltage sensitivity on the slow conductance term. That is, in [9], Izhikevich proposed the novel model

$$\begin{cases} \dot{x} = & \hat{f}(x) + y(x - \hat{E}) + \hat{I} \\ \dot{y} = & a(bx - y) \end{cases} \tag{1.3}$$

in which we impose a discontinuous reset just as before, and all variables and parameters are analogous to those above except $\hat{E} \in \mathbb{R}$ is a conductance reversal energy. Changing coordinates, time, and parameters

$$x = \frac{a}{b}v \qquad f(x) := \frac{b}{a^2}\hat{f}\left(\frac{a}{b}x\right) \tag{1.4}$$

$$y = au \qquad E := \frac{b}{a}\hat{E} \tag{1.5}$$

$$t = \frac{1}{a}T \qquad I := \frac{b}{a^2}\hat{I} \tag{1.6}$$

we obtain the model

$$\begin{cases} \dot{v} = & f(v) + u(v - E) + I \\ \dot{u} = & v - u \\ v \geqslant & v_{max} \Rightarrow v \leftarrow c, u \leftarrow u + d \end{cases} \tag{1.7}$$

where v is the dimensionless membrane voltage, u is the dimensionless voltage-sensitive slow conductance of some ionic species (called the recovery variable), E is the dimensionless reversal voltage for the conductance, I is the dimensionless DC input current, and f is some convex C^k function for $k \geqslant 2$. The parameter v_{max} denotes the maximum cut-off voltage to signify an action potential, c is the after-spike reset voltage, and d is the gain in conductance due to the action potential. All parameters and variables here are dimensionless. We can assume that $f(0) = 0$ since during change of coordinates, parameters, and time, we can wrap the constant term of f into I.

We require that $f(v)$ scale faster than linearly for sufficiently large v in order for membrane voltage to blow up in finite time. If this is the case, then any value for v_{max} will be suitable presuming it is sufficiently large and positive. Touboul [13] demonstrated that the condition $\lim_{v\to\infty} f(v) \geqslant \alpha v^{1+\epsilon}$ for some $\alpha, \epsilon > 0$ is sufficient for v to blow up in finite time for the original Izhikevich model 1.2. Further, unless $\epsilon > 1$, the recovery variable u may also blow up in finite time, leading to a biologically implausible sensitivity to the cutoff voltage v_{max}. Model 1.7 also exhibits this behavior, which is proven in Appendix A.

Hybrid models are popular because they are minimal with respect to computational expense while retaining the capability to reproduce most computational properties of neurons. Indeed, the original Izhikevich simple model is two orders of magnitude faster to simulate than the original Hodgkin-Huxley model, and by using the function $f(v) = v^4 + 2av$ used by Touboul, that model is capable of a very rich set of dynamical regimes despite its computational efficiency. In contrast to model 1.2, which did not incorporate voltage-sensitive conductance, we see that model 1.7 has a voltage-sensitive conductance term. The role in neural dynamics played by voltage-sensitive conductance reversal is unclear. Herein, we investigate model 1.7 and the computational properties and bifurcations of which the model is capable.

1.1. Neurocomputational Properties and Bifurcations

Neurons capable of stable spiking cycle are referred to as excitable, and determining the conditions under which neurons are excitable motivated much of 20^{th} century neuroscience. Researchers originally suspected that excitability was a function of input current, and with a sufficiently strong, excitatory input, a neuron would fire a spike. Hence, much effort has historically been put forth to determine the excitability threshold of a spiking neuron. Excitable neurons were originally classified by Hodgkin as either Class 1 or Class 2 [4]. Class 1 neurons ideally can exhibit an arbitrarily

small firing rate and smoothly increase that rate as input current increases. Class 2 neurons, on the other hand, have a minimum firing rate which is fairly insensitive to input current above the threshold current.

Unfortunately, this picture is oversimplified. Indeed, there exist at least two ubiquitous neurocomputational properties of excitable neurons entirely missed by this model: resonance and bistability. Resonant neurons experience sub-threshold oscillations and have a resonance frequency. A properly timed burst of presynaptic spikes will trigger a resonant neuron to spike; therefore, resonators act as frequency detectors. Integrator neurons, on the other hand, act as coincidence detectors. With a sufficient number of recent spikes, they will fire. Note all neurons transition into stable spiking with sufficient excitatory input.

The other property is bistability. Stable spiking states are mutually exclusive with stable resting states in monostable neurons. With a sufficiently small mean input current, they can only fire a single spike, whereas with a sufficiently large input current, they constantly spike. Bistable neurons can be shocked into a spiking state when at rest, and then shocked back into rest from a spiking state without changing their mean input current. Hence, we can categorize neurons into four distinct categories; monostable integrators, bistable integrators, monostable resonators, and bistable resonators.

We can summarize these neurocomputational properties succinctly with a dynamical systems model. Indeed, the resting state of a resonator neuron is a spiral (or focus) equilibrium, whereas the resting state of an integrator is a node. Further, bistable neurons will exhibit the coexistence of a stable resting state and a periodic spiking limit cycle, whereas monostable neurons can either have a stable resting state or a stable spiking limit cycle, but not both.

Figure 1.1 (a) shows the basic fold (or saddle-node) bifurcation associated with the transition in bistable integrators between resting state and stable spiking limit

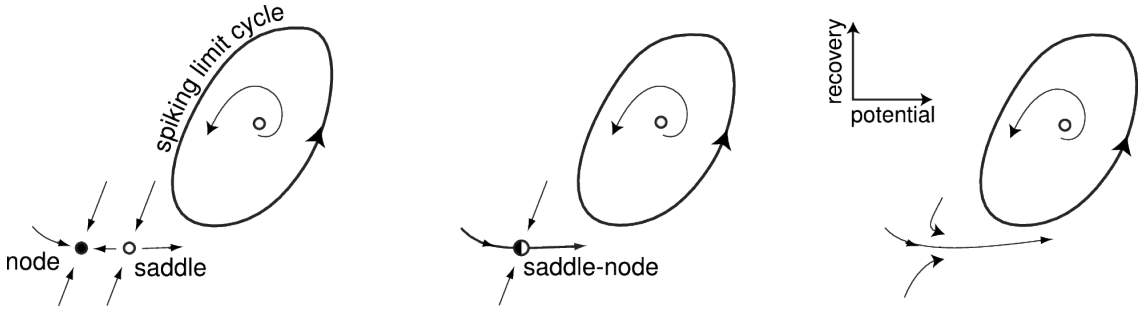

(a) A fold bifurcation

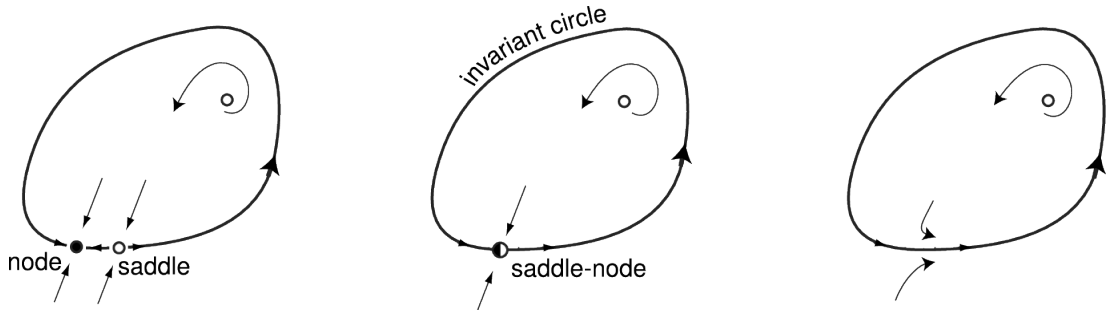

(b) Fold-on-invariant-circle bifurcation

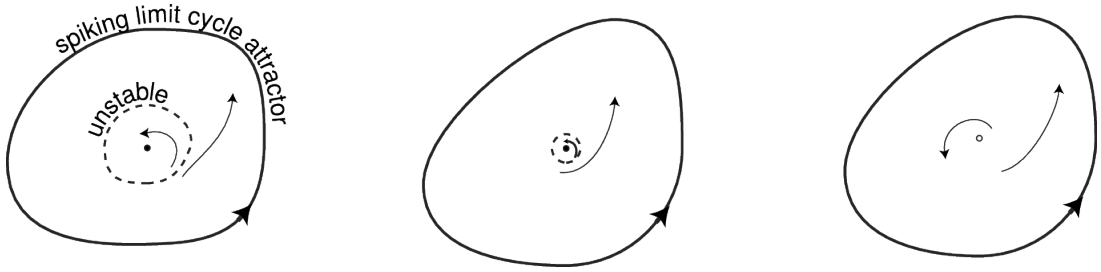

(c) subcritical Andronov-Hopf bifurcation

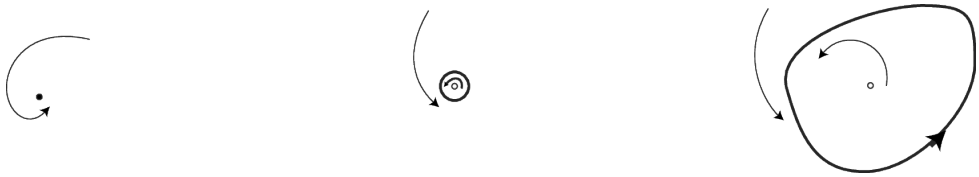

(d) Supercritical Andronov-Hopf bifurcation

Figure 1.1: Bifurcation transitions between stable states and spiking cycles. Figure 1.1a illustrates bistable integrators, Figure 1.1b illustrates monostable integrators, Figure 1.1c illustrates bistable resonators, and Figure 1.1d illustrates monostable resonators. Figure from [8] printed with permission from E.M. Izhikevich.

cycles. Figure (b) shows the fold-on-invariant-circle bifurcation associated with monostable integrators. Figure (c) shows the subcritical Andronov-Hopf bifurcation associated with bistable resonators. Finally, Figure (d) shows the supercritical Andronov-Hopf bifurcation associated with monostable resonators. Neuronal models of interest must be capable of the four dynamical behaviors presented in Figure 1.1, and hence must be capable of undergoing bifurcations to transition between the different regimes.

1.2. Other Neurocomputational Properties

Bistability and resonance are not the only neurocomputational properties of interest, although together they can be used to recreate a very wide variety of biologically plausible neuronal behaviors. Recreating these behaviors is one way to assess the utility of a neural model.

Most notions of spiking can be extended to the notion of a burst. Indeed, a neuron may be capable of *tonic bursting* in which a neuron fires bursts periodically. A neuron may be capable of firing a *rebound spike* or *burst* in response to a brief inhibitory pulses of current. A neuron may be capable of both bursting and spiking in a *mixed mode* fashion. The inter-spike interval of a tonically firing neuron may grow over time as a neuron adapts to a constant input current in the phenomenon of *spike frequency adaptation*. Neurons may exhibit *spike latency*, in which a neuron fires a spike after a delay in response to a super-threshold input current. A neuron may also exhibit *threshold variability*, in which a particular amplitude of input current is not sufficient to trigger a spike unless an inhibitory pulse of input current precedes it. A neuron may also exhibit a *depolarizing after-potential* in which membrane voltage experiences a post-spike hump during which time it is sensitive to firing another spike.

Finally, a neuron may be capable of *accommodation*, in which case a slow ramping of input current to a particular amplitude does not elicit a spike, but a brief shock at the same amplitude will elicit a spike. Accommodation occurs when input current is

changing slowly with respect to the fast active processes in the neural membrane. A neuron may also be capable of *inhibition-induced spiking* or *bursting* in response to a sustained inhibitory input current. Model 1.7 can reproduce many of these observed biological behaviors, as illustrated by Figure 4.4 in Chapter 4.

CHAPTER 2. DYNAMICAL SYSTEMS AND BIFURCATIONS

Bifurcation theory, roughly speaking, is the analysis of the topological properties of dynamical systems, how those properties change as parameters vary, and the conditions under which a system's behavior undergoes a transition between qualitatively distinct regimes. A bifurcation portrait is a partition of parameter space into dynamically equivalent regimes, together with representative phase portraits from each regime, including the borders between distinct dynamical regimes. In this section, we discuss the framework for analyzing the bifurcations for an autonomous continuous-time dynamical system. As always, we begin with a definition:

Definition 2.1. A *dynamical system* is a triple $\left(X, T, \{\phi^t\}_{t\in T}\right)$ consisting of a phase space (a manifold X, usually a complete metric space), an ordered time set closed under addition (T, usually $\mathbb{R}$ or $\mathbb{Z}$), and a family of evolution operators $\phi^t : X \to X$ such that $\phi^{t+s}(x) = \phi^t \circ \phi^s x$ for any $t, s \in T$ and $x \in X$ and such that $\phi^0(x) = x$ for any $x \in X$.

We oftentimes restrict our attention to small neighborhoods of the phase space. We will say that the phase portraits of two systems $\left(X, T, \{\phi^t\}_{t\in T}\right)$ and $\left(Y, S, \{\psi^s\}_{s\in S}\right)$ are *locally topologically equivalent at the respective points* x_0 *and* y_0 if there exists a pair of open neighborhoods $X' \subseteq X$ with $x_0 \in X'$, $Y' \subseteq Y$ with $y_0 \in Y'$, and a homeomorphism $h : X' \to Y'$ such that $h(x_0) = y_0$ and such that h carries trajectories within X' to trajectories within Y' preserving the direction of time.

Continuous-time dynamical systems take $T = \mathbb{R}$ and are governed by differential equations whereas discrete-time dynamical systems take $T = \mathbb{Z}$ and are governed by some map $x \mapsto f(x)$. Analysis of dynamical systems begins with partitions of X in terms of *invariant sets*. A set $S \subseteq X$ is *invariant* if for any $x \in S, t \in T$, $\phi^t x \in S$.

Particular examples of invariant sets abound. A singleton $\{x_0\} \subset X$ such that $\phi^t x_0 = x_0$ for any $t \in T$ is invariant. In continuous-time systems, they are known as

equilibria, and in discrete-time systems, they are *fixed points*. An *orbit starting at* x_0 is the invariant set $\{x \in X : x = \phi^t(x_0) \text{ for some } t \in T\}$. One can think of an orbit as the (usually unique) trajectory passing through x_0, or as the trajectory generated by x_0. A *cycle* is a periodic orbit. An *isolated cycle* is a cycle such that an open neighborhood contains the cycle of interest but lacks other cycles. A *center* is a collection of non-isolated cycles.

2.1. Equivalence Relations on Dynamical Systems

In order to compare two systems, we need a notion of equivalence; essentially we require some abstract notion of equality that is reflexive, symmetric, and transitive.

Definition 2.2. Two dynamical systems are said to be *topologically equivalent* if there exists a homeomorphism mapping the trajectories of one system onto the trajectories of the other system preserving the direction of time.

Example 2.3. The following example demonstrates global topological equivalence. Take both state spaces X and Y to be the punctured plane $\mathbb{R}^2\backslash(0,0)$, let both time sets be $T = S = \mathbb{R}$, and consider the pair of continuous-time differential equations models:

$$\begin{cases} \dot{x_1} = & -x_1 \\ \dot{y_1} = & -y_1 \end{cases} \qquad \begin{cases} \dot{x_2} = & -x_2 - y_2 \\ \dot{y_2} = & x_2 - y_2 \end{cases} \tag{2.1}$$

Representative phase portraits for these two systems are illustrated in Figure 2.1(a) and (b), respectively. Notice both systems exclude the origin. Consider an orbit $(x_1(t), y_1(t))$ in X (respectively $(x_2(t), y_2(t))$ in Y). We can represent any point in $\mathbb{R}^2$ away from the origin in polar coordinates. We perform the standard polar coordinate

change

$$x_1 = r_1 \cos\theta_1 \qquad y_1 = r_1 \sin\theta_1$$
$$x_2 = r_2 \cos\theta_2 \qquad y_2 = r_2 \sin\theta_2$$

where $r_1, r_2 > 0$. We also interpret θ_1, θ_2 as real numbers in the interval $[0, 2\pi)$ with the understanding that θ_1, θ_2 are equivalence classes of real numbers under the usual equivalence relation $\theta \sim \theta'$ if and only if $\theta - \theta' = 2k\pi$ for some integer k. This yields the system of differential equations:

$$\begin{cases} \dot{r_1} = & -r_1 \\ \dot{\theta_1} = & 0 \end{cases} \qquad \begin{cases} \dot{r_2} = & -r_2 \\ \dot{\theta_2} = & 1 \end{cases}$$

Then the map $\Psi : X \to Y$ defined by

$$\Psi\left(\begin{pmatrix} r_1 \\ \theta_1 \end{pmatrix}\right) = \begin{pmatrix} r_1 \\ \theta_1 - \ln(r_1) \end{pmatrix}$$

is a homeomorphism mapping the orbits from X into the orbits of Y.

Of course, an astute reader will notice that the map in the above example is not differentiable (or even defined) at the origin; there is no way to connect a node equilibrium and a spiral equilibrium with a diffeomorphism. This brings us to a stronger version of topological equivalence:

Definition 2.4. Two systems that are topologically equivalent via a diffeomorphism h are called *smoothly equivalent*.

Example 2.3 demonstrates that the equilibria in two topologically equivalent, but not smoothly equivalent systems, may exhibit some qualitatively different behavior, i.e.

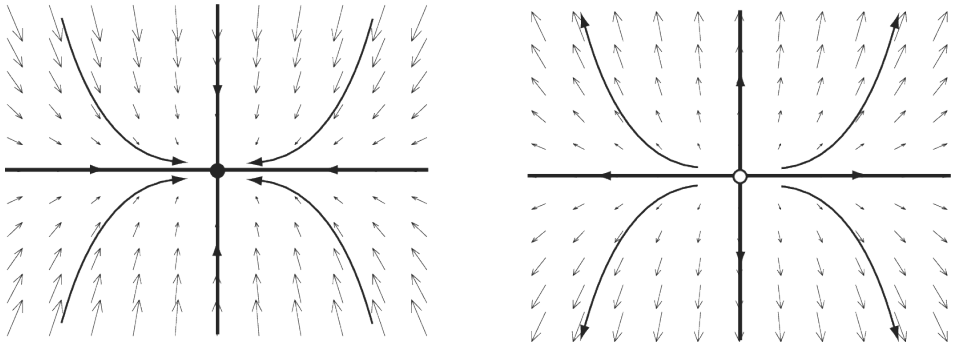

(a) Node equilibria

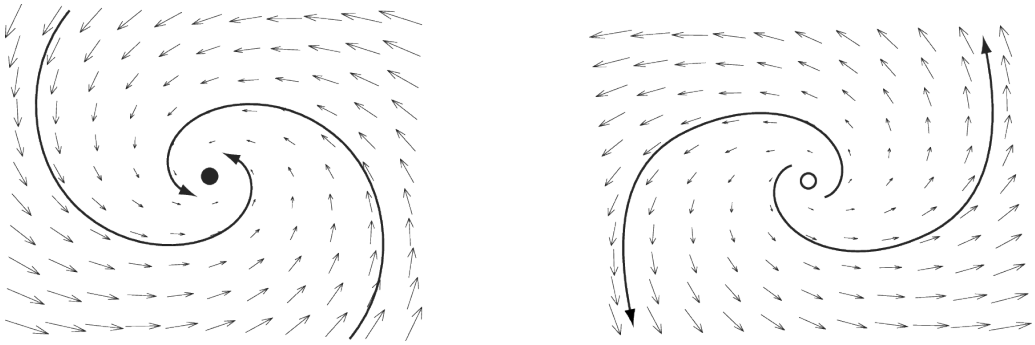

(b) Spiral equilibria

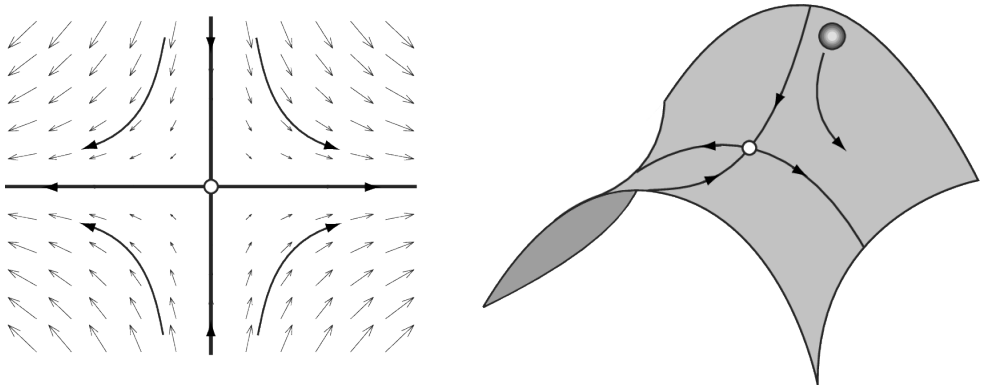

(c) Saddle equilibrium

Figure 2.1: Vector fields and representative trajectories near various equilibria. Figure 2.1a: vector field and representative trajectories near a stable (left) and unstable (right) node equilibrium. Figure 2.1b: vector field and representative trajectories near a stable (left) and unstable (right) spiral equilibrium. Figure 2.1c: vector field and representative trajectories near a saddle equilibrium. Figure from [8] printed with permission from E.M. Izhikevich.

node equilibria as opposed to spiral equilibria. Smoothly equivalent systems are "more equivalent" than topologically equivalent systems.

When a bifurcation occurs, we wish to find the simplest way to describe the system as it transitions through the qualitatively different behavioral regimes. To this end, we wish to find a smooth equivalence to a topological normal form (see section 2.3.1). Before we discuss this, however, we must define bifurcations and topological normal forms (see section 2.3). It must be noted that computing specific diffeomorphisms is usually a headache. However, there are a variety of theorems at our disposal in order to prove the existence of equivalences without the computational nightmare involved in finding specific morphisms.

2.2. Characterizing Invariant Sets

Bifurcation analysis includes characterization of the properties of orbits near equilibria and limit cycles. Analyzing behavior near equilibria in autonomous systems is accomplished by considering the eigenvalues of the Jacobian matrix of the system evaluated at that equilibrium. Analyzing behavior near limit cycles involves the method of Poincaré cross-sections, in which we restrict our attention to a manifold intersecting the limit cycle transversally. This induces a discrete-time dynamical system using that manifold as the state space. Fixed points in the Poincaré cross-section are in one-to-one correspondence with cycles of the original continuous-time system, and analyzing the cycles of a continuous-time dynamical system will often reduce to analyzing the fixed points of the induced discrete-time dynamical system. However, our analysis does not use Poincaré cross-sections in the sequel; we only include this description for completeness. Hence, in this section, we describe only the characterization of equilibria.

The eigenvalues of the Jacobian matrix evaluated at the equilibria (or fixed points) characterize behavior near those equilibria (or fixed points). At the risk of abusing

vocabulary, rather than referring to the eigenvalue of the Jacobian matrix of the system evaluated at the equilibrium, we will refer to the eigenvalue of the equilibrium. For example, if an eigenvalue λ of the Jacobian matrix evaluated at the equilibrium satisfies $\lambda = 0$, then we will say that the equilibrium has a zero eigenvalue (or an eigenvalue that vanishes), and so on.

We are concerned with three traits of equilibria and fixed points: hyperbolicity, stability, and monotonicity.

Definition 2.5. An equilibrium in a continuous-time dynamical system is *hyperbolic* if none of its eigenvalues are on the imaginary axis. A fixed point of a discrete-time dynamical system is hyperbolic if none of its eigenvalues lie on the unit circle in the complex plane.

Hyperbolicity ensures a variety of nice, equivalent properties, including structural stability, shadowing, and the ability to define stable and unstable manifolds. Indeed, a bifurcation is classically considered the loss of structural stability or rather a change of topological equivalence. We say that a *local bifurcation of an equilibrium* has occurred as a parameter varies whenever topological equivalence changes. If a hyperbolic equilibrium loses hyperbolicity in a generic and transversal manner, then topological equivalence has changed and we say a bifurcation has occurred. Given a hyperbolic equilibrium, we are also generally concerned with two properties: asymptotic stability and oscillations so as to classify the behavior of trajectories near that equilibrium.

Definition 2.6. An invariant set S of a dynamical system with an evolution operator ϕ is *Lyapunov stable* if for any open U containing S, there exists some open $V \subseteq U$ containing S such that any orbit with its initial condition in V will thereafter remain in U for all time.

An invariant set S has the *asymptotic property* if there exists an open neighborhood U containing S such that, for any $x \in U$, $\phi^t x \to S$. That is, orbits starting sufficiently close to S tend toward S in the Hausdorff metric as time proceeds to infinity.

An invariant set S is *asymptotically stable* if it is both Lyapunov stable and has the asymptotic property.

The eigenvalues of stable equilibria have strictly negative real parts. In two-dimensional continuous-time dynamical systems, stability is equivalent to requiring the trace of the Jacobian to be strictly negative with a strictly positive determinant. Each eigenvalue is associated with an eigenvector. If all eigenvalues are real and all eigenvectors have real components, the sign of an eigenvalue determines the stability of the equilibrium in the direction of its associated eigenvector. If the sign is negative, then the equilibrium is stable in the direction of the associated eigenvector, and if the sign is positive, then the equilibrium is unstable in the direction of the associated eigenvector. If one eigenvalue is negative and one eigenvalue is positive, the equilibrium is a saddle point. This occurs if and only if the determinant is negative.

For example, in the first system in example 2.3, we have one equilibrium (the origin) with the Jacobian

$$\begin{pmatrix} -1 & 0 \\ 0 & -1 \end{pmatrix}$$

which has determinant 1, trace -2, and a (not simple) eigenvalue -1. The second system on the other hand has Jacobian

$$\begin{pmatrix} -1 & -1 \\ 1 & -1 \end{pmatrix}$$

with determinant 2, trace -2, and eigenvalues $-1 \pm i$. In both systems, the origin is stable. Indeed, Figure 2.1 portrays the phase portraits of these systems.

Finally, we are also concerned with whether trajectories monotonically approach a stable equilibrium or whether they oscillate on their approach. Monotonic equilibria are known as nodes (first system in example 2.3 and left phase portrait in Figure 2.1), and oscillatory equilibria are spirals (second system in example 2.3 and right phase portrait in Figure 2.1). Although nodes and spirals are topologically equivalent (presuming they are both stable or both unstable), they are not smoothly equivalent.

In a planar system, an equilibrium is a spiral or a center if at least one eigenvalue has a nonzero imaginary part. Complex eigenvalues come in complex-conjugate pairs, and we will be dealing with two dimensional systems exclusively. Hence, an equilibrium is a spiral if and only if both eigenvalues have a nonzero imaginary part in our context.

2.3. Local Bifurcations of Equilibria

In practice, we wish to find the Taylor expansion of a dynamical system's vector field at an equilibrium and then find a suitable coordinate system in which some or all of the linear terms of the Taylor expansion vanish. Most of the difficulty in bifurcation theory involves verifying that these terms vanish in a generic way.

Local bifurcations of equilibria occur when an equilibrium loses hyperbolicity as a parameter varies. Therefore, we consider parameter-dependent systems by augmenting our state space X with a parameter space A. Hyperbolicity is lost if at least one eigenvalue crosses the imaginary axis. Of course, such a bifurcation must occur at an equilibrium, satisfying an *equilibrium condition*. The subset $A' \subset A$ of parameter space upon which the eigenvalue crosses the imaginary axis is the *bifurcation curve* (and requiring that our parameters are in this subset is the *bifurcation condition*). This is all we need to guarantee that the bifurcation occurs, although it may not unfold completely, and it may not occur in a generic manner (i.e. more complicated bifurcations may be occurring).

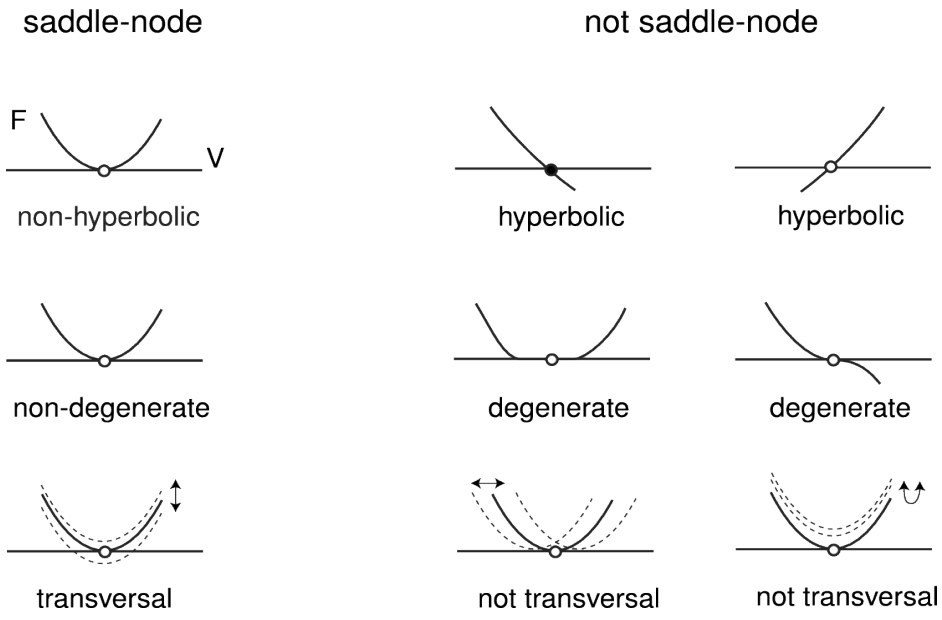

Figure 2.2: Various conditions of the fold bifurcation. Figure from [8] printed with permission from E.M. Izhikevich.

If the eigenvalue crosses the imaginary axis with a nonzero velocity, then we have satisfied the *transversality condition*, guaranteeing that the bifurcation unfolds completely. To guarantee that the bifurcation is occurring in a generic manner, we also have *genericity conditions*. The genericity conditions are a set of inequalities ensuring that the parameters lie upon non-degenerate regions of the bifurcation curve. If the equilibrium, bifurcation, transversality, and genericity conditions are all satisfied, then the system is smoothly equivalent to the topological normal form of the bifurcation (see section 2.3.1).

We can graphically visualize these conditions as follows, using the fold bifurcation as a starting point. The fold bifurcation (in one dimension) occurs in a parameter-dependent system $\dot{x} = f(x;\alpha)$ when $f(x^*;\alpha^*) = 0$ at some (x^*,α^*) and $\frac{\partial f}{\partial x}(x^*;\alpha^*) = 0$. Indeed, in Figure 2.2 we see how $f(x;\alpha)$ interacts with the x-axis as we vary α in a generic, transversal saddle-node bifurcation occurring at a non-hyperbolic equilibrium in the left column. We see examples of how each of these fail in the right column. Non-

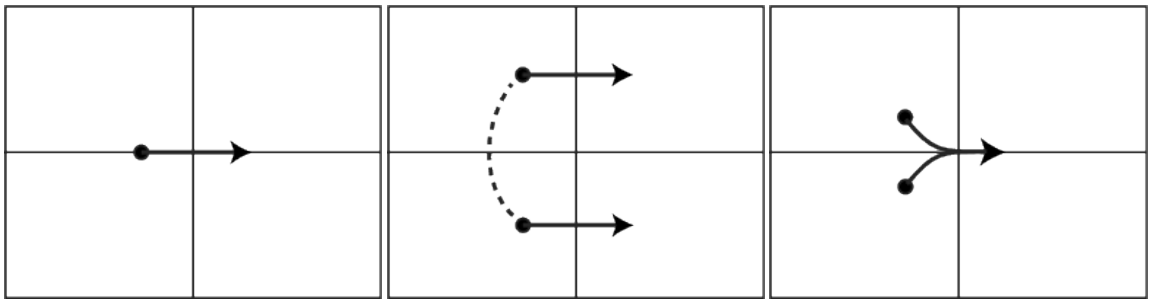

(a) Fold bifurcation (b) Andronov-Hopf bifurcation (c) Bogdanov-Takens bifurcation

Figure 2.3: The behavior of eigenvalues during different bifurcations. In a fold bifurcation, a single real eigenvalue crosses the imaginary axis (Figure 2.3a). In an Andronov-Hopf bifurcation, a pair of complex conjugate eigenvalues cross the imaginary axis together (Figure 2.3b). In a Bogdanov-Takens bifurcation, both of these occur simultaneously (Figure 2.3c). Figure from [8] printed with permission from E.M. Izhikevich.

hyperbolicity requires that an eigenvalue vanish ($\frac{\partial f}{\partial x}(x^*;\alpha^*) = 0$). Genericity requires that $f(x;\alpha)$ act like a parabola crossing the x-axis near the bifurcation point (x^*,α^*). Transversality requires that, as we vary bifurcation parameters, the bifurcation unfolds completely (i.e. $f(x;\alpha)$ crosses the x-axis completely as we vary α, rather than sliding along it, or touching it and then lifting back off).

With the idea of losing hyperbolicity in mind, there are only a few ways an equilibrium can lose hyperbolicity since we only have two eigenvalues. Either a single real eigenvalue can approach and cross the imaginary axis (corresponding to the fold or the cusp bifurcations, as in Figure 2.3a), a pair of complex-conjugate eigenvalues approach and cross the imaginary axis (corresponding to the Andronov-Hopf or Bautin/Generalized Hopf bifurcation, as in Figure 2.3b), or both of these can occur as a pair of complex conjugate eigenvalues become zero and cross the imaginary axis (corresponding to the Bogdanov-Takens bifurcation, as in Figure 2.3c). This is an exhaustive list of all possible local bifurcations of equilibria that can occur in a two-dimensional system.

Our model cannot produce a cusp bifurcation because it has at most two equilibria. Indeed, if a cusp bifurcation occurs generically and transversally, then three equilibria approach and annihilate as in the fold bifurcation [10]. Hence, the fold, Andronov-Hopf, and Bogdanov-Takens bifurcations are the only local bifurcations of equilibria that can occur in our model.

2.3.1. Topological Normal Forms

In this section, we will discuss the manner in which bifurcations are embedded in state- and parameter-space and how we reduce systems into the simplest possible form for analysis. Indeed, bifurcations occur on *center manifolds* in $A \times X$, we measure their complexity by their *codimension*, and we endeavor to find their simplest possible representations in terms of the *topological normal form*.

First, let us elaborate on the center manifold. Consider a linear system of differential equations $\dot{x} = Lx$ with $x \in \mathbb{R}^n$, L an $n \times n$ matrix, and equilibrium x^*. The matrix L divides $\mathbb{R}^n$ into three distinct invariant sets which also happen to be subspaces. The *stable subspace* is spanned by the generalized eigenvectors corresponding to the eigenvalues with strictly negative real parts, the *unstable subspace* is spanned by the generalized eigenvectors corresponding to the eigenvalues with the strictly positive real parts, and the *center subspace* is spanned by the generalized eigenvectors corresponding to the eigenvalues with precisely zero real part.

The Center Manifold Theorem claims that when a dynamical system $\dot{x} = f(x)$ with $x \in \mathbb{R}^n$ has equilibrium at the origin and that equilibrium has n_0 eigenvalues on the imaginary axis, there exists a locally defined smooth n_0-dimensional invariant manifold M called the *center manifold* that has some nice properties. First, M is locally tangent to the center eigenspace, i.e. the space spanned by the eigenvectors associated with the eigenvalues lying on the imaginary axis. Second, there exists a neighborhood

U of the equilibrium such that if an orbit $x(t) \in U$ for all $t \geqslant 0$ ($t \leqslant 0$), then $x(t) \to M$ in the Hausdorff metric as $t \to \infty$ ($t \to -\infty$).

Since we can always perform a change of coordinates so as to center a dynamical system on any of its equilibria, the Center Manifold Theorem guarantees an n_0-dimensional center manifold for each equilibrium. Hyperbolic equilibria only have eigenvalues off of the imaginary axis, so their center manifolds are 0-dimensional. Nonhyperbolic equilibria are undergoing a bifurcation, on the other hand, and have a nontrivial center manifold. Since a center manifold M is tangent to the center subspace of the linearized version of the system, we can locally describe that manifold by projecting the system onto the critical eigenbasis of the linearized system.

The complexity or rarity of a bifurcation is determined by its *codimension*, defined as the difference between the dimensionality of the parameter space and the dimensionality of the center manifold; for our purposes, the codimension is precisely the number of equality conditions we require to meet the bifurcation conditions.

Finally, we wish to find the simplest (say, polynomial) representation of a bifurcation. Presume we have a system $\dot{\xi} = g\left(\xi, \beta; \sigma\right)$, for $\xi \in \mathbb{R}^n$, $\beta \in \mathbb{R}^k$, $\sigma \in \mathbb{R}^\ell$, in which g is polynomial in ξ_i with vector of coefficients σ. Presume this system has equilibrium at the origin for all $\left|\beta\right|$ sufficiently small and undergoes a particular bifurcation of codimension k in the most generic manner possible when $\beta = 0$.

Also presume we have a system $\dot{x} = f\left(x, \alpha\right)$, where $x \in \mathbb{R}^n$ and $\alpha \in \mathbb{R}^k$ which has equilibrium at the origin for all $|\alpha|$ sufficiently small. Also presume that when $\alpha = 0$, $\dot{x} = f(x, \alpha)$ undergoes the same codimension k bifurcation that the system $\dot{\xi} = g(\xi, \beta; \sigma)$ undergoes when $\beta = 0$, and with the same degree of genericity. We have the following definition of the topological normal form of the bifurcation:

Definition 2.7. The system $\dot{\xi} = g\left(\xi, \beta; \sigma\right)$ is called a *topological normal form* for the bifurcation if any generic system $\dot{x} = f(x, \alpha)$ undergoing that bifurcation is locally

topologically equivalent near the origin to the system $\dot{\xi} = g(\xi, \beta; \sigma)$ for some values of the coefficients σ.

A generic system can be written as a linear combination of coordinates on the center, stable, and unstable manifolds $\xi = \xi_c + \xi_s + \xi_u$. On the stable and unstable manifolds, the system is smoothly equivalent to its linearization, i.e. trajectories exponentially grow or shrink thanks to the Hartman-Grobman theorem [3]. This provides the system

$$\begin{cases} \dot{\xi}_c &= \hat{g}\left(\xi_c, \beta; \sigma\right) \\ \dot{\xi}_s &= -\xi_s \\ \dot{\xi}_u &= \xi_u \end{cases}$$

where $\hat{g}$ represents the system restricted to the center manifold. The reduction principle, first proved by Pliss [11], provides the existence of some C^k homeomorphism (for some $k \geqslant 1$) mapping this system into the restricted system $\dot{\xi}_c = \hat{g}\left(\xi_c, \beta; \sigma\right)$. This allows us to disregard the stable and unstable manifolds, and the genericity conditions ensure that the restricted system is smoothly equivalent to the topological normal form.

The "interesting" part of the system is *suspended by the standard saddle*; orbits starting off of M act as if they are near a saddle point, whose dynamics are well-known. The *reduction principle* allows us to strip off everything except the center manifold, whose dynamics are under study. We can then demonstrate transversality and genericity to ensure the system is smoothly equivalent to the topological normal form via a sequence of (possibly nonlinear) changes in variables, parameters, and time.

Note that transforming the system into its normal form is not necessary to demonstrate transversality and genericity, and in fact is to be avoided if possible. Indeed, demonstrating the genericity and transversality of the fold and Andronov-Hopf bifurcation does not require transforming the system into the topological normal form. Further, we only need to go "half-way" to the Bogdanov-Takens bifurcation normal form

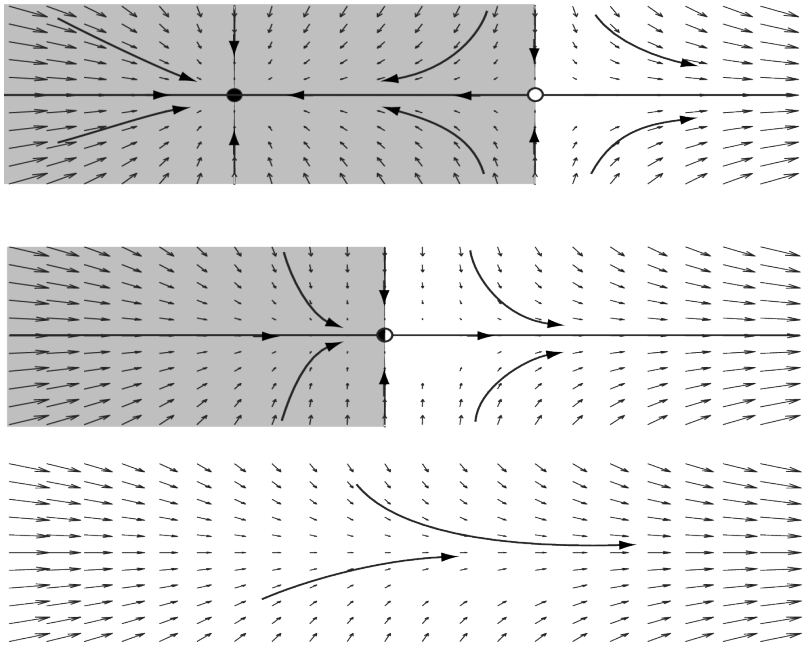

Figure 2.4: A generic unfolding of the fold bifurcation in a planar system. The shaded region denotes the basin of attraction of the stable fixed point. Figure from [8] printed with permission from E.M. Izhikevich.

in order to demonstrate transversality and genericity. The complete transformation into the normal form is tedious and not particularly illuminating.

2.3.2. Fold Bifurcation

We first seek the lowest-hanging bifurcative fruit, the *fold* (or *saddle-node*) *bifurcation*. Consider the parameter-dependent system $\dot{x} = f(x, \alpha)$, where $x \in \mathbb{R}^n$ and $\alpha \in \mathbb{R}$. The fold bifurcation condition is the existence of an equilibrium $x = x^*$ dependent on a critical parameter choice $\alpha = \alpha^*$ such that an eigenvalue vanishes and no other eigenvalues lie on the imaginary axis. If genericity and transversality conditions are satisfied, the fold bifurcation geometrically corresponds to a stable equilibrium approaching a saddle, the two equilibria colliding with nonzero velocity, and then disappearing in the process. In the most generic case, the stable equilibrium is a node, and for this reason, the fold bifurcation is often known as a saddle-node bifurcation. A complete unfolding of the fold bifurcation in a planar system is depicted in Figure 2.4.

The eigenvector associated with this vanishing eigenvalue is referred to as *critical*. The center manifold theorem and the reduction principle ensure that it is sufficient to consider the dynamical system projected onto the critical eigenspace. The fold bifurcation takes on the one-dimensional topological normal form $\dot{y} = \beta \pm y^2$ where $\beta \in \mathbb{R}$.

If the fold bifurcation, genericity, and transversality conditions are satisfied, then a homeomorphism exists taking a system of interest (restricted to its center manifold) into the topological normal form. The bifurcation condition guarantees that the linear part of the system vanishes. The genericity condition guarantees that the quadratic part of the Taylor expansion of the system is non-vanishing. The transversality condition guarantees that the derivative of the vector field with respect to the bifurcation parameters is non-vanishing at the bifurcation point. Following Kuznetsov [10] pp. 174-177, we have the following conditions ensuring the generic occurrence of a fold bifurcation:

(i) (Equilibrium condition) For the critical parameter value $\alpha = \alpha^*$, we have an equilibrium $x = x^*$ dependent on α^* (that is, $f(x^*, \alpha^*) = 0$).

(ii) (Bifurcation condition) The equilibrium x^* has an eigenvalue $\lambda(\alpha^*) = 0$, with no other eigenvalues on the imaginary axis.

(iii) (Transversality condition) The eigenvalue vanishes transversally with respect to α and so has a nonzero derivative with respect to α evaluated at $(x, \alpha) = (x^*, \alpha^*)$.

(iv) (Genericity condition) The quadratic term of the Taylor expansion of the system restricted to the critical eigenspace is nonzero.

Let us endeavor to make these conditions more precise. In a two-dimensional system, if we denote τ as the trace of the Jacobian at an equilibrium and Δ as the

determinant, then the eigenvalues satisfy the characteristic polynomial $\lambda^2 - \tau\lambda + \Delta = 0$. Indeed, given a Jacobian

$$\begin{pmatrix} a & b \\ c & d \end{pmatrix}$$

we have the characteristic polynomial $\lambda^2 - \tau\lambda + \Delta = 0$, where $\tau = a + d$ and $\Delta = ad - bc$. Thus we have a simple zero eigenvalue if and only if $\Delta = 0$ and $\tau \neq 0$.

Transversality is equivalent to requiring that the first derivative of the restricted vector field with respect to the bifurcation parameter does not vanish at the bifurcation point. Genericity is equivalent to requiring that the quadratic term of the Taylor expansion of this vector field does not vanish. Hence, we need to compute our restricted system.

Let us presume that we have a planar autonomous system $\dot{x} = f(x, \alpha)$ where $x \in \mathbb{R}^2$, $\alpha \in \mathbb{R}$, and f is smoothly dependent on x and α. Presume further that for $\alpha = \alpha^*$, the system has the equilibrium $x = x^*$ with one eigenvalue $\lambda_1 = 0$ and one eigenvalue $\lambda_2 < 0$. The Center Manifold Theorem implies the existence of a smooth invariant center manifold locally defined near $(x, \alpha) = (x^*, \alpha^*)$ and tangent to the subspace spanned by the eigenvector associated with $\lambda_1 = 0$ at this point. Since the second eigenvalue is strictly real and negative, this center manifold is attracting. We denote the Jacobian matrix evaluated at the equilibrium as L and we write

$$x = \begin{pmatrix} x_1 \\ x_2 \end{pmatrix},\ q = \begin{pmatrix} q_1 \\ q_2 \end{pmatrix},\ p = \begin{pmatrix} p_1 \\ p_2 \end{pmatrix},\ f(x, \alpha) = \begin{pmatrix} f_1(x, \alpha) \\ f_2(x, \alpha) \end{pmatrix}$$

where q is the eigenvector corresponding to the annihilated eigenvalue (i.e. $Lq = 0$), and p is its adjoint ($\overline{L}^\top p = L^\top p = 0$ since all quantities are real).

We can without loss of generality choose q and p so that $\langle p, q \rangle = 1$. We restrict the system to the basis spanned by q by writing any $x = yq + u + x^*$ for some vector u

orthogonal to p. Following Kuznetsov, [10], pp. 177, at $\alpha = \alpha^*$, the restricted system will now have the form $\dot{y} = a_2 y^2 + O(y^3)$ where

$$\begin{aligned} a_2 &= \frac{1}{2}\frac{\partial^2}{\partial y^2}\langle p, f(yq + x^*)\rangle \mid_{(y,\alpha)=(0,\alpha^*)} \\ &= \frac{1}{2}\left\langle p, \begin{pmatrix} q_1^2 (f_1)_{x_1x_1} + 2q_1q_2 (f_1)_{x_1x_2} + q_2^2 (f_1)_{x_2x_2} \\ q_1^2 (f_2)_{x_1x_1} + 2q_1q_2 (f_2)_{x_1x_2} + q_2^2 (f_2)_{x_2x_2} \end{pmatrix} \right\rangle \Bigg|_{(x,\alpha)=(x^*,\alpha^*)} \end{aligned}$$

where $\langle v, w\rangle = v_1w_1 + v_2w_2$. If $a_2 \neq 0$, the system depends generically on a_2, and the system satisfies some transversality conditions, then we obtain the topological normal form. Define $\sigma = \text{sgn}(a_2)$, and let $a \in \mathbb{R}$ be a new parameter; we obtain the topological normal form

$$\dot{y} = a + \sigma y^2 + O\left(y^3\right)$$

Following Kuznetsov [10], pp. 84, 177, the transversality and genericity conditions, respectively, are

$$\text{(iii)} \quad \left\langle p, \frac{\partial}{\partial \alpha} f\left(yq + x^*, \alpha\right)\right\rangle \Bigg|_{(y,\alpha)=(0,\alpha^*)} \neq 0$$

$$\text{(iv)} \quad a_2 = \frac{1}{2}\left\langle p, \begin{pmatrix} q_1^2 (f_1)_{x_1x_1} + 2q_1q_2 (f_1)_{x_1x_2} + q_2^2 (f_1)_{x_2x_2} \\ q_1^2 (f_2)_{x_1x_1} + 2q_1q_2 (f_2)_{x_1x_2} + q_2^2 (f_2)_{x_2x_2} \end{pmatrix} \right\rangle \Bigg|_{(x,\alpha)=(x^*,\alpha^*)} \neq 0$$

where $(f_i)_{**}$ denotes second partial derivatives. Hence, any system satisfying the following four conditions is smoothly equivalent to the topological normal form of the fold bifurcation:

(i) (Equilibrium) $f(x^*, \alpha^*) = 0$

(ii) (Bifurcation) When $(x, \alpha) = (x^*, \alpha^*)$, $\Delta = 0$ and $\tau \neq 0$

(iii) (Transversality) $\left\langle p, \frac{\partial}{\partial \alpha} f\left(yq + x^*, \alpha\right)\right\rangle \Bigg|_{(x,\alpha)=(x^*,\alpha^*)} \neq 0$

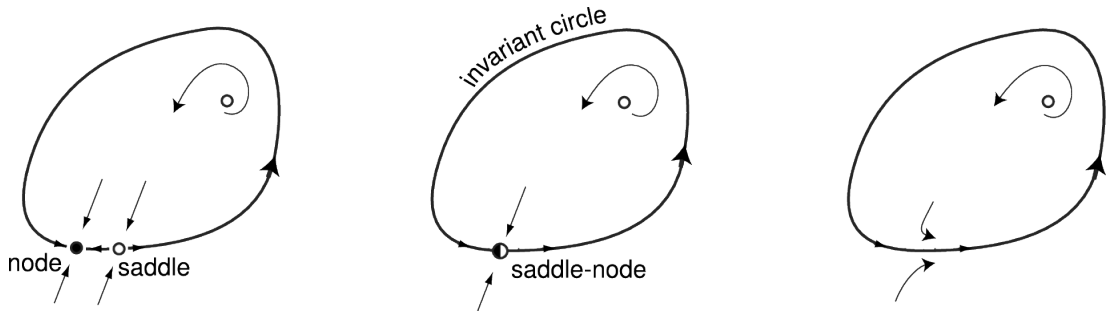

Figure 2.5: A generic unfolding of the fold-on-invariant-circle bifurcation. Figure from [8] printed with permission from E.M. Izhikevich.

$$\text{(iv)}\quad \text{(Genericity)}\quad \left\langle p, \begin{pmatrix} q_1^2 (f_1)_{x_1x_1} + 2q_1q_2 (f_1)_{x_1x_2} + q_2^2 (f_1)_{x_2x_2} \\ q_1^2 (f_2)_{x_1x_1} + 2q_1q_2 (f_2)_{x_1x_2} + q_2^2 (f_2)_{x_2x_2} \end{pmatrix} \right\rangle \Bigg|_{(x,\alpha)=(x^*,\alpha^*)} \neq 0$$

We are also interested in a slightly different flavor of the fold bifurcation, the fold-on-invariant-circle bifurcation, as illustrated in Figures 1.1b and 2.5.

The fold-on-invariant-circle bifurcation proceeds as the fold bifurcation, however, the the unstable manifold of the saddle connects with a stable node forming a heteroclinic loop. The nomenclature is clear: this loop is an invariant set and is homeomorphic to a circle. After the fold bifurcation occurs, the heteroclinic loop becomes a limit cycle, as in Figure 2.5.

2.3.3. Andronov-Hopf Bifurcation

Presume we have some system $\dot{x} = f(x, \alpha)$ where $x \in \mathbb{R}^2$ and $\alpha \in \mathbb{R}$ with fixed equilibrium $x^* = 0$ for all $|\alpha|$ sufficiently small. Geometrically, the Andronov-Hopf bifurcation occurs when a spiral equilibrium changes stability. However, it is a local bifurcation, and so trajectories outside of a small neighborhood of the equilibrium remain unperturbed (up to smooth equivalence). For example, if an equilibrium becomes unstable, trajectories outside of a small neighborhood of the equilibrium will still be approaching the neighborhood. This apparent paradox is resolved with the creation of a stable limit cycle surrounding the equilibrium, preserving the behavior beyond the neighborhood. If an Andronov-Hopf bifurcation is associated with the (dis)appearance

of a stable limit cycle, it is referred to as *supercritical* (Figure 2.6, left), and if it is associated with the (dis)appearance of an unstable limit cycle, it is *subcritical* (Figure 2.6, right).

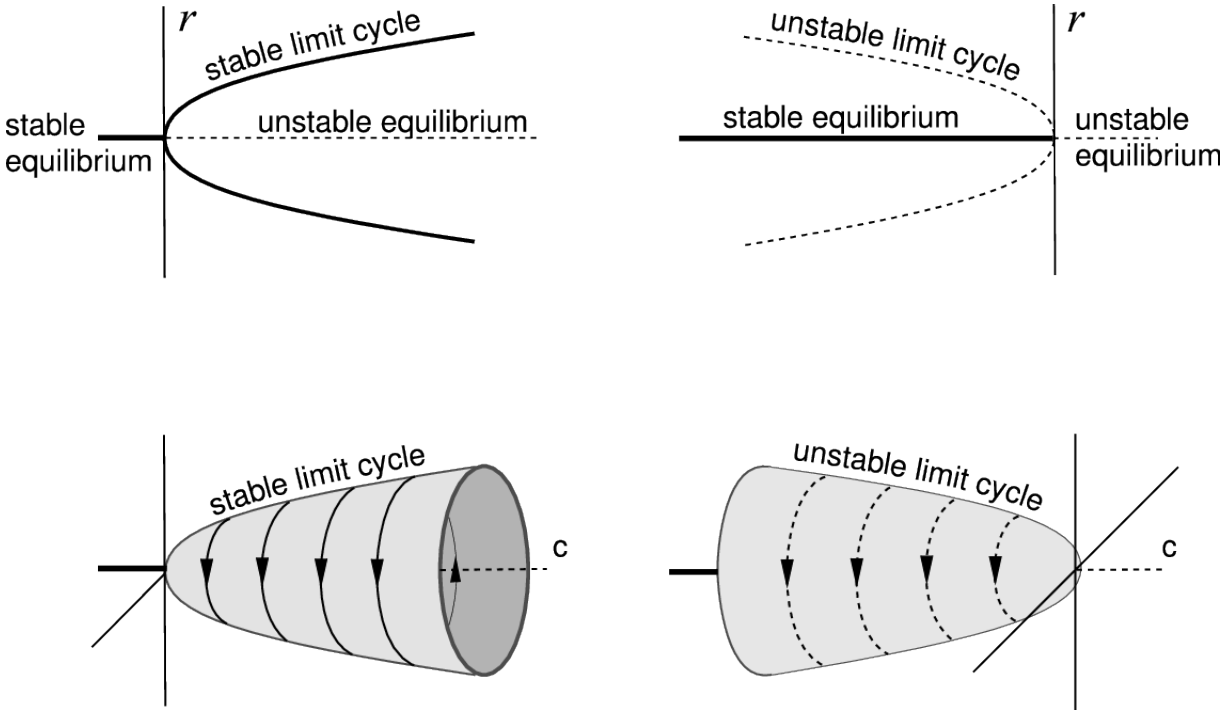

Figure 2.6: Generically unfolding Andronov-Hopf bifurcations. On left, a generic unfolding of a supercritical Andronov-Hopf bifurcation corresponding to the (dis)appearance of a stable limit cycle. On right, a generic unfolding of a subcritical Andronov-Hopf bifurcation. Figure from [8] printed with permission from E.M. Izhikevich.

The Andronov-Hopf bifurcation condition demands that two complex-conjugate eigenvalues cross the imaginary axis. Transversality demands that the real part of these eigenvalues vanish transversally. Genericity demands that the first Lyapunov coefficient not vanish. As before, we wish to make these conditions more precise.

The center manifold is locally described by the critical eigenbasis, comprised of two linearly independent eigenvectors. As before, for a 2×2 Jacobian matrix L with trace τ and determinant Δ, the eigenvalues of L in a two-dimensional system satisfy

$\lambda^2 - \tau\lambda + \Delta = 0$. Further, a pair of complex conjugate eigenvalues meets the imaginary axis if and only if $\tau = 0$ and $\Delta > 0$.

The Andronov-Hopf bifurcation takes the topological normal form

$$\begin{cases} \dot{r} = & \frac{\tau}{2} r + \ell_1 r^3 \\ \dot{\theta} = & \frac{1}{2}\sqrt{4\Delta - \tau^2} + \delta r^2 \end{cases} \tag{2.2}$$

Further, δ describes the sensitivity of an orbit's oscillation frequency to the square of the distance from equilibrium, and ℓ_1 is known as the *first Lyapunov coefficient*, describing the sensitivity of the radius of oscillation to the cube of that distance. The computation of ℓ_1 and δ are often nontrivial in the general setting. We can use a convenient formula for ℓ_1, but we will ignore δ since it is not involved in demonstrating the genericity of the bifurcation.

Following the procedure described by Kuznetsov ([10] pp. 89-96), we compute the genericity conditions, which demand that the first Lyapunov coefficient be non vanishing. If it does vanish, a generalized Hopf (or Bautin) bifurcation may be occurring, which is of codimension at least 2 (see Section 2.3.4). The first Lyapunov coefficient results from a series of coordinate and parameter changes, but can be computed directly using formulas from Kuznetsov to simplify the process. For the parameter-dependent system $\dot{x} = f(x, \alpha)$ with equilibrium at the origin for all sufficiently small $|\alpha|$ undergoing an Andronov-Hopf bifurcation when $\alpha = 0$, let $q(\alpha)$ be an eigenvector associated with the eigenvalue on the imaginary axis (i.e. $L(\alpha)q(\alpha) = \lambda(\alpha)q(\alpha)$), $p(\alpha)$ be its adjoint ($\overline{L(\alpha)}^{\top} p(\alpha) = \overline{\lambda(\alpha)} p(\alpha)$), and define $\omega(\alpha) := \sqrt{\Delta(\alpha)}$. Then we have the eigenvalues $\left\{\lambda(\alpha), \overline{\lambda(\alpha)}\right\} = \{\pm i\omega\}$ when $\alpha = 0$. Projecting any point x onto the coordinate system afforded by $q(\alpha)$ and $\bar{q}(\alpha)$ provides $x = zq(\alpha) + \bar{z}\bar{q}(\alpha)$ on the complex plane. We use symmetric multi-linear functions in the partial derivatives with respect to z and $\bar{z}$ to compute the Taylor expansion of the vector field in these

coordinates:

$$g_{kl} = \left\langle p(\alpha), \frac{\partial^{k+l}}{\partial z^k \partial \bar{z}^l} f\left(zq(\alpha) + \bar{z}\bar{q}(\alpha), \alpha\right) \right\rangle \Bigg|_{(z,\alpha)=(0,0)} \tag{2.3}$$

The first Lyapunov coefficient is $\ell_1 = \left(2\omega^2\right)^{-1} \mathrm{Re}\left(ig_{20}g_{11} + \omega g_{21}\right)$ at the bifurcation point (following [10] and others). Checking to ensure genericity, then, is equivalent to checking that $\mathrm{Re}\left(ig_{20}g_{11} + \omega g_{21}\right) \neq 0$.

Hence, we have the following conditions ensuring the generic occurrence of an Andronov-Hopf bifurcation:

(i) (Equilibrium) $f(0, \alpha) = 0$ for small $|\alpha|$,

(ii) (Bifurcation) $\tau = 0$ and $\Delta > 0$ when $(x, \alpha) = (0, 0)$,

(iii) (Transversality) $\frac{\partial \tau}{\partial \alpha} |_{(x,\alpha)=(0,0)} \neq 0$

(iv) (Genericity) $\mathrm{Re}\left(ig_{20}g_{11} + \omega g_{21}\right) |_{(x,\alpha)=(0,0)} \neq 0$

As an aside, our usage of the symmetric multi-linear functions of the partial derivatives of z and $\bar{z}$ is not concerned with linear terms. Hence, it is sufficient to consider only the nonlinear terms in the Taylor expansion centered on the equilibrium. Indeed, this expansion will be $f(x) = Lx + F(x)$ where L is the Jacobian of the system, which can be disregarded; to compute any g_{kl} with $k + l \geqslant 2$, we can use F instead of f. Indeed, for g_{kl}, we only need terms of order $k + l$ in the Taylor expansion of F.

The Andronov-Hopf bifurcation is of codimension 1 as the Andronov-Hopf bifurcation curve is defined implicitly by one and only one parameter curve, $\tau = 0$. The first dimension of our topological normal form takes the form $\dot{r} = \frac{1}{2}\tau r + \ell_1 r^3$, where ℓ_1 is the 1^{st} Lyapunov coefficient. If the first Lyapunov coefficient vanishes at the bifurcation point, then genericity fails and a Bautin bifurcation of codimension at least 2 may be occurring. In general, checking whether Lyapunov coefficients vanish

is not trivial. We are tasked with assessing the richness of the voltage-sensitive neuron model's bifurcation behavior; if genericity is failed, then a candidate Bautin point has been reached, and expected Bautin behavior will be checked numerically.

Finally, we can classify an Andronov-Hopf bifurcation as either subcritical or supercritical depending on the sign of the first Lyapunov coefficient. Geometrically, supercritical Andronov-Hopf bifurcations correspond to the appearance or disappearance of a stable limit cycle, which occurs when $\text{sgn}\left(\ell_1\right) = -1$. Otherwise, we have a subcritical Andronov-Hopf bifurcation, corresponding to the appearance of an unstable limit cycle when $\text{sgn}\left(\ell_1\right) = +1$.

2.3.4. Bautin Bifurcation

If a dynamical system satisfies the Andronov-Hopf equilibrium and bifurcation condition for some equilibrium and critical parameter value $(x, \alpha) = (x^*, \alpha^*)$, but fails the genericity condition, i.e. has vanishing first Lyapunov coefficient, then the point (x^*, α^*) is a candidate Bautin bifurcation point. To verify that a Bautin bifurcation is occurring generically and transversally, one must compute the value of the second Lyapunov coefficient and verify a transversality condition. Doing this for a general system is not easy.

Any neighborhood in parameter space of a generic and transversal Bautin bifurcation point will contain a supercritical Andronov-Hopf bifurcation point, a subcritical Andronov-Hopf bifurcation point, and a (global) fold-limit-cycle bifurcation point. The subcritical Andronov-Hopf bifurcation is associated with the appearance of an unstable limit cycle, and the supercritical Andronov-Hopf bifurcation is associated with the appearance of a stable limit cycle, and near a Bautin point, these limit cycles appear nested within one another. The fold-limit-cycle bifurcation occurs when the inner cycle grows or the outer cycle shrinks, and the cycles annihilate in a fold-like bifurcation.

Numerically verifying the presence of a Bautin bifurcation is straightforward. We demonstrate phase portraits from each qualitatively distinct region surrounding the candidate Bautin point. This numerically demonstrates the coexistence of stable-unstable limit cycle pairs before a fold-limit-cycle bifurcation, the hallmark behavior associated with the Bautin bifurcation.

2.3.5. Bogdanov-Takens Bifurcation

Geometrically, the Bogdanov-Takens bifurcation is more complicated than the Andronov-Hopf and fold bifurcations since it is of codimension 2. The fold bifurcation has two dynamical regimes and one degenerate case: before the two equilibria collide, after they collide, and the degenerate case in which we have a single half-stable equilibrium. The Andronov-Hopf bifurcation likewise has two dynamical regimes with a degenerate border: before the spiral changes stability, after it changes stability, and the degenerate case in which we have a neutrally stable center (a family of non-isolated cycles). The unfolding of the Bogdanov-Takens bifurcation depends on whether the Andronov-Hopf bifurcation in question is subcritical or supercritical.

Indeed, we have four distinct dynamical regimes with three degenerate border cases. Figure 2.7 illustrates both the supercritical and the subcritical case. As in the Andronov-Hopf bifurcation, the criticality is determined by the sign of a coefficient s computed via a series of parameter, time, and coordinate changes. Let a and b be the bifurcation parameters, and consider the subcritical Bogdanov-Takens bifurcation. Beginning in region 1 of Figure 2.7 and moving counterclockwise, we begin with a stable spiral and saddle pair of equilibria. Crossing the SHO line triggers a saddle-homoclinic orbit in which the stable and unstable manifolds of the saddle form a homoclinic loop. This loop pinches off in section 2 into an unstable limit cycle surrounding the stable spiral equilibrium. An Andronov-Hopf bifurcation occurs at AH as the unstable limit cycle shrinks and collides with the stable spiral inside, leaving an unstable spiral behind

in region 3. Crossing from region 3 into region 4 across SN_1 triggers a saddle-node bifurcation in which the unstable spiral and the saddle collide and annihilate. In region 4, we have no equilibria, and crossing SN_2 triggers another saddle-node bifurcation giving birth to our original stable spiral and saddle pair of equilibria. The supercritical Bogdanov-Takens bifurcation unfolds similarly, except with time reversed.

The Bogdanov-Takens (or double zero) bifurcation occurs when the system has two zero eigenvalues. As before, we wish to make the conditions of the Bogdanov-Takens bifurcation precise. Presume we have a planar system dependent on two parameters, $\dot{x} = f(x, \alpha)$ with $x, \alpha \in \mathbb{R}^2$ where f is smoothly dependent on x and α. Furthermore, suppose that for $\alpha = 0$, the equilibrium $x = 0$ has two zero eigenvalues, $\lambda_{1,2} = 0$. Denote the Jacobian evaluated at the equilibrium as L, its trace as τ, and its determinant as Δ.

The Bogdanov-Takens bifurcation condition demands that both eigenvalues vanish so $\tau = \Delta = 0$. Transversality demands that they vanish transversally, and so we require the map $(x, \alpha)^\top \mapsto \left(f(x, \alpha), \tau, \Delta\right)^\top$ to be regular (has a nonzero determinant) at the origin. The Center Manifold Theorem implies the existence of a smooth invariant center manifold locally defined near $(x, \alpha) = (0, 0)$. To discuss genericity, we project the system onto the center manifold, or at least its linerization near the bifurcation point, which is spanned by its critical (generalized) eigenvectors.

We project the system onto the subspace spanned by the generalized critical eigenvectors q_0 and q_1 using their adjoints p_1 and p_0; we have $Lq_0 = 0$ and $Lq_1 = q_0$ and that $\overline{L}^\top p_1 = 0$ and $\overline{L}^\top p_0 = p_1$. Since L consists of real entries, $\overline{L} = L$, so this reduces to $L^\top p_1 = 0$ and $L^\top p_0 = p_1$. These eigenvectors are also associated with the Jordan normal form of the Jacobian matrix evaluated at the equilibrium; q_0 and q_1 form the columns of the passage matrix of the Jacobian to the Jordan normal form and p_0 and p_1 form the rows of the inverse passage matrix. Since both eigenvalues of L are

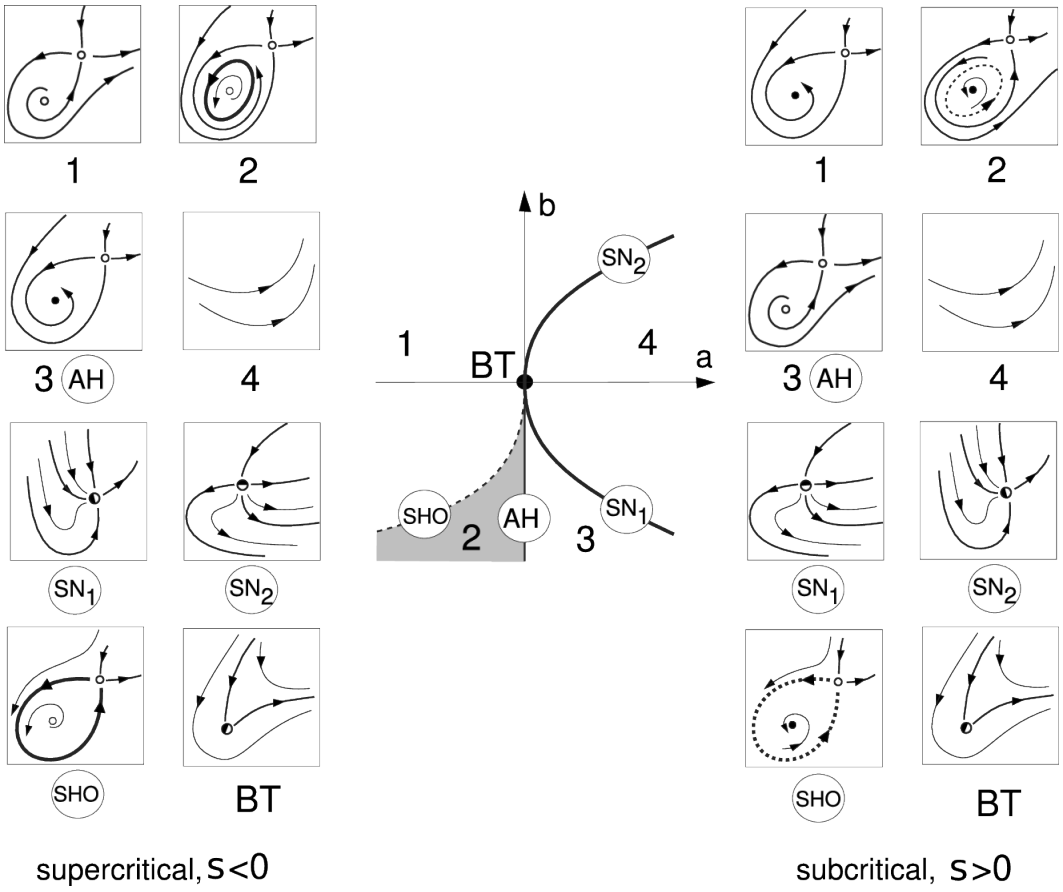

Figure 2.7: Generically unfolding Bogdanov-Takens bifurcation. Complete bifurcation portrait of the Bogdanov-Takens topological normal form illustrating a generically unfolding BT bifurcation. Image taken from [8], printed with permission from E.M. Izhikevich.

zero, and since L is 2×2, the Jordan normal form for L is

$$\begin{pmatrix} 0 & 1 \\ 0 & 0 \end{pmatrix}$$

Without loss of generality we can assume the generalized eigenvectors have been normalized so that $\langle p_0, q_0 \rangle = \langle p_1, q_1 \rangle = 1$ and $\langle p_0, q_1 \rangle = \langle p_1, q_0 \rangle = 0$.

When we set $y = \binom{y_1}{y_2}$ and represent a point x in this coordinate system as $x = y_1 q_0 + y_2 q_1$, we obtain

$$\begin{cases} \dot{y}_1 = & \langle p_0, f(y_1 q_0 + y_2 q_1, \alpha) \rangle \\ \dot{y}_2 = & \langle p_1, f(y_1 q_0 + y_2 q_1, \alpha) \rangle \end{cases} \tag{2.4}$$

which is a system with equilibrium at the origin for $\alpha = 0$. If we consider the Taylor expansion of this system about the origin, we obtain coefficients that vary as functions of α. Since q_0 and q_1 form the columns of the passage matrix of the Jacobian to the Jordan normal form (and p_0 and p_1 form the rows of the inverse passage matrix), we always have a system of the form

$$\dot{y} = \begin{pmatrix} 0 & 1 \\ 0 & 0 \end{pmatrix} \begin{pmatrix} y_1 \\ y_2 \end{pmatrix} + \begin{pmatrix} a_0 + a_{10} y_1 + a_{01} y_2 + \frac{1}{2} a_{20} y_1^2 + a_{11} y_1 y_2 + \frac{1}{2} a_{02} y_2^2 + O\left(\|y\|^3\right) \\ b_0 + b_{10} y_1 + b_{01} y_2 + \frac{1}{2} b_{20} y_1^2 + b_{11} y_1 y_2 + \frac{1}{2} b_{02} y_2^2 + O\left(\|y\|^3\right) \end{pmatrix} \tag{2.5}$$

where each coefficient is a function of α. Furthermore, when $\alpha = 0$, we have that $a_0, a_{10}, a_{01}, b_0, b_{10}$, and b_{01} each vanish.

Kuznetsov [10] provides that the genericity conditions of the Bogdanov-Takens bifurcation demands $a_{20} + b_{11} \neq 0$, $b_{20} \neq 0$. Hence, we have the following conditions for the Bogdanov-Takens bifurcation:

(i) (Equilibrium) Equilibrium at the origin ($f(0,0) = 0$)

(ii) (Bifurcation) When $(x, \alpha) = (0,0)$, the trace and determinant both vanish with nonzero Jacobian ($\tau = \Delta = 0, L \neq 0$)

(iii) (Transversality) The map $(x, \alpha)^\top \mapsto \left(f(x, \alpha), \tau, \Delta\right)^\top$ is regular at the point $(x, \alpha) = (0,0)$ (and so has a nonzero determinant)

(iv) (Genericity) The following holds when $\alpha = 0$:

(a) $a_{20} + b_{11} \neq 0$

(b) $b_{20} \neq 0$

The normal form is

$$\begin{cases} \dot{\xi}_1 = & \xi_2 \\ \dot{\xi}_2 = & \beta_1 + \beta_2 \xi_1 + \xi_1^2 + \sigma \xi_1 \xi_2 \end{cases} \tag{2.6}$$

where $\sigma = \operatorname{sgn}\left(b_{20}\left(a_{20} + b_{11}\right)\right)$, and the parameters β_1, β_2 are computed from the parameters of our system 2.5 in the following manner summarized by Kuznetsov [10]. Notice that we have guaranteed that $\sigma \neq 0$ due to our genericity conditions. The parameters β_1, β_2 in the topological normal form are used to parameterize the saddle-homoclinic-orbit bifurcation curve associated with a Bogdanov-Takens bifurcation point, as discussed below. Following Kuznetsov [10], pp. 318, we take system 2.5 and reduce

it to a nonlinear oscillator with a change of coordinates

$$\begin{cases} u_1 &= y_1 \\ u_2 &= y_2 + a_{00} + a_{10}y_1 + a_{01}y_2 + \frac{1}{2}a_{20}y_1^2 + a_{11}y_1y_2 + \frac{1}{2}a_{02}y_2^2 + O\left(\|y\|^3\right) \end{cases}$$

yielding the system

$$\begin{cases} \dot{u_1} &= u_2 \\ \dot{u_2} &= g_{00} + g_{10}u_1 + g_{01}u_2 + \frac{1}{2}g_{20}u_1^2 + g_{11}u_1u_2 + \frac{1}{2}g_{02}u_2^2 + O\left(\|u\|^3\right) \end{cases}$$

where each g_{kl} is a function of α. We then perform a parameter-dependent shift:

$$\begin{cases} u_1 &= v_1 + \delta(\alpha) \\ u_2 &= v_2 \end{cases}$$

A choice of $\delta(\alpha) \approx -\frac{g_{01}(\alpha)}{g_{11}(0)}$ will yield the system

$$\begin{cases} \dot{v_1} &= v_2 \\ \dot{v_2} &= h_{00} + h_{10}v_1 + \frac{1}{2}h_{20}v_1^2 + h_{11}v_1v_2 + \frac{1}{2}h_{02}v_2^2 + O\left(\|v\|^3\right) \end{cases}$$

where each h_{kl} is a smooth function of α. From here, we can compute the topological normal form 2.6 directly. Define the following:

$$\begin{cases} A &:= \frac{1}{2}\left(h_{20} - h_{10}h_{02}\right) \\ B &:= h_{11} \\ \mu_1 &:= h_{00} \\ \mu_2 &:= h_{10} - \frac{1}{2}h_{00}h_{02} \end{cases}$$

Then in system 2.6 we have:

$$\begin{cases} \beta_1 &= \dfrac{B^4}{A^3}\mu_1 \\ \beta_2 &= \dfrac{B^2}{A^2}\mu_2 \end{cases}$$

The existence of the Bogdanov-Takens bifurcation, which is local, implies the existence of the global saddle-homoclinic-orbit bifurcation, which is global (see section 2.4). Kuznetsov provided the following Lemma for $\beta = \binom{\beta_1}{\beta_2}$ ([10] pp. 325):

Lemma 2.8. There is a unique smooth curve P corresponding to a SHO bifurcation in system 2.6 that originates at $\beta = 0$ and has the local representation

$$P = \left\{ (\beta_1, \beta_2) \mid k\beta_1 = -\frac{6}{25}\beta_2^2 + o(\beta_2^2), \beta_2 < 0 \right\}$$

Moreover, for $\|\beta\|$ small, system 2.6 has a unique limit cycle for parameter values inside the region bounded by the Hopf bifurcation curve and the SHO bifurcation curve P, and no cycles outside this region. This cycle is stable if $\sigma < 0$ and unstable if $\sigma > 0$.

2.4. Global Bifurcations and Non-smooth Bifurcations

Global bifurcations affect the entire state-space, rather than a single invariant set. The existence of high-codimension (at least 2) local bifurcations of equilibria implies the existence of global bifurcations of lower codimension; without the existence of these local bifurcations, global bifurcations are very difficult to detect and handle computationally. We will ignore them except in the case of the saddle-homoclinic-orbit bifurcation (whose existence is implied by the Bogdanov-Takens bifurcation), the fold-limit-cycle bifurcation (whose existence is implied by the Bautin bifurcation), and the "big" saddle-homoclinic-orbit bifurcation (which occurs due to the hybrid nature of our model).

More interestingly, perhaps, is that our model is not strictly smooth. Indeed, we have a discontinuous reset, and so it is a hybrid system, which both "flows" and

“jumps.” Hybrid systems exhibit more complicated behaviors that are technically not global bifurcations, but have the same consequences as global bifurcations. For example, the (dis)appearance of limit cycles do not always coincide with Andronov-Hopf bifurcations. We will observe some interesting phenomena that arise due to the hybrid nature of our model in Chapter 4.

We are not interested in interactions between the equilibria and the jump, as this would compromise the local topological equivalence between our model and previous models. However, the interaction between the jump, limit cycles, and the stable and unstable manifolds of the equilibria are of interest, as these interactions maintain a biological interpretation. Indeed, in Chapter 4 we numerically demonstrate that model 3.1 is capable of hybrid equivalents of both (global) "big" saddle-homoclinic-orbit bifurcations and (local) fold-on-invariant-circle bifurcations (see Figure 2.8). These phenomena create (or destroy) stable spiking limit cycles, and the hybrid “big” SHO and hybrid fold-on-invariant circle bifurcation-like behaviors seem to occur together in model 3.1 ubiquitously. However, we must be careful; since our system is not strictly smooth, we cannot classify these interactions as a bifurcation in the smooth sense. However, the phenomena have the same ramifications as bifurcations.

Techniques are available for analyzing non-smooth bifurcations, but we do not pursue this line of inquiry. Coombes, Thul, and Wedgewood present an interesting analysis of non-smooth dynamics in hybrid spiking models in [2].

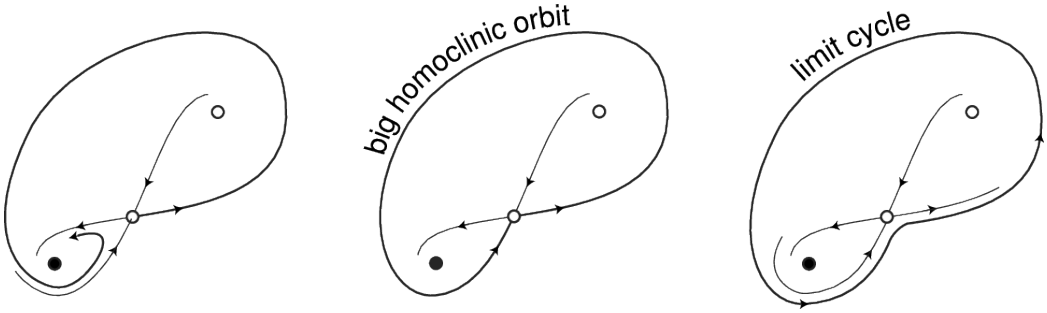

Figure 2.8: Depiction of a “big” saddle-homoclinic-orbit bifurcation. The unfolding of a “big” saddle-homoclinic-orbit bifurcation. Thanks to the discontinuous reset in our model, we are able to observe a non-smooth analog to this bifurcation. Figure from [8] printed with permission from E.M. Izhikevich.

CHAPTER 3. THE MODEL AND ITS SMOOTH BIFURCATIONS

From here, we analyze the following continuous-time model; we have implemented the parameter reduction as described in Chapter 1, in which $I, E \in \mathbb{R}$:

$$\begin{cases} \dot{v} &= f(v) + u(v - E) + I \\ \dot{u} &= v - u \end{cases} \tag{3.1}$$

We also assume that $f \in C^2(\mathbb{R})$, is convex, and has a unique minimum. Later, we will strengthen our assumptions to presume that $f \in C^3(\mathbb{R})$. We assume convexity because the hybrid spiking model [7] was first proposed so as to retain local topological equivalence with the Hodgkin-Huxley model near that model's resting state equilibrium. The dynamics in this neighborhood can be locally well-described with convex functions. Izhikevich used quadratic functions [8], Brette and Gerstner used exponential functions [1], and Touboul used quartics [12].

3.1. Characterization of Equilibria

Ultimately we wish to construct a bifurcation portrait; to this end, we first investigate local bifurcations of equilibria. We establish the existence of at most two equilibria and then determine the subsets of parameter space under which those equilibria lose hyperbolicity. One equilibrium is a saddle and is hence always hyperbolic, but the other equilibrium loses hyperbolicity in a few ways.

First we develop some tools. Certainly $(v, u) = (v_0, u_0)$ is an equilibrium point if and only if $u_0 = v_0$ and $f(v_0) + v_0(v_0 - E) + I = 0$. Also, notice the Jacobian at the equilibrium can be written

$$L = \begin{pmatrix} f'(v_0) + v_0 & v_0 - E \\ 1 & -1 \end{pmatrix} \tag{3.2}$$

Define, for each $v \in \mathbb{R}$, $E^*(v) := f'(v) + 2v$. Since f is convex, $E^* \in C^1(\mathbb{R})$ is strictly increasing with $\frac{d}{dv}E^* \geqslant 2$. Define $V^*(E)$ as the inverse of E^*; since $E^* \in C^1(\mathbb{R})$, we have that $V^* \in C^1(\mathbb{R})$, and since $\frac{d}{dv}E^* \geqslant 2$, we have that $\frac{d}{dE}V^* \in \left(0, \frac{1}{2}\right]$.

We shall first be interested in determining when equilibria exist, i.e. choices for E and I when solutions to $f(v)+v(v-E)+I=0$ exist. Define $I^*(E) := -\min_{v\in\mathbb{R}}(f(v)+v(v-E))$; we prove in the next Lemma that this is precisely the curve dividing the parameter space into regions with and without equilibria. Notice that v minimizes $f(v)+v(v-E)$ if and only if $f'(v)+2v-E=0$, i.e. $E = E^*(v)$ or $v = V^*(E)$. That is, $I^*(E) = V^*(E)E - f(V^*(E)) - V^{*2}(E)$.

$I^*(E)$ admits some helpful properties: $I^*(E) \in C^2(\mathbb{R})$, $I^*(E)$ is strictly convex with a unique minimum, and $\frac{d}{dE}I^* = V^*(E)$. Indeed, the chain rule yields the following:

$$\frac{d}{dE}I^*(E) = \frac{d}{dE}\left(-f(V^*(E)) - V^*(E)(V^*(E)-E)\right) \tag{3.3}$$

$$= -\left(f'(V^*(E)) + 2V^*(E) - E\right)\frac{dV^*}{dE}(E) + V^*(E) \tag{3.4}$$

$$= -(E^*(V^*(E)) - E)\frac{dV^*}{dE}(E) + V^*(E) \tag{3.5}$$

$$= V^*(E) \tag{3.6}$$

Of course, since $\frac{d}{dE}V^*(E) > 0$, I^* must be strictly convex. Consequently, the curve $I = I^*(E)$ has a minimum occurring at the value E given by $\frac{dI}{dE} = V^*(E) = 0$, i.e. $E = E^*(0) = f'(0)$. Hence, the minimum occurs at $(E, I) = (f'(0), -f(0))$.

Next define $T(v) := f'(v) + v - 1$, the trace τ of the Jacobian, and $\Delta(v) := E - E^*(v)$, i.e. the determinant of the Jacobian. Since $E^* \in C^1(\mathbb{R})$ is strictly increasing with $\frac{d}{dv}E^* \geqslant 2$, we have that $\Delta \in C^1(\mathbb{R})$, is strictly decreasing, and $\frac{d}{dv}\Delta \leqslant -2$. Further, note that v is the minimum of $f(v)+v(v-E)$ if and only if $\Delta = 0$, $E = E^*(v)$, or $v = V^*(E)$. That is, $I^*(E)$ is our candidate fold bifurcation curve, since, for any choice $(E, I) = (E, I^*(E))$ with equilibrium $(v, u) = (v_0, v_0)$ will have $\Delta = 0$.

Also observe that the convexity of f implies that $T \in C^1(\mathbb{R})$ and $\frac{d}{dv}T \geqslant 1$. Define V^{**} as the unique root of T; note that V^{**} depends solely on the properties of f. Since all eigenvalues satisfy $\lambda^2 + \tau\lambda + \Delta = 0$, notice that the second eigenvalue of V^* is precisely $T(V^*)$. These definitions and observations lead naturally to the following lemma:

Lemma 3.1. For $E \in \mathbb{R}$, given model 3.1, we have a strictly convex critical input current $I^*(E) = V^*(E)E - V^{*2}(E) - f(V^*(E)) \in C^2(\mathbb{R})$ with a unique minimum such that:

(i) if $I > I^*(E)$, then the model has no equilibria,

(ii) if $I = I^*(E)$, then the model has a unique non-hyperbolic equilibrium, $(v,u) = (V^*(E), V^*(E))$ with a zero eigenvalue and whose other eigenvalue is precisely $T(V^*(E))$, and

(iii) if $I < I^*(E)$, then the model has precisely two equilibria, $(v,u) = (v_-(E,I), v_-(E,I))$ and $(v,u) = (v_+(E,I), v_+(E,I))$ satisfying the following:

  (a) the ordering $v_-(E,I) < V^*(E) < v_+(E,I)$;

  (b) for a fixed E, $v_+(E,I)$ is a strictly decreasing function of I mapping $(-\infty, I^*(E))$ onto $(V^*(E), \infty)$ and is always a saddle; and

  (c) for a fixed E, $v_-(E,I)$ is a strictly increasing function of I mapping $(-\infty, I^*(E))$ onto $(-\infty, V^*(E))$.

Proof. Of course, we have already proven that $I^*(E) = V^*(E)E - f(V^*(E)) - V^{*2}(E)$.

If $I > I^*(E)$, then $f(v) + v(v - E) + I > 0$ for any $v \in \mathbb{R}$, and hence no (v,u) can possibly be an equilibrium. On the other hand, if $I = I^*(E)$, then $f(V^*(E)) + V^*(E)(V^*(E) - E) + I^*(E) = 0$ by definition. Hence, $(v,u) = (V^*(E), V^*(E))$ is an equilibrium. Since $I = I^*(E)$, the determinant of the Jacobian at V^* is zero. The

eigenvalues then satisfy $\lambda^2 - \tau\lambda = 0$, and hence we have a zero eigenvalue, violating hyperbolicity.

Since $f \in C^2(\mathbb{R})$ is convex with a unique minimum, so is $f(x) + x(x-E)$ for any $E \in \mathbb{R}$; such functions intersect level subsets once, twice, or never. By the definition of I^*, if $I < I^*(E)$, there exist two solutions which, necessarily, satisfy $v_-(E,I) < V^*(E) < v_+(E,I)$.

Finally note that an equilibrium $v_0 \in \{v_-, v_+\}$ must satisfy the relation $f(v_0) + v_0(v_0 - E) + I = 0$ and is hence continuous. We obtain

$$0 = \frac{\partial}{\partial I}\left(f(v_0) + v_0(v_0 - E) + I\right) \tag{3.7}$$

$$= (f'(v_0) + 2v_0 - E)\frac{\partial v_0}{\partial I} + 1 \tag{3.8}$$

$$\frac{\partial v_0}{\partial I} = \frac{1}{E - E^*(v_0)} \tag{3.9}$$

which is continuous since $v_0 \neq V^*(E)$ and therefore $\det L \neq 0$. Moreover, $\frac{\partial v_-}{\partial I} > 0$ and $\frac{\partial v_+}{\partial I} < 0$ since the determinant is strictly decreasing. It remains to be shown the mappings are onto their ranges and that v_+ is a saddle.

Let $E \in \mathbb{R}$ and $c \geqslant V^*(E)$. Then define $I_{c,E} := -f(c) - c(c-E)$ and note that $(E, I_{c,E})$ will have $v_+(E, I_{c,E}) = c$. Hence, the mapping v_+ is onto. The same argument, *mutatis mutandis*, demonstrates that the map v_- is also onto.

Finally, we have that $\Delta(v)$ is strictly decreasing, vanishes at $V^*(E)$, $v_+ > V^*$, and any equilibrium with a negative determinant is a saddle. □

Observe that, if $v_0 \neq V^*(E)$ then $\frac{\partial v_0}{\partial E} = \frac{-v_0}{E - E^*(v_0)}$, which is continuous, although we won't use this fact. Also note that we are generally unconcerned with the eigenvalues of a saddle. Finally, although we can easily classify v_+ as a saddle, it is a more delicate task to classify the behavior of v_-.

3.2. Fold Bifurcation

We have equilibrium conditions, bifurcation conditions, a transversality condition, and a genericity condition to check on our candidate bifurcation curve $I^*(E)$, following Section 2.3.2. Here the determinant vanishes, so $-f'(V^*(E)) - 2V^*(E) + E = 0$, but we require that the trace does not, so we require that $f'(V^*(E)) + V^*(E) - 1 \neq 0$. Equivalently, we require $E \neq 1 + V^*(E)$. Thus, our bifurcation conditions are, for any $E \in \mathbb{R}$,

(i) (Equilibrium) $u = v = V^*(E)$

(ii) (Bifurcation 1) $I = I^*(E)$

(iii) (Bifurcation 2) $E \neq 1 + V^*(E)$

The transversality condition requires that the first derivative of the vector field (in the critical eigenspace) with respect to I is nonzero. Similarly, the genericity condition demands that the second derivative with respect to the state-space variables of the vector field not vanish.

We have the Jacobian

$$L = \begin{pmatrix} f(V^*) + V^* & V^* - E \\ 1 & -1 \end{pmatrix}$$

and if we have a vanishing eigenvalue with eigenvector $q = \binom{q_1}{q_2}$, then clearly $q_1 = q_2$. Hence, we can choose the eigenvector associated with the vanishing eigenvalue $q = \binom{1}{1}$ with adjoint (normalized as in Section 2.3.2) $p = \binom{p_1}{p_2} = (V^* - E + 1)^{-1} \binom{1}{V^* - E}$. This normalization allows us some intuition about why we require $V^* \neq E - 1$. Note that if

the determinant vanishes, then the Jacobian is

$$L = \begin{pmatrix} E - V^* & V^* - E \\ 1 & -1 \end{pmatrix}$$

and the other eigenvalue is precisely the trace, $E - V^* - 1$. Hence, transversality requires that

$$\left\langle p, \frac{\partial}{\partial I}\begin{pmatrix} \dot{v} \\ \dot{u} \end{pmatrix} \right\rangle \Bigg|_{(v^*, v^*, I^*)} \neq 0$$

$$\left\langle p, \begin{pmatrix} 1 \\ 0 \end{pmatrix} \right\rangle \neq 0$$

$$\frac{1}{V^* - E + 1} \neq 0$$

Therefore, transversality is always assured. Our genericity condition requires that

$$0 \neq \left\langle p, \left(q_1^2 \frac{\partial^2}{\partial v^2} + 2q_1 q_2 \frac{\partial^2}{\partial u \partial v} + q_2^2 \frac{\partial^2}{\partial u^2} \right) \begin{pmatrix} \dot{v} \\ \dot{u} \end{pmatrix} \right\rangle \Bigg|_{(V^*, V^*, I^*)}$$

$$0 \neq \left\langle p, \begin{pmatrix} q_1^2 f''(V^*) + 2q_1 q_2 \\ 0 \end{pmatrix} \right\rangle$$

$$0 \neq \frac{f''(V^*) + 2}{V^* - E + 1}$$

Certainly convexity provides $f'' + 2 \geqslant 2$. Hence, genericity is always satisfied, proving the following Lemma. We will see that if this exceptional condition is violated, then a Bogdanov-Takens bifurcation occurs.

Lemma 3.2. Let $E \in \mathbb{R}$. If $E \neq 1 + V^*$ then a generic and transversal fold bifurcation occurs at the point $(v, u, E, I) = (V^*(E), V^*(E), E, I^*(E))$.

3.3. Andronov-Hopf Bifurcation

We now turn our attention to the Andronov-Hopf bifurcation, when the trace vanishes transversally with a positive determinant, following Section 2.3.3. In this section, we assume $f \in C^3(\mathbb{R})$ so as to allow discussion of the first Lyapunov coefficient. The Andronov-Hopf bifurcation is associated with a spiral equilibrium changing stability; since v_+ is always a saddle, this must occur at $v_-(E,I)$ or $V^*(E)$. However, $V^*(E)$ is associated with the fold bifurcation (or a bifurcation with higher codimension when genericity fails). Hence, we only concern ourselves with $v_-(E,I)$. This can only exist for $I < I^*(E)$. Of course, $\Delta > 0$ in this region following from the monotonicity of $E - E^*(v)$. We, again, begin with a few introductory tools.

To analyze an equilibrium $(v,u) = (v_-, v_-)$, observe that the real part of the eigenvalue has the same sign as the trace, i.e. $\mathrm{Sgn}\left(T(v_-(E,I))\right) = \mathrm{Sgn}\left(\mathrm{Re}(\lambda)\right)$. Hence, since $T(v)$ is monotonically increasing and $T(V^{**}) = 0$, an equilibrium is stable if and only if $v_-(E,I) < V^{**}$. Recall that $v_-(E,I)$ maps onto $(-\infty, V^*(E))$ and $V^*(E)$ ranges from $-\infty$ to ∞, following Lemma 3.1. Hence, for any $c \in \mathbb{R}$, the contour $v_-(E,I) = c$ exists and is well-defined in parameter space. Indeed, since v_- is an equilibrium, this curve satisfies the relation $I = cE - c^2 - f(c)$. We make some remarks about these lines through parameter space.

For any $c \in \mathbb{R}$, the curve $I^*(E)$ intersects the line $I = cE - c^2 - f(c)$ at the point

$$(E,I) = (E^*(c), I^*(E^*(c))) = \left(f'(c) + 2c, c^2 - f(c) + cf'(c)\right)$$

Furthermore, $\frac{d}{dE} I^*(E) \mid_{E=E^*(c)} = V^*(E^*(c)) = c$, and the curve $I^*(E)$ is strictly convex (see Lemma 3.1). Hence, each of these lines is beneath the curve $I^*(E)$ and is tangent to that curve at the point $E = E^*(c)$. Since $I^*(E)$ is strictly convex following Lemma 3.1, the tangent line lies entirely below $I^*(E)$ except at the point of tangency. The point

of tangency therefore divides the tangent line into two open half-lines with $E < E^*(c)$ and $E > E^*(c)$, each of which lies entirely below $I^*(E)$.

Lemma 3.3. Let $c \in \mathbb{R}$ and define L_c as the right half-line $I = cE - c^2 - f(c)$ defined on $E > E^*(c)$. The family $\mathscr{L} := \{L_c \mid c \in \mathbb{R}\}$ partitions the region $D := \{(E, I) \mid I < I^*(E)\}$.

Proof. We observed that each half-line is strictly beneath $I^*(E)$. Hence, $\cup_{c\in\mathbb{R}} L_c \subseteq D$. Let $(E, I) \in D$. By Lemma 3.1, there exists two equilibria, $v_-(E, I)$ and $v_+(E, I)$. Certainly $(E, I) \in L_{v_-(E,I)}$. Indeed, $I = v_-(E, I)E - v_-(E, I)^2 - f(v_-(E, I))$ and $v_-(E, I) < V^*(E)$, we have that $E^*(v_-(E, I)) < E$. So (E, I) is on at least one half-line in $\mathscr{L}$, in particular, $L_{v_-(E,I)}$. Thus, $D = \cup_{c\in\mathbb{R}} L_c$. It remains to be shown that no point (E, I) can be on two distinct half-lines $L_{v_-(E,I)}$ and L_c.

To this end, let $(E, I) \in D$ on $L_{v_-(E,I)}$ as above, and also assume that $(E, I) \in L_c$ for some $c \neq v_-(E, I)$. Then $I = cE - c^2 - f(c)$ and $E > E^*(c)$. However, $f(x) + x(x - E) + I = 0$ has only two possible solutions, $v_-(E, I)$ and $v_+(E, I)$. Since $c \neq v_-(E, I)$, we conclude $c = v_+(E, I)$. However $v_+(E, I) > v^*(E)$, so $E^*(v_+(E, I)) > E$, which is a contradiction. Hence, each point $(E, I) \in D$ is on one and only one half-line $L_{v_-(E,I)} \in \mathscr{L}$, and $\mathscr{L}$ must therefore partition D. □

We pause to remark about the transition between a node and a spiral. First, this transition does not correspond to a loss in hyperbolicity, i.e. this transition is not a bifurcation transition. However, we can divide the region $I < I^*(E)$ into two subregions, one in which v_- is a node, and one in which v_- is a spiral in the following manner. Recall that any eigenvalue λ satisfies $\lambda^2 - \tau\lambda + \Delta = 0$ where τ is the trace and Δ is the determinant, and for any $c \in \mathbb{R}$, the equilibrium $v_- = c$ exists and corresponds to L_c, the open half-line $I = cE - c^2 - f(c)$ in parameter space. Recall that the family $\{L_c \mid c \in \mathbb{R}\}$ partitions $I < I^*(E)$ by Lemma 3.3. Further, for this equilibrium, $\tau = f'(c) + c - 1$ and $\Delta = E - E^*(c)$. Hence, the eigenvalues for $v_- = c$ are real (i.e. v_- is a node) if $\frac{1}{4}(f'(c) + c - 1) - (E - E^*(c)) > 0$, and the eigenvalues are complex

conjugate (i.e. v_- is a spiral) if $\frac{1}{4}(f'(c)+c-1)-(E-E^*(c))<0$. For each $c\in\mathbb{R}$, define the discriminant $E_c := \frac{1}{4}(f'(c)+c-1)^2+E^*(c)$. It is clear, then, that on each half-line L_c, the equilibrium is a node for any $E^*(c)<E<E_c$ and a spiral for any $E>E_c$. Hence, we can parametrically represent a point (E,I) on the spiral-node transition curve as $E=E_c$, $I=cE-c^2-f(c)$ for any $c\in\mathbb{R}$.

Now, reconsider the family of half-lines. A remarkable fact about these half-lines is that the trace $T(v)$ is a constant on each half-line. Indeed, let (E,I) be an ordered pair on some half-line L_c; then $v_-=c$ and $T(v_-)=f'(c)+c-1$. That is, by defining $\mathscr{S} := \{L_c \mid T(c)<0\}$ and $\mathscr{U} := \{L_c \mid T(c)>0\}$, we see that v_- is stable in the region $R_S=\cup_{L_c\in\mathscr{S}}L_c$ and unstable in the region $R_U=\cup_{L_c\in\mathscr{U}}L_c$. Further, there always exists a unique equilibrium V^{**} with $T(V^{**})=0$ and we always have a candidate Andronov-Hopf half-line $I=V^{**}E-V^{**2}-f(V^{**})$. Observe that the half-line $L_{V^{**}}$ includes the point $(E^*(V^{**}),I^*(E^*(V^{**})))$ which is not an allowable point on the candidate Hopf curve since the determinant is precisely zero on $I^*(E)$. Observe that the node-spiral transition curve, which divides the region $I<I^*(E)$ into the node- and spiral subregions, will also divide R_S and R_U, so the region $I<I^*(E)$ can (in general) be divided into four subregions, corresponding to stable nodes, stable spirals, unstable nodes, and unstable spirals.

The second bifurcation condition demands that we have a positive determinant, so we require that $E>E^*(V^{**})$. Of course, $E^*(V^{**})=f'(V^{**})+2V^{**}$, and since V^{**} is the point at which the trace vanishes, we have that $f'(V^{**})=1-V^{**}$. Thus, $E^*(V^{**})=1+V^{**}$.

Thus, the candidate Hopf curve always exists as precisely the half-line $I^{**}(E)=V^{**}E-V^{**2}-f(V^{**})$ where $E>1+V^{**}$. That is, the Andronov-Hopf conditions are:

(i) (Equilibrium) $v=u=V^{**}$

(ii) (Bifurcation 1) $I^{**}=V^{**}E-V^{**2}-f(V^{**})$

(iii) (Bifurcation 2) $1 + V^{**} < E$

In Section 2.3.3, we lay out the general method of checking transversality and genericity of the Andronov-Hopf bifurcation; herein, we recapitulate that method for our specific model. To check transversality, we require that the trace must vanish transversally as we vary our bifurcation parameter, I. That is, we require that

$$0 \neq \frac{\partial}{\partial I}\left(f'(v) + v - 1\right)|_{v=V^{**}}$$
$$0 \neq \left(f''(V^{**}) + 1\right)\left(\frac{\partial v}{\partial I}\right)|_{v=V^{**}}$$

Convexity yields that $f'' + 1 \geqslant 1$ and we have seen that $\frac{\partial v_{\pm}}{\partial I}$ is continuous and nonzero in this region since $\Delta > 0$. Thus, transversality is always satisfied, and we only need to demonstrate genericity.

The Andronov-Hopf bifurcation occurs generically if and only if the first Lyapunov coefficient is nonvanishing. This coefficient has the same sign as $\mathrm{Re}\left(ig_{20}g_{11} + \omega g_{21}\right) \neq 0$, where $\omega = \sqrt{\Delta}$ and each g_{kl} is defined as in Equation 2.3 in Section 2.3.3. We begin by changing parameters $I = J + I^{**}$ so that the Andronov-Hopf bifurcation occurs with parameter $J = 0$. This yields the system of differential equations

$$\begin{cases} \dot{v} &= f(v) + uv - Eu + I^{**} + J \\ \dot{u} &= v - u \end{cases} \tag{3.10}$$

Since $I^{**} = -f(V^{**}) - V^{**2} + EV^{**}$, we can rewrite this as

$$\begin{cases} \dot{v} &= \left[f(v) - f(V^{**})\right] + \left[uv - V^{**2}\right] + E\left[V^{**} - u\right] + J \\ \dot{u} &= v - u \end{cases} \tag{3.11}$$

in which each term in square brackets vanishes at the point $(v,u) = (V^{**},V^{**})$, and for which the equilibrium is at this point for $J = 0$. We make a parameter-dependent change of coordinates

$$\begin{cases} v &= x + X(J) \\ u &= y + Y(J) \end{cases} \tag{3.12}$$

such that $X(0) = Y(0) = V^{**}$ yielding the system of differential equations

$$\begin{cases} \dot{x} &= \left[f\left(x + X(J)\right) - f(V^{**})\right] + \left[(x + X(J))(y + Y(J)) - V^{**2}\right] \\ &\quad + E\left[V^{**} - y - Y(J)\right] + J \\ \dot{y} &= x - y + X(J) - Y(J) \end{cases} \tag{3.13}$$

The Implicit Function Theorem allows us to make a choice for $X(J)$ and $Y(J)$ such that the resulting system has an equilibrium at the origin for all sufficiently small $|J|$. However, if this has equilibrium at the origin for all sufficiently small $|J|$, then inspection of $\dot{y}$ reveals that $Y(J) = X(J)$ for all sufficiently small $|J|$. Define $\hat{f}(x)$ to be the (parameter-dependent) function $\hat{f}(x) := f(x + X(J)) - f'(X(J))x - f(X(J))$. It is easily seen that $\hat{f} \in C^3(\mathbb{R})$, is convex, has a unique minimum, has no linear terms, and passes through the origin when $J = 0$. Furthermore, $\hat{f}''(x) = f''(x + X(J))$. We obtain the system

$$\begin{cases} \dot{x} &= \hat{f}(x) + \left[(x + X(J))(y + X(J)) - V^{**2}\right] + E\left[V^{**} - y - X(J)\right] \\ &\quad + f'(X(J))x + f(X(J)) - f(V^{**}) + J \\ \dot{y} &= x - y \end{cases} \tag{3.14}$$

Note that the Jacobian, L, evaluated at the equilibrium (i.e. the origin), is now

$$L = \begin{pmatrix} f'(X(J)) + X(J) & X(J) - E \\ 1 & -1 \end{pmatrix}.$$

Let $q = \binom{q_1}{q_2}$ be an eigenvector so that $Lq = \lambda q$ and $p = \binom{p_1}{p_2}$ be its adjoint, where λ, q, and p each depend on J. Then we have

$$q = \begin{pmatrix} 1+\lambda \\ 1 \end{pmatrix} \qquad\qquad p = \frac{1}{2\mathrm{Im}(\lambda)} \begin{pmatrix} i \\ -i(1+\lambda) \end{pmatrix}$$

Let $F\binom{x}{y}$ be the nonlinear components of the vector field governing the model 3.14:

$$F\begin{pmatrix} x \\ y \end{pmatrix} = \begin{pmatrix} F_1(x,y) \\ F_2(x,y) \end{pmatrix} = \begin{pmatrix} xy + \hat{f}(x) \\ 0 \end{pmatrix}$$

We desire to compute $F(zq + \bar{z}\bar{q})$ and find its inner product with p before taking higher order derivatives. Since the second dimension of F is zero, we only need the first component of p and F. We have:

$$\langle p, F(zq + \bar{z}\bar{q})\rangle = \frac{-i}{2\mathrm{Im}(\lambda)} \left[(1+\lambda)z^2 + 2z\bar{z} + (1+\bar{\lambda})\bar{z}^2 + \hat{f}\left((1+\lambda)z + (1+\bar{\lambda})\bar{z} \right) \right] \tag{3.15}$$

Recall from Equation 2.3 that $g_{kl} = \left\langle p, \frac{\partial^{k+l}}{\partial z^k \partial \bar{z}^l} F\left(zq + \bar{z}\bar{q}\right) \right\rangle \Big|_{\alpha=\alpha^*, z=0}$. Further recall that when $J = 0$, we have that $X(0) = V^{**}$ and $\lambda = i\omega$. We are primarily interested in the second and third derivatives so as to obtain $\mathrm{Re}(ig_{20}g_{11} + \omega g_{21})$. To this end, we

compute using Equation 3.15 and recalling that $\hat{f}''(0) = f''(V^{**})$:

$$\frac{\partial^2}{\partial z^2} F_1\left(zq + \bar{z}\bar{q}\right) = 2(1+\lambda) + (1+\lambda)^2 \hat{f}''\left((1+\lambda)z + (1+\bar{\lambda})\bar{z}\right) \tag{3.16}$$

$$g_{20} = \frac{-i}{2\omega}\left[2(1+i\omega) + (1+i\omega)^2 f''(V^{**})\right] \tag{3.17}$$

Similarly, we obtain:

$$\frac{\partial^2}{\partial z \partial \bar{z}} F_1\left(zq + \bar{z}\bar{q}\right) = 2 + (1+\lambda)(1+\bar{\lambda})\hat{f}''\left((1+\lambda)z + (1+\bar{\lambda})\bar{z}\right)$$

$$g_{11} = \frac{-i}{2\omega}\left(2 + (1+\omega^2) f''(V^{**})\right) \tag{3.18}$$

$$\frac{\partial^3}{\partial z^2 \partial \bar{z}} F_1\left(zq + \bar{z}\bar{q}\right) = (1+\lambda)^2(1+\bar{\lambda})\hat{f}'''\left((1+\lambda)z + (1+\bar{\lambda})\bar{z}\right)$$

$$g_{21} = \frac{-i}{2\omega}(1+\omega^2)(1+i\omega) f'''(V^{**}) \tag{3.19}$$

We obtain:

$$\mathrm{Re}\left(i g_{20} g_{11} + \omega g_{21}\right) = \frac{1}{2\omega}(1 + f''(V^{**}))(2 + (1+\omega^2) f''(V^{**})) + \frac{\omega}{2}(1+\omega^2) f'''(V^{**}) \tag{3.20}$$

Hence, the first Lyapunov coefficient vanishes if and only if

$$0 = \left(f''(V^{**}) + 1\right)\left((1+\omega^2) f''(V^{**}) + 2\right) + (1+\omega^2)\omega^2 f'''(V^{**}) \tag{3.21}$$

More to the point, $\omega^2 = E - V^{**} - 1$ here; this boils down to the following:

$$0 = \left(f''(V^{**}) + 1\right)\left(2 + (E - V^{**}) f''(V^{**})\right) + (E - V^{**})(E - V^{**} - 1) f'''(V^{**}) \tag{3.22}$$

Hence, if $f'''(V^{**}) < 0$ then an Andronov-Hopf bifurcation may lose genericity as we vary E. Further, this formula is quadratic in E, and hence will vanish at most twice as we vary E. Consequently, the Andronov-Hopf bifurcation can lose genericity for at most two points on the half-line $L_{V^{**}}$ corresponding to the roots of 3.22 in E. All that remains is to study the criticality which depends on the sign of $\mathrm{Re}(ig_{20}g_{11} + \omega g_{21})$, given by Equation 3.20, as described in Section 2.3.3; this informs our analysis of the limit cycles associated with the Andronov-Hopf bifurcation. Of course, it follows immediately from the definition of the criticality of the Andronov-Hopf bifurcation that if this sign is positive, then we have a subcritical bifurcation, and vice versa.

Hence, we proved the following lemma:

Lemma 3.4. Let $V^{**} \in \mathbb{R}$ be the unique solution to $f'(x) + x - 1 = 0$. If $E > 1 + V^{**}$ and $I^{**}(E) = V^{**}E - V^{**2} - f(V^{**})$ and

$$0 \neq \left(f''(V^{**}) + 1\right)\left(2 + (E - V^{**})f''(V^{**})\right) + (E - V^{**})(-1 + E - V^{**})f'''(V^{**}) \quad (3.23)$$

then an Andronov-Hopf bifurcation occurs at the point $(v, u, E, I) = (V^{**}, V^{**}, E, I^{**}(E))$ which is subcritical (respectively supercritical) if the sign of the right side of Equation 3.23 is positive (negative).

3.4. Bogdanov-Takens Bifurcation

The Bogdanov-Takens bifurcation occurs when the fold and Andronov-Hopf bifurcations occur together; we obtained in Sections 3.2 and 3.3 the fold and Hopf conditions, and in Section 2.3.5, we lay out the general method of checking genericity and transversality of a Bogdanov-Takens bifurcation. Herein, we check the specific model of choice. Define $\hat{E} := E^*(V^{**})$ and $\hat{I} := I^*(E^*(V^{**}))$. Any candidate Bogdanov-Takens point has vanishing trace and determinant; to this end, let (v, u) be a candidate Bogdanov-Takens point. Since the trace vanishes, $v = V^{**}$ is the equilibrium and since

the determinant vanishes, $I = I^*(E)$. That is, $E = \hat{E}$ and $I = \hat{I}$, yielding $(v,u) = (V^{**},V^{**})$ with parameters $(E,I) = (\hat{E},\hat{I})$.

If $f'(V^{**}) = 1 - V^{**}$ then $\hat{E} = f'(V^{**}) + 2V^{**} = 1 + V^{**}$. This also yields that $\hat{I} = V^{**}\hat{E} - V^{**2} - f(V^{**}) = V^{**} - f(V^{**})$. Hence, our bifurcation and equilibrium conditions of interest are the following:

(i) (Equilibrium) $(v,u) = (V^{**},V^{**})$

(ii) (Bifurcation 1) $E = \hat{E} = 1 + V^{**}$

(iii) (Bifurcation 2) $I = \hat{I} = V^{**} - f(V^{**})$

and, since both the trace and the determinant vanish at this equilibrium, the Jacobian evaluated at this equilibrium becomes

$$L = \begin{pmatrix} 1 & -1 \\ 1 & -1 \end{pmatrix}.$$

We begin checking genericity and transversality by making the following change of coordinates and parameters:

$$\begin{aligned} v &= x_1 + V^{**}, & I &= a_1 + \hat{I} \\ u &= x_2 + V^{**}, & E &= a_2 + \hat{E} \end{aligned}$$

This yields the system of differential equations:

$$\begin{cases} \dot{x_1} = & f(x_1 + V^{**}) - f(V^{**}) + x_1x_2 + V^{**}x_1 - (1 + a_2)x_2 + (a_1 - a_2V^{**}) \\ \dot{x_2} = & x_1 - x_2 \end{cases} \tag{3.24}$$

Here we write $f(x_1+V^{**}) = f(V^{**}) + f'(V^{**})x_1 + \frac{f''(V^{**})}{2}x_1^2 + g(x_1)$ for some $g(x_1) = O(x_1^3)$. Since $f'(V^{**}) + V^{**} = 1$, we obtain

$$\begin{cases} \dot{x_1} &= g\left(x_1\right) + \frac{f''(V^{**})}{2}x_1^2 + x_1x_2 + x_1 - (1+a_2)x_2 + (a_1 - a_2V^{**}) \\ \dot{x_2} &= x_1 - x_2 \end{cases} \tag{3.25}$$

We now have the Jacobian

$$\begin{aligned} L &= \begin{pmatrix} g'(x_1) + f''(V^{**})x_1 + x_2 + 1 & x_1 - 1 - a_2 \\ 1 & -1 \end{pmatrix} \\ &= \begin{pmatrix} f'(x_1+V^{**}) - f'(V^{**}) + x_2 + 1 & x_1 - 1 - a_2 \\ 1 & -1 \end{pmatrix} \end{aligned} \tag{3.26}$$

To demonstrate transversality and genericity, we must check a few things. First, we must verify the Jacobian is nonzero at the bifurcation point. Certainly this is the case since the bottom row is nonzero. Next, we must check regularity of the following map evaluated at the bifurcation point:

$$\begin{pmatrix} x_1 \\ x_2 \\ a_1 \\ a_2 \end{pmatrix} \mapsto \begin{pmatrix} \dot{x_1} \\ \dot{x_2} \\ \tau(L) \\ \Delta(L) \end{pmatrix}$$

$$\begin{pmatrix} x_1 \\ x_2 \\ a_1 \\ a_2 \end{pmatrix} \mapsto \begin{pmatrix} g\left(x_1\right) + \frac{f''(V^{**})}{2} x_1^2 + x_1 x_2 + x_1 - (1+a_2)x_2 + (a_1 - a_2 V^{**}) \\ x_1 - x_2 \\ f'(x_1 + V^{**}) - f'(V^{**}) + x_2 \\ f'(V^{**}) - f'(x_1 + V^{**}) - x_1 - x_2 + a_2 \end{pmatrix}$$

This is equivalent to verifying that the following determinant is nonzero:

$$0 \neq \begin{vmatrix} g'(x_1) + f''(V^{**})x_1 + x_2 + 1 & 1 & f''(x_1 + V^{**}) & -(f''(x_1 + V^{**}) + 1) \\ x_1 - (1 + a_2) & -1 & 1 & -1 \\ 1 & 0 & 0 & 0 \\ -(x_2 + V^{**}) & 0 & 0 & 1 \end{vmatrix}$$

$$0 \neq \begin{vmatrix} 1 & f''(x_1 + V^{**}) & -(f''(x_1 + V^{**}) + 1) \\ -1 & 1 & -1 \\ 0 & 0 & 1 \end{vmatrix}$$

$$0 \neq \begin{vmatrix} 1 & f''(x_1 + V^{**}) \\ -1 & 1 \end{vmatrix} \neq 1 + f''(x_1 + V^{**})$$

Of course, this follows from convexity, i.e. $f'' + 1 \geqslant 1$. All that remains is to check genericity.

We have the eigenvector $q_0 = \binom{1}{1}$, its generalized eigenvector $q_1 = \binom{2}{1}$ and their adjoints $p_0 = \binom{-1}{2}$ and $p_1 = \binom{1}{-1}$, normalized as in Section 2.3.5. We project system 3.25 onto the coordinate system afforded by q_0 and q_1 by writing $\binom{x_1}{x_2} = y_1 q_0 + y_2 q_1$.

This yields the system:

$$\begin{cases} \dot{y}_1 &= y_2 + (a_2 V^{**} - a_1) + a_2 y_1 + a_2 y_2 - \frac{1}{2}(2 + f''(V^{**}))y_1^2 - (3 + 2f''(V^{**}))y_1 y_2 \\ &\quad -\frac{1}{2}(4 + 4f''(V^{**}))y_2^2 + g(y_1 + 2y_2) \\ \dot{y}_2 &= a_1 - a_2 V^{**} - a_2 y_1 - a_2 y_2 + \frac{1}{2}(2 + f''(V^{**}))y_1^2 + (3 + 2f''(V^{**}))y_1 y_2 \\ &\quad +\frac{1}{2}(4 + 4f''(V^{**}))y_2^2 + g(y_1 + 2y_2) \end{cases} \tag{3.27}$$

Using the notation from Section 2.3.5, we have $\dot{y}_1 = y_2 + \sum_{j,k\geqslant 0} a_{jk} y_1^j y_2^k$ and $\dot{y}_2 = \sum_{j,k\geqslant 0} b_{jk} y_1^j y_2^k$, yielding the genericity conditions:

$$a_{20} + b_{11} = (-2 - f''(V^{**})) + (3 + 2f''(V^{**})) = f''(V^{**}) + 1 \neq 0$$
$$b_{02} = 4(1 + f''(V^{**}) \neq 0$$

which are both guaranteed by the convexity of f. We do not compute the saddle-homoclinic orbit curve with this level of generality. Hence, we have proven the following lemma:

Lemma 3.5. Let V^{**} be the unique root of $f'(x)+x-1=0$, let $I = \hat{I} = V^{**} - f(V^{**})$, let $E = \hat{E} = 1 + V^{**}$. Then a generic and transversal Bogdanov-Takens bifurcation occurs at the point $(v, u, E, I) = (V^{**}, V^{**}, \hat{E}, \hat{I})$.

Observe that the genericity and transversality of this bifurcation implies that the first Lyapunov coefficient at the Bogdanov-Takens point is always nonzero; hence, the Bogdanov-Takens bifurcation and the Bautin bifurcation never occur together.

3.5. Bifurcation Portrait

We have established the following theorem:

Theorem 3.6. Consider model 3.1 with $f \in C^3(\mathbb{R})$, convex, with a unique minimum. Define $I^*(E) := V^*(E)E - (V^*(E))^2 - f(V^*(E))$. Let V^{**} be the root of $f'(v) + v = 1$ and define $\hat{E} := V^{**} + 1$, $\hat{I} := I^*(V^{**})$. Then:

(1) $I = I^*(E) \in C^2(\mathbb{R})$ is strictly convex, has a unique minimum $(E, I) = (f'(0), -f(0))$ and is such that:

   (i) if $I > I^*(E)$, then the model has no equilibria,

   (ii) if $I = I^*(E)$, then the model has a unique non-hyperbolic equilibrium, $v = V^*(E)$ with a zero eigenvalue whose other eigenvalue is precisely $T(V^*(E))$, and

   (iii) if $I < I^*(E)$, then the model has precisely two equilibria, $v_-(E, I) < V^*(E) < v_+(E, I)$ satisfying the following.

      (a) for a fixed E, $v_-(E, I)$ is strictly increasing function of I from $(-\infty, I^*(E))$ onto $(-\infty, V^*(E))$;

      (b) for a fixed E, $v_+(E, I)$ is strictly decreasing function of I from $(-\infty, I^*(E))$ onto $(V^*(E), \infty)$; and

      (c) the equilibrium $(v, u) = (v_+(E, I), v_+(E, I))$ is always a saddle.

(2) For each $c \in \mathbb{R}$, the half-line L_c defined by $I = cE - c^2 - f(c)$ for $E > E^*(c)$ is tangent to $I = I^*(E)$ when $E = E^*(c)$. Furthermore, the family of half-lines $\{L_c \mid c \in \mathbb{R}\}$ partitions the region $\{(E, I) \mid E \in \mathbb{R}, I < I^*(E)\}$.

(3) If $E \neq \hat{E}$ and $I = I^*(E)$ then a generic and transversal fold bifurcation occurs at the point $(v, u, E, I) = (V^*(E), V^*(E), E, I^*(E))$.

(4) If $E > \hat{E}$ and $I = I^{**}(E) := V^{**}(E - \hat{E}) + \hat{I}$ (the half-line $L_{V^{**}}$), and if

$$0 \neq \left(f''(V^{**}) + 1\right)\left((E - V^{**})f''(V^{**}) + 2\right) + (E - V^{**})(-1 + E - V^{**})f'''(V^{**}) \tag{3.28}$$

then an Andronov-Hopf bifurcation occurs at $(v, u, E, I) = (V^{**}, V^{**}, E, I^{**}(E))$. This bifurcation is subcritical when Equation 3.28 is positive and supercritical when Equation 3.28 is negative. This condition can fail at most twice for $E > \hat{E}$, yielding up to two candidate Bautin bifurcation points.

(5) Finally, if $E = \hat{E}$ and $I = \hat{I}$, then a generic and transversal Bogdanov-Takens bifrucation occurs at the point $(v, u, E, I) = (V^{**}, V^{**}, \hat{E}, \hat{I})$.

Theorem 3.6 also yields the existence of at least one global bifurcation curve, in particular a saddle-homoclinic-orbit bifurcation curve implied by the Bogdanov-Takens. In order to verify the genericity of the candidate Bautin bifurcation points, stronger assumptions are required of f as well as a much more extensive analysis. In particular, we would require that $f \in C^5(\mathbb{R})$ in order to compute the second Lyapunov coefficient. This is beyond the scope of this analysis. However, if this Bautin bifurcation were to be verified to be generic, this would also imply the existence of a fold-limit-cycle bifurcation.

We have enough information to develop a generic local bifurcation portrait. Indeed, the saddle-node curve has the parameterization

$$E = E^*(c), \quad I = I^*(E) = cE - c^2 - f(c), \quad c \in \mathbb{R}$$

which is always convex with unique minimum at $(f'(0), -f(0))$. The Andronov-Hopf curve is the half-line

$$\left\{(E,I) \mid I = V^{**}E - V^{**2} - f(V^{**}), E \geqslant E^*(V^{**})\right\}$$

and we can parametrically represent the spiral-node transition curve

$$E = \frac{1}{4}(f'(c) + c - 1)^2 + E^*(c), \quad I = cE(c) - c^2 - f(c), \quad c \in \mathbb{R}.$$

This, together with up to two Bautin bifurcation points on the Andronov-Hopf line, yields a bifurcation diagram as in Figure 3.1.

Note, however, that the spiral-node transition curve is not properly a bifurcation curve as it is not related to loss of hyperbolicity, i.e. eigenvalues crossing the imaginary axis. Further note that while we have some information about the shape of the fold- and Andronov-Hopf bifurcation curves, the shape of the spiral-node transition curve is sensitive to our choice of f and our analysis has not revealed much information about its properties.

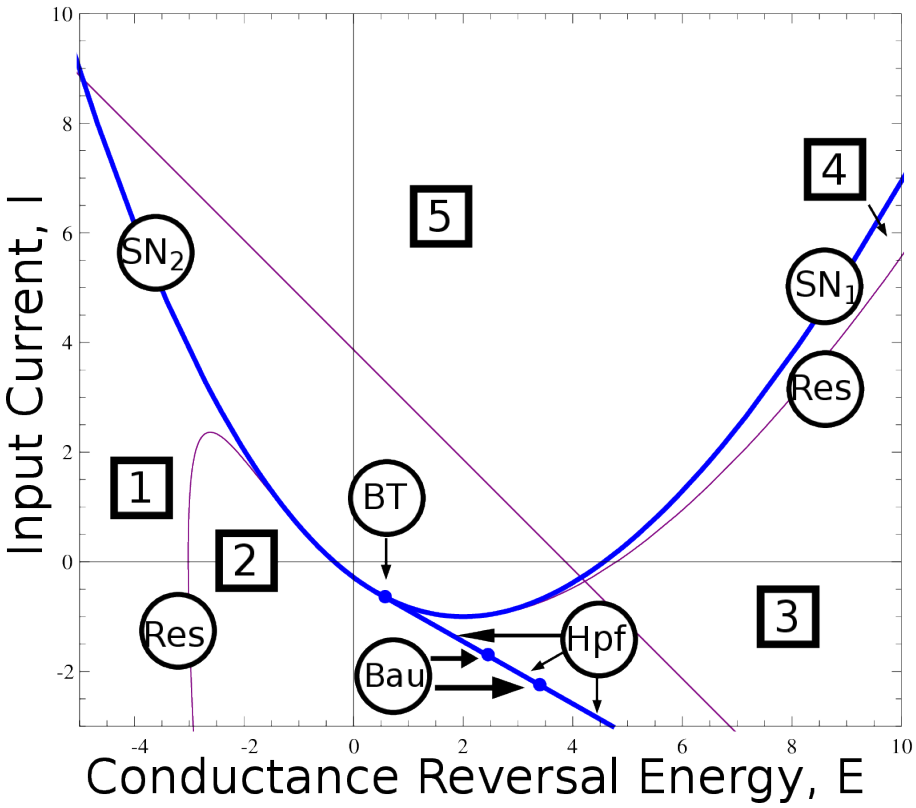

Figure 3.1: Partition of parameter space via bifurcation curves in general model 3.1. In region 1, the equilibrium $(v,u) = (v_{\_}(E,I), v_{\_}(E,I))$ is a stable node. In region 2, $v_{\_}$ is a stable spiral. In region 3, $v_{\_}$ is an unstable spiral. In region 4, $v_{\_}$ is an unstable node, and in region 5, no equilibria exist whatsoever. Point BT denotes the Bogdanov-Takens point, whose existence is always assured, and points Bau denote the candidate Bautin bifurcation points, of which there are at most two. The curves SN_1 and SN_2 denote the fold bifurcation curves, and the candidate Bautin points lie on the Andronov-Hopf bifurcation line, Hpf, which is tangent with the the fold bifurcation curve at the Bogdanov-Takens point. The spiral-node transition curve is denoted Res.

3.6. Examples

With this theorem in hand, we provide a few examples. Both have very similar spike activation functions $f(x)$, and yet have very different Hopf behaviors.

Example 3.7. Let $f(x) = x^4 + x$. Then $E^*(v) = 4v^3 + 2v + 1$ and if we define $\gamma(E)$ such that

$$\gamma^3(E) := -9 + 9E + \sqrt{105 - 162E + 81E^2}$$

then $V^*(E) = \gamma(E)/\sqrt[3]{72} - (\sqrt[3]{3}\gamma(E))^{-1}$ and $I^*(E) = V^*(E)E - V^{*2}(E) - V^{*4}(E) - V^*(E)$.

We apply the results of Theorem 3.6. The critical input current curve $I = I^*(E)$ has a unique minimum at the point $(E, I) = (f'(0), -f(0)) = (1, 0)$. Notice that V^{**}, the unique root of $f'(v) + v - 1 = 0$, is precisely $V^{**} = 0$. For $E \neq V^{**} + 1 = 1$, a generic fold bifurcation occurs at the point $(v, u, E, I) = (V^*(E), V^*(E), E, I^*(E))$. Furthermore, $E^*(V^{**} = 1$ and $I^*(E^*(V^{**})) = 0$. The Andronov-Hopf bifurcation curve is the open half-line $I = 0$ for $E > 1$.

If $E > 1$, then an Andronov-Hopf bifurcation occurs at the point $(v, u, E, I) = (0, 0, E, 0)$. Furthermore, $f''(V^{**}) = f'''(V^{**}) = 0$, and so the sign of 3.23 is always positive, and the Andronov-Hopf bifurcation is always subcritical.

Finally, a generic and transversal Bogdanov-Takens bifurcation occurs at the point $(v, u, E, I) = (0, 0, 1, 0)$. This implies the existence of a smooth saddle-homoclinic-orbit bifurcation curve. Following the procedure in Chapter 2 and the equation in Lemma 2.8, we use *Mathematica* to obtain the local approximation to the saddle-homoclinic orbit curve

$$I(E) = \frac{1}{888}\left(84 - 109E + 5\sqrt{-144 + 120E + 49E^2}\right) + o((E-1)^2) \tag{3.29}$$

We investigate the accuracy of this curve by numerically finding SHO bifurcation points; we plot the approximate curve as a dashed blue line and the numerically-

verified "true" SHO bifurcation points as solid purple points on Figure 3.2. Near the Bogdanov-Takens point, the approximation curve is above the true SHO bifurcation curve. At some point near $E \approx 2.8$, the approximate SHO curve and the true SHO bifurcation curve intersect. It numerically appears that for any greater value of E, the approximate SHO bifurcation curve is below the true SHO bifurcation curve in (E, I)-plane. For values $E > 5.5$, the approximation gets progressively worse. We summarize our numerical results in Table 3.2.

Figure 3.2 shows the partition of parameter space into regions of distinct dynamical behavior, as well as particular (E, I) ordered pairs of interest and the spiral-node transition curve. Figure 3.3 shows representative phase portraits, associated nullclines, separatrices, and equilibria from the three regions of richest behaviors. Parameter values used to generate those figures can be found in Table 3.1, and are plotted on Figure 3.2.

Point	Parameter E	Parameter I
A	6.5	-0.192
B	6.75	-0.096
C	6.5	0.384

Table 3.1: Parameter values used to generate Figure 3.3 in Example 3.7.

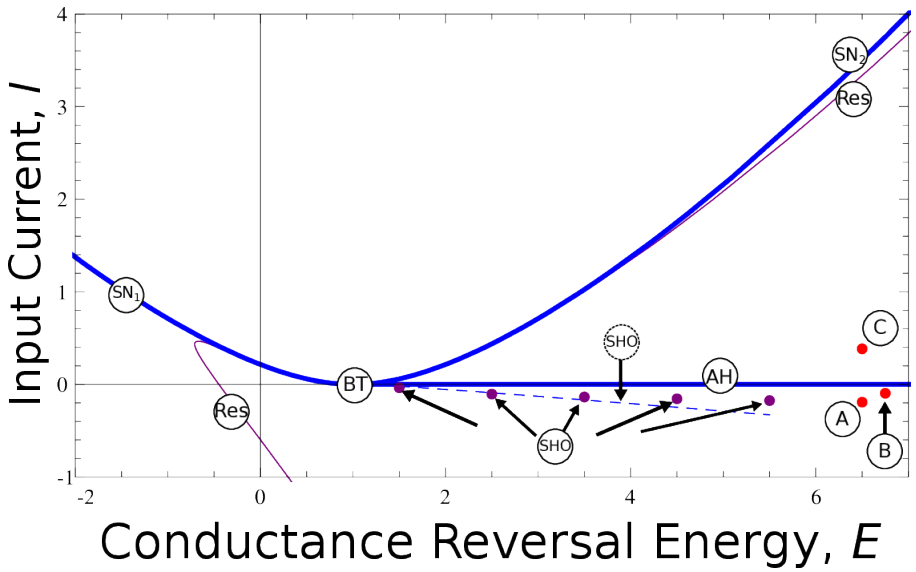

Figure 3.2: Complete partition of parameter space for Example 3.7. We include some other interesting features. Local bifurcation curves (resp. points) appear as blue solid lines (resp. points): fold bifurcation curve SN_1 and SN_2, Andronov-Hopf bifurcation half-line AH, and Bogdanov-takens point BT. The saddle-node non-bifurcation transition curve appears as the purple solid line Res. The points representing parameter values used to generate phase portraits in Figure 3.3 appear as red points A, B, and C, whose numerical values are reported in Table 3.1. The approximate SHO bifurcation curve from Equation 3.29 appears as a blue dashed line and numerical, hand-tuned, "true" SHO bifurcation points appear as purple points. The numerical values of the "true" SHO points are reported in Table 3.2 and compared with the approximate SHO bifurcation curve.

Example 3.8. Although this Example has a similar spike activation function $f(x)$ to the previous Example, the behavior is much more rich. The Example does exhibit a candidate Bautin bifurcation, as well as a saddle-homoclinic-orbit bifurcation above the Andronov-Hopf line. Let $f(x) = x^4 + 6x$. Then $E^*(v) = 4v^3 + 2v + 6$, and if we

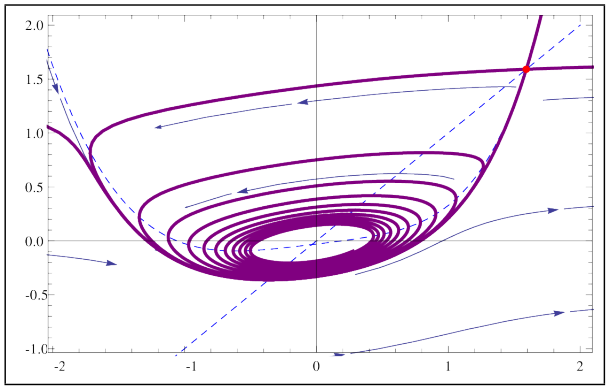

(a) Stable spiral equilibrium

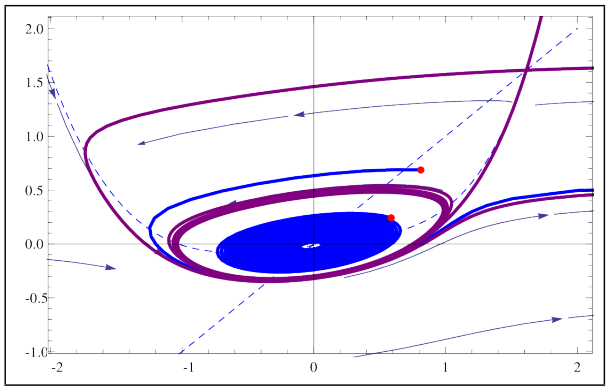

(b) Unstable limit cycle around stable spiral equilibrium

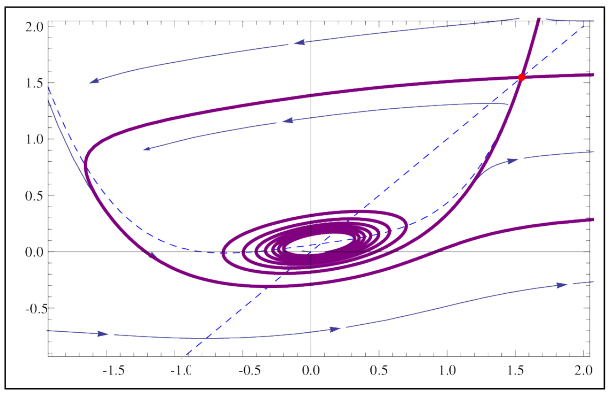

(c) Unstable spiral equilibrium

Figure 3.3: Depiction of Example 3.7 undergoing bifurcation cascade. Example 3.7 displaying the expected behavior from a Bogdanov-Takens bifurcation. In figure (a), the model is near a saddle-homoclinic-orbit bifurcation for $(E, I) = (6.5, -0.192)$ (point A on Figure 3.2), and displays a single stable spiral equilibrium. In figure (b), the model exhibits an unstable limit cycle surrounding a stable equilibrium near a subcritical Andronov-Hopf bifurcation for $(E, I) = (6.75, -0.096)$ (point B on Figure 3.2). In figure (c), the model has undergone a subcritical Andronov-Hopf bifurcation and only an unstable equilibrium remains for $(E, I) = (6.5, 0.384)$ (point C on Figure 3.2).

E	I_{APX}	I_{SHO}	Error $= I_{\text{SHO}} - I_{\text{APX}}$
1.5	-0.021	-0.038	-0.017
2.5	-0.091	-0.105	-0.014
3.5	-0.168	-0.136	0.032
4.5	-0.248	-0.156	0.092
5.5	-0.329	-0.175	0.154
6.5	-0.410	-0.192	0.218

Table 3.2: Accuracy of SHO approximation in Example 3.7. For each value of E, we list the expected values I_{APX} for input current I that triggers an SHO bifurcation according to our approximation in Equation 3.29. We compared this approximation to measured "true" SHO currents I_{SHO} discovered by hand-tuning, and we list the error $I_{\text{SHO}} - I_{APX}$ for each value of E.

define $\gamma(E)$ such that

$$\gamma^3(E) = -54 + 9E + \sqrt{2940 - 972E + 81E^2}$$

then $V^*(E) = \gamma(E)/\sqrt[3]{72} - (\sqrt[3]{3}\gamma(E))^{-1}$ and $I^*(E) = V^*(E)E - V^{*2}(E) - V^{*4}(E) - 6V^*(E)$.

We apply the results of Theorem 3.6. The critical input current curve $I = I^*(E)$ has a unique minimum at the point $(E, I) = (f'(0), -f(0)) = (6, 0)$. Notice that V^{**}, the unique root of $f'(v)+v-1 = 0$, is precisely $V^{**} = -1$. For $E \neq V^{**}+1 = 0$, a generic fold bifurcation occurs at the point $(v, u, E, I) = (V^*(E), V^*(E), E, I^*(E))$. Furthermore, $E^*(V^{**} = 0$ and $I^*(E^*(V^{**})) = 4$. The Andronov-Hopf bifurcation curve is the open half-line $I = 4 - E$ for $E > 0$.

It remains to check the first Lyapunov coefficient. Indeed, $f''(V^{**}) = 12$ and $f'''(V^{**}) = -24$, yielding

$$\text{sgn}(\ell_1) = \text{sgn}\left(\left(f''(-1)+1\right)\left((E+1)f''(-1)+2\right) + E(E+1)f'''(-1)\right) \tag{3.30}$$

$$= \text{sgn}\left(13(12E+14) - 24(E+1)E\right) \tag{3.31}$$

One root occurs for $E < 0$, but the other root occurs when $E = \frac{33+\sqrt{2181}}{12} \approx 6.64$; the Andronov-Hopf bifurcation loses genericity at this point. Further, for any $E < \frac{33+\sqrt{2181}}{12}$, the Andronov-Hopf bifurcation is subcritical, corresponding to the appearance of an unstable limit cycle, and for any $E > \frac{33+\sqrt{2181}}{12}$, the Andronov-Hopf bifurcation is supercritical, corresponding to the appearance of a stable limit cycle. This implies the existence of a candidate Bautin bifurcation point at

$$(v,u,E,I) = (-1,-1,\frac{33+\sqrt{2181}}{12}, 4-\frac{33+\sqrt{2181}}{12})$$

Thus, if $E \in (0, \frac{33+\sqrt{2181}}{12})$ then a subcritical Andronov-Hopf bifurcation occurs at the point $(v,u,E,I) = (0,0,E,4-E)$, and if $E > \frac{33+\sqrt{2181}}{12}$, then a supercritical Andronov-Hopf bifurcation occurs at the point $(v,u,E,I) = (0,0,E,4-E)$.

A generic and transversal Bogdanov-Takens bifurcation occurs at $(v,u,E,I) = (0,0,0,4)$. This implies the existence of a smooth saddle homoclinic orbit bifurcation manifold. Following the procedure in Chapter 2 and the equation in Lemma 2.8, we use *Mathematica* to obtain the local approximation to the saddle-homoclinic orbit curve

$$I(E) = \frac{1}{2080272}\left(8291513 - 2145493E + 65\sqrt{91}\sqrt{2275 + E(10034+91E)}\right) + o(E^2) \tag{3.32}$$

We investigate the accuracy of this curve by numerically finding SHO bifurcation points, illustrated in Table 3.3. The true SHO bifurcation curve, approximate SHO bifurcation curve (Equation 3.32, and the Andronov-Hopf line are each tangent to $I^*(E)$ at the Bogdanov-Takens bifurcation point. Near the Bogdanov-Takens point $E = 0$, the approximation curve is an over-estimate of true SHO bifurcation curve, and both the approximation curve and the true SHO curve lie below the Andronov-Hopf half-line. At some point near $E \approx 3.70$, the approximate SHO curve and the true SHO bifurcation

curve intersect and the approximation becomes an under-estimate. For values of $3.70 < E < 6.50$, the true SHO curve is above the approximation, but below the Andronov-Hopf half-line. When $E \approx 6.50$, the true SHO curve intersects the Andronov-Hopf bifurcation half-line at a point near $E \approx 6.50$. Further, it seems that, for any value $E > 6.50$, the true SHO curve lies above the Andronov-Hopf bifurcation half-line in parameter space and the approximation lies below the Andronov-Hopf line. While the approximation curve 3.32 has an accuracy within 0.2 for values up to $E \leqslant 7$, the approximation curve does not lie in the correct region of parameter space for any value of $E > 6.50$ and therefore the approximation is not particularly accurate for $E > 6.50$.

We also numerically investigate the fold-limit-cycle (FLC) bifurcation curve. We found examples of FLC bifurcation points for values of E in the interval $[6.28, 6.57]$, illustrated in Table 3.4, and we compared these findings to the SHO and Andronov-Hopf half-lines. The FLC curve is very close to both the true SHO curve and the Andronov-Hopf half-line, so finding numerical examples of the FLC bifurcation for $6.57 < E < E_{\text{Bau}}$ leads to numerical difficulties. This is consistent with the expected behavior of a Bautin bifurcation, whose FLC bifurcation curve in the topological normal form is a half-parabola extending away from the Bautin point and tangent to the Andronov-Hopf half-line at the Bautin point. However, the curve does appear to naturally terminate near $E \approx 6.27$. On this entire interval, the FLC curve is below both the true SHO curve and the Andronov-Hopf half-line.

The presence of the candidate Bautin point near the SHO curve leads to interesting results. As Table 3.4 demonstrates, the SHO curve, the Andronov-Hopf half line, and the FLC curves are very close together in parameter space; they vary by a small error in I usually on the order of 10^{-2} or smaller. Hence, model behavior is rich with bifurcation cascades that occur in rapid succession near Andronov-Hopf bifurcations. Holding E constant near the Bautin value $E \approx 6.64$ and varying I as a bifurcation

E	I_{SHO}	I_{APX}	Error $= I_{\text{SHO}} - I_{\text{APX}}$
1.5	-0.021	-0.038	-0.017
0.500	3.493	3.4956	-0.0026
1.500	2.4620	2.4782	-0.0162
2.500	1.4380	1.4572	-0.0192
3.500	0.4300	0.4345	-0.0045
4.500	-0.5610	-0.5891	0.0281
5.500	-1.5380	-1.6135	0.0755
6.000	-2.0210	-2.1258	0.1049
6.100	-2.1170	-2.2284	0.1114
6.200	-2.2130	-2.3309	0.1179
6.300	-2.3080	-2.4334	0.1254
6.350	-2.3567	-2.4846	0.1279
6.400	-2.4044	-2.5359	0.1315
6.450	-2.4520	-2.5871	0.1351
6.480	-2.4805	-2.6179	0.1374
6.500	-2.4996	-2.6384	0.1388
6.550	-2.5471	-2.6896	0.1425
6.600	-2.5940	-2.7409	0.1469
6.610	-2.6040	-2.7512	0.1472
6.620	-2.6130	-2.7614	0.1484
6.630	-2.6230	-2.7717	0.1487
6.640	-2.6320	-2.7819	0.1499
6.642	-2.6338	-2.7837	0.1500
6.650	-2.6420	-2.7921	0.1502
6.660	-2.6510	-2.8024	0.1514
6.670	-2.6620	-2.8127	0.1507
6.680	-2.6700	-2.8229	0.1529
6.690	-2.6790	-2.8332	0.1547
6.700	-2.6890	-2.8434	0.1544
6.800	-2.7830	-2.9459	0.1629
6.900	-2.9724	-3.1510	0.1786
8.000	-3.9000	-4.1764	0.2765

Table 3.3: Accuracy of SHO approximation in Example 3.7. For each value of E, we list the expected values I_{APX} for input current I that triggers an SHO bifurcation according to our approximation in Equation 3.32. We compared this approximation to measured "true" SHO currents I_{SHO} discovered by hand-tuning, and we list the error $I_{\text{SHO}} - I_{APX}$ for each value of E.

E	I_{SHO}	I_{Hopf}	I_{FLC}	$I_{\text{Hopf}} - I_{\text{SHO}}$	$I_{\text{Hopf}} - I_{\text{FLC}}$
6.29	-2.2994	-2.29	-2.2995	0.0094	0.0095
6.30	-2.3080	-2.3	-2.3090	0.008	0.009
6.31	-2.3185	-2.31	-2.3186	0.00854	0.00855
6.32	-2.3280	-2.32	-2.3281	0.008	0.0081
6.33	-2.3376	-2.33	-2.3377	0.0076	0.0077
6.34	-2.3471	-2.34	-2.3473	0.0071	0.0073
6.35	-2.3567	-2.35	-2.3569	0.0067	0.0069
6.36	-2.3662	-2.36	-2.3665	0.0062	0.0065
6.37	-2.3758	-2.37	-2.3761	0.0058	0.0061
6.38	-2.3853	-2.38	-2.3856	0.0053	0.0056
6.39	-2.3948	-2.39	-2.3953	0.0048	0.0053
6.40	-2.4044	-2.4	-2.4050	0.0044	0.005
6.41	-2.4139	-2.41	-2.4145	0.0039	0.0045
6.42	-2.4234	-2.42	-2.4243	0.0034	0.0043
6.43	-2.4329	-2.43	-2.4336	0.0029	0.0036
6.44	-2.4425	-2.44	-2.4434	0.0025	0.0034
6.45	-2.4520	-2.45	-2.4531	0.002	0.0031
6.46	-2.4615	-2.46	-2.4629	0.0015	0.0029
6.47	-2.4710	-2.47	-2.4726	0.001	0.0026
6.48	-2.4805	-2.48	-2.4821	0.0005	0.0021
6.49	-2.4901	-2.49	-2.4917	0.0001	0.0017
6.50	-2.4996	-2.5	-2.5016	-0.0004	0.0016
6.51	-2.5091	-2.51	-2.5113	-0.0009	0.0013
6.52	-2.5186	-2.52	-2.5214	-0.0014	0.0014
6.53	-2.5281	-2.53	-2.5311	-0.0019	0.0011
6.54	-2.5376	-2.54	-2.5408	-0.0024	0.0008
6.55	-2.5471	-2.55	-2.5507	-0.0029	0.0007
6.56	-2.5566	-2.56	-2.5603	-0.0034	0.0003
6.57	-2.5661	-2.57	-2.5703	-0.0039	0.0003

Table 3.4: Comparison of various bifurcation curves for Example 3.8. For each value of E, we display the numerically measured "true" SHO current I_{SHO}, the analytically known Andronov-Hopf current $I_{\text{Hopf}} = 4 - E$, and the numerically measured FLC current I_{FLC}. We compare the numerically measured values I_{SHO} and I_{FLC} to I_{Hopf} to demonstrate when the SHO curve crosses the Andronov-Hopf half-line, and to demonstrate that the FLC curve always lies below the Andronov-Hopf half-line. Inspection reveals that the FLC curve also lies below the SHO curve.

parameter yields four qualitatively distinct cascades of bifurcations near the Andronov-Hopf half-line, and in particular near the Bautin point. We completely characterize the bifurcation behavior near the Bautin point by illustrating each of the four cases, providing strong numerical evidence that the candidate Buatin bifurcation is generic and transversal.

In Figure 3.4, we illustrate the first distinct cascade. For $0 < E < 6.27$, no FLC points were found and the SHO curve is below the Hopf half-line. For $I << 0$, we have a single stable equilibrium. As I increases, our system passes the true SHO curve, and this creates an unstable limit cycle surrounding the stable equilibrium. Biologically speaking, this allows for the coexistence of a spiking limit cycle with a stable resting state, and that resting state has a relatively small basin of attraction. As I increases further and passes the Hopf half-line, the unstable limit cycle shrinks and merges with the stable equilibrium, leaving an unstable equilibrium behind.

In Figure 3.5, we illustrate the second distinct cascade, the first in which a fold-limit-cycle bifurcation occurs, and so the first that has interesting Bautin behavior. For $6.27 < E < 6.50$, the FLC curve exists and the SHO curve is below the Hopf half-line. Hence, for $I << 0$, we have a single stable equilibrium. As I increases, an FLC bifurcation is triggered, creating a stable-unstable pair of limit cycles surrounding the stable equilibrium. Biologically, this describes a neuron capable of both endogenous subthreshold oscillation as well as a resting state equilibrium, which is a desirable property of neural models. As I increases further, the SHO bifurcation is triggered, destroying the stable limit cycle, leaving behind an unstable limit cycle surrounding the stable equilibrium. Biologically, this is equivalent to a resting state with a small basin of attraction as in the previous case. As I increases further, we cross the Hopf half-line; the unstable limit cycle shrinks, merging with the stable equilibrium, leaving an unstable equilibrium behind.

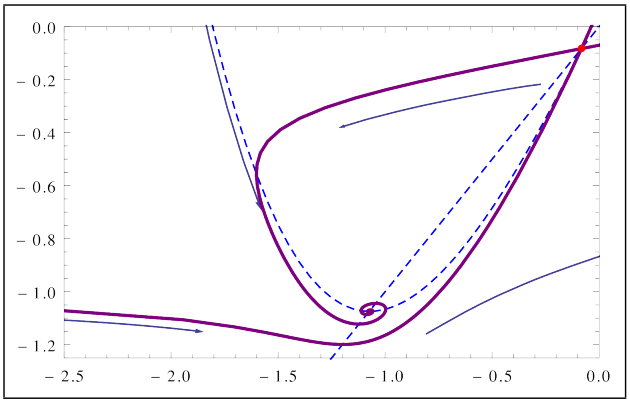

(a) Stable spiral equilibrium

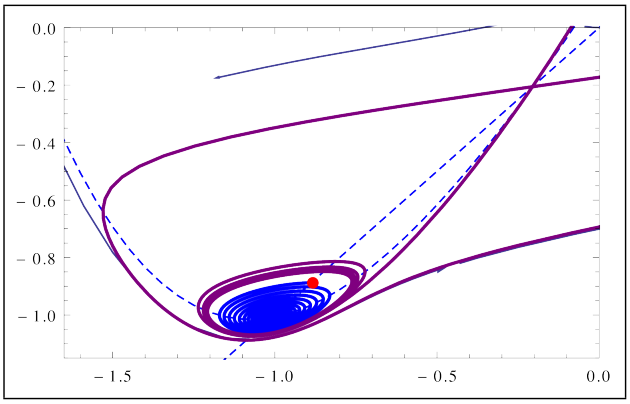

(b) Unstable limit cycle surrounding stable spiral equilibrium

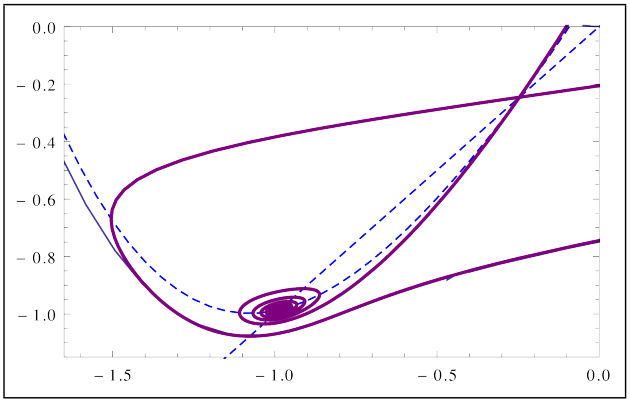

(c) Unstable spiral equilibrium

Figure 3.4: First bifurcation cascade from Example 3.7. For $0 < E < 6.27$, as I increases from $-\infty$ to ∞, two distinct bifurcations occur in rapid succession near the subcritical part of the Andronov-Hopf half-line. First, the SHO bifurcation curve is crossed, creating an unstable limit cycle, and then the subcritical Andronov-Hopf half-line is crossed, causing that limit cycle to merge with the resting state equilibrium. Phase portraits generated with (a) $(E,I) = (3.5, 0.2)$, (b), $(E,I) = (3.5, 0.47)$, and (c) $(E,I) = (3.5, 0.55)$.

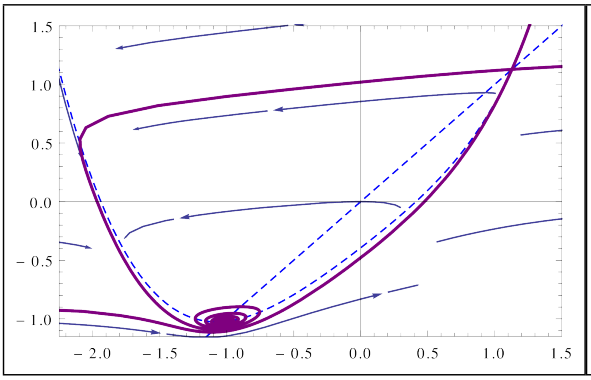

(a) Stable spiral equilibrium

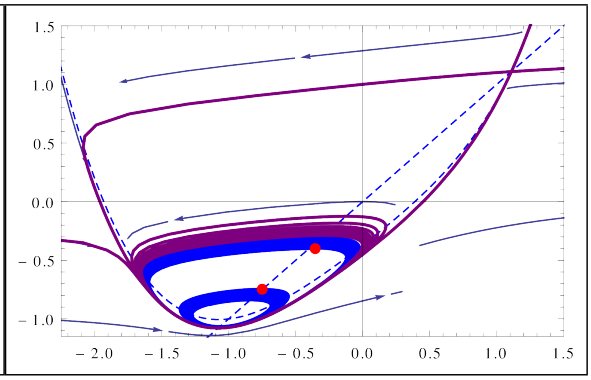

(b) Stable and unstable limit cycles surrounding stable spiral equilibrium

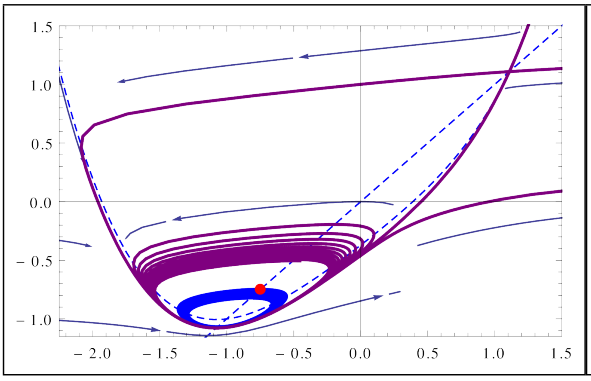

(c) Unstable limit cycle surrounding stable spiral equilibrium

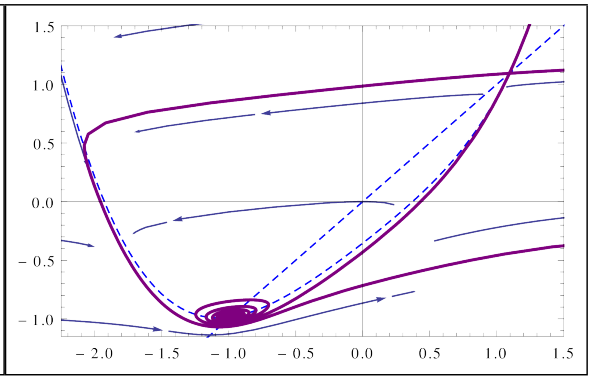

(d) Unstable spiral equilibrium

Figure 3.5: Second bifurcation cascade for Example 3.8. For $6.27 < E < 6.50$, as I increases from $-\infty$ to ∞, three distinct bifurcations occur in rapid succession near the subcritical part of the Andronov-Hopf half-line. First, the fold-limit-cycle bifurcation curve is crossed, creating a stable limit cycle surrounding an unstable limit cycle, both of which surround a stable spiral equilibrium. Next, the SHO curve is crossed as the outer stable limit cycle expands and is annihilated, leaving an unstable limit cycle surrounding a stable spiral equilibrium. Finally, a subcritical Andronov-Hopf bifurcation occurs as the unstable limit cycle shrinks and merges with the stable spiral equilibrium, leaving an unstable equilibrium behind. Phase portraits generated with (a) $(E,I) = (6.35,-2.5)$, (b) $(E,I) = (6.35,-2.3568)$, (c) $(E,I) = (6.35,-2.3566)$, and (d) $(E,I) = (6.35,-2.25)$.

In Figure 3.6, we illustrate the third cascade, in which the FLC bifurcation curve exists, but the SHO bifurcation curve is above the Hopf line. For $6.50 < E < 6.64$ and $I << 0$, we have a single stable equilibrium. As I increases, an FLC bifurcation is triggered, creating a stable-unstable pair of limit cycles surrounding the stable equilibrium. As before, this corresponds to the coexistence of endogenous subthreshold oscillations with a quiescent resting state in the neuron. As I increases further, the Hopf bifurcation is triggered, shrinking the unstable limit cycle and causing it to merge with the stable equilibrium, leaving behind a stable limit cycle surrounding an unstable equilibrium. Biologically, there now exists only subthreshold oscillations and no resting state. Finally, as I increases even further, the SHO bifurcation occurs, destroying the stable limit cycle leaving only an unstable spiral equilibrium.

In Figure 3.7, we illustrate the fourth distinct change of dynamical regime. For $E_{Bau} < E$, the Hopf line is below the SHO curve. Hence, as I increases from $-\infty$ to ∞, two distinct bifurcations occur in rapid succession. As we cross the supercritical Andronov-Hopf half-line, a stable limit cycle surrounds an unstable spiral equilibrium. As we cross the SHO curve, the stable limit cycle swells and annihilates with the stable and unstable manifolds of the saddle.

In Table 3.5, we summarize the (E, I) ordered pairs used to generate the phase portraits in Figures 3.4, 3.5, 3.6, and 3.7. Figure 3.8 shows the partition of parameter space by the Hopf half-line and the fold bifurcation curves for $f(x) = x^4 + 6x$, as well as the Bogdanov-Takens point and the candidate Bautin point.

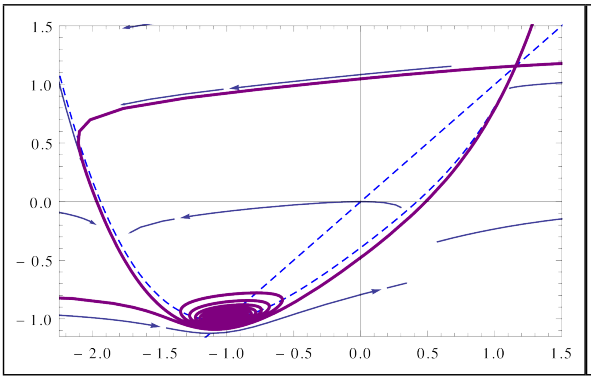

(a) Stable spiral equilibrium

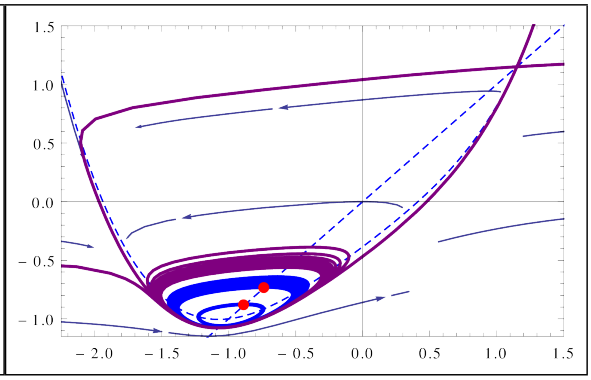

(b) Stable and unstable limit cycles surrounding stable spiral equilibrium

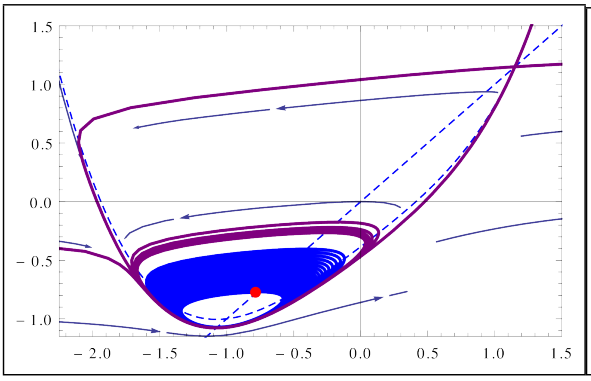

(c) Stable limit cycle surrounding unstable spiral equilibrium

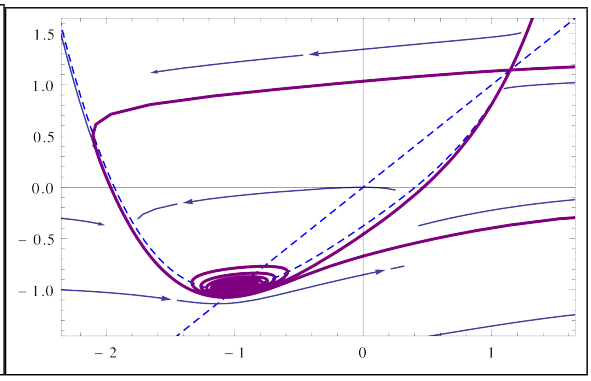

(d) Unstable spiral equilibrium

Figure 3.6: Third bifurcation cascade for Example 3.8. For $6.50 < E < E_{Bau} \approx 6.64$, as I increases from $-\infty$ to ∞, three distinct bifurcations occur in rapid succession. First, the fold-limit-cycle bifurcation curve is crossed, creating a stable limit cycle surrounding an unstable limit cycle, both of which surround a stable spiral equilibrium. Next, the subcritical Andronov-Hopf bifurcation curve is crossed as the interior unstable limit cycle shrinks and merges with the stable spiral equilibrium. This leaves a stable limit cycle surrounding an unstable equilibrium. Finally, the SHO curve is crossed as the stable limit cycle swells and annihilates as it collides with the stable and unstable manifolds of the saddle point, leaving only an unstable spiral equilibrium. Phase portraits generated with (a) $(E,I) = (6.5,-2.55)$, (b) $(E,I) = (6.5,-2.501)$, (c) $(E,I) = (6.5,-2.4999)$, and (d) $(E,I) = (6.5,-2.45)$.

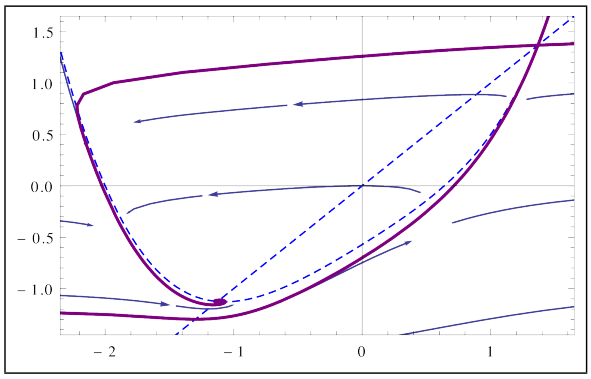

(a) Stable spiral equilibrium

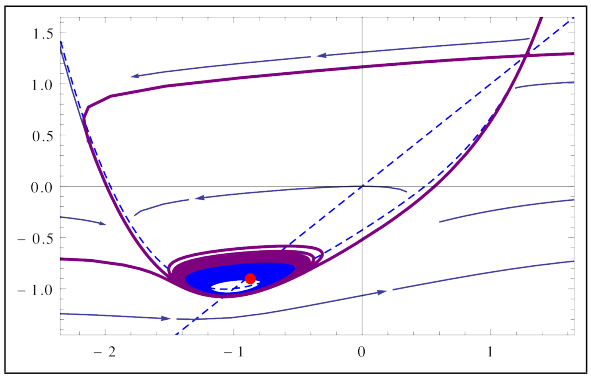

(b) Stable limit cycle surrounding unstable spiral equilibrium

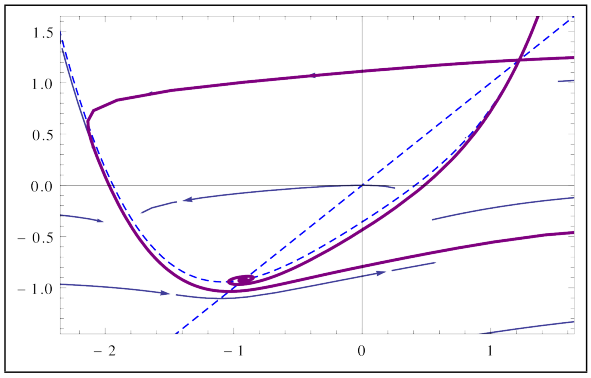

(c) Unstable spiral equilibrium

Figure 3.7: Fourth bifurcation cascade for Example 3.8. For $E_{Bau} < E$, as I increases from $-\infty$ to ∞, two distinct bifurcations occur in rapid succession. First, the supercritical Andronov-Hopf bifurcation curve is crossed, creating an stable limit cycle surrounding an unstable spiral equilibrium. Next, the stable limit cycle swells and annihilates with the stable and unstable manifolds of the saddle in an SHO bifurcation. Phase portraits generated with (a) $(E,I) = (7.0,-4.0)$, (b), $(E,I) = (7.0,-2.9862)$, and (c) $(E,I) = (7.0,-2.5)$.

E	I	$I_{\text{Hopf}} - I = \Delta I$	Behavior
3.5	0.2	0.3	Stable spiral equilibrium, Figure 3.4 (a)
3.5	0.47	0.03	Unstable limit cycle surrounding stable spiral equilibrium, Figure 3.4 (b)
3.5	0.55	-0.05	Unstable spiral equilibrium,, Figure 3.4 (c)
6.35	-2.5	0.15	Stable spiral equilibrium,, Figure 3.5 (a)
6.35	-2.3568	0.0068	Stable limit cycle around unstable limit cycle around stable spiral equilibrium,, Figure 3.5 (b)
6.35	-2.3566	0.0066	Unstable limit cycle around stable spiral equilibrium,, Figure 3.5 (c)
6.35	-2.25	-0.1	Unstable spiral equilibrium, Figure 3.5 (d)
6.5	-2.55	0.05	Stable spiral equilibrium, Figure 3.6 (a)
6.5	-2.501	0.001	Stable limit cycle around unstable limit cycle around stable spiral equilibrium, Figure 3.6 (b)
6.5	-2.4999	-0.001	Stable limit cycle around unstable equilibrium, Figure 3.6 (c)
6.5	-2.45	-0.05	Unstable spiral equilibrium, Figure 3.6 (d)
7.0	-4	1	Stable spiral equilibrium, Figure 3.7 (a)
7.0	-2.9862	-0.0138	Stable limit cycle around unstable spiral equilibrium, Figure 3.7 (b)
7.0	-2.5	-0.5	Unstable spiral equilibrium, Figure 3.7 (c)

Table 3.5: Parameter values used to generate phase portraits and their behaviors.

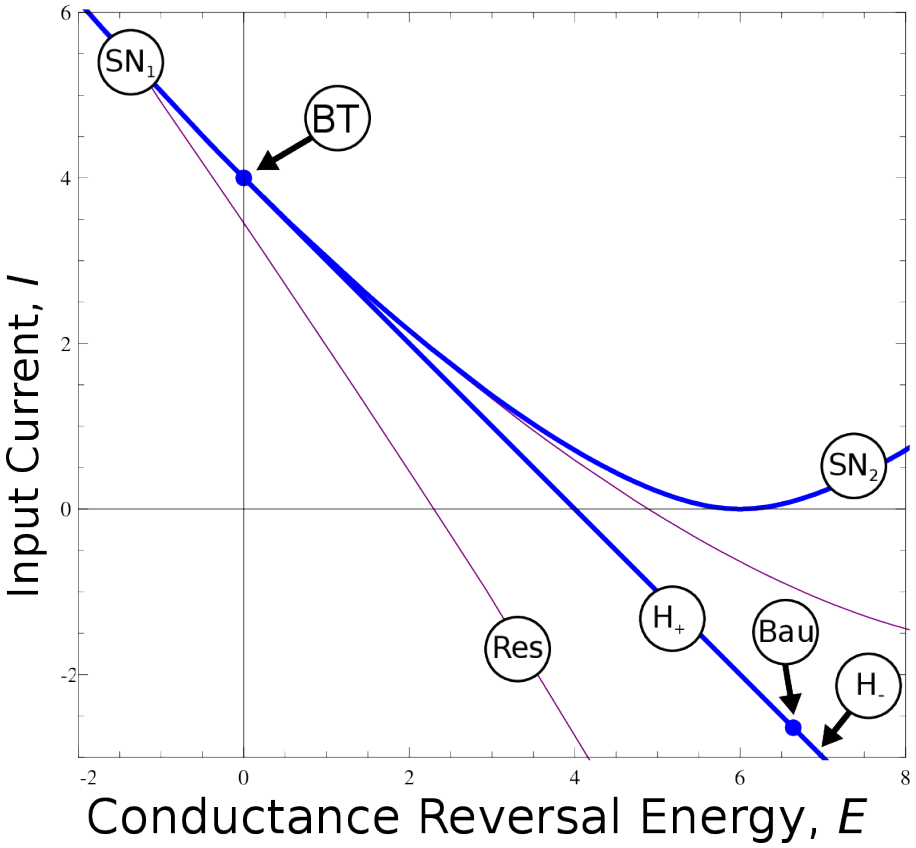

Figure 3.8: Partition of parameter space for Example 3.8. We include the fold bifurcation curves SN_1 and SN_2, the subcritical Andronov-Hopf bifurcation curves H_+, the supercritical Andronov-Hopf bifurcation curve H_-, the Bautin point Bau, the Bogdanov-Takens point BT, and the spiral-node transition curve Res.

CHAPTER 4. COMPARISON WITH BIOLOGICAL NEURONS

In this section, we investigate some behavior resulting from the nonsmooth component of our model. This behavior resembles global bifurcations and gives rise to some interesting behavior that can be interpreted biologically. We also investigate some of the extent to which our model can approximate biological neurons.

4.1. Nonsmooth Bifurcations

We have demonstrated the existence of the smooth fold bifurcation, the sub- and super-critical Andronov-Hopf bifurcations, corresponding to bistable integrators, and bistable and monostable resonators. However, the smooth behavior of our model does not end the story. The interactions between the stable and unstable manifolds extending from the saddle point and the instantaneous reset in our model can lead to interesting behavior. Indeed, post-spike trajectories can be "dumped" into the basin of attraction of the resting state or not, and this can lead to the creation or destruction of heteroclinic loops in our model. In this section, we observe some numerical simulations that lead to some bifurcation-like behavior. However, we must impose another assumption on f.

In particular, we assume there exists some $\epsilon, \alpha > 0$ such that $f(v) \geqslant \alpha v^{2+\epsilon}$ for sufficiently large v. This assumption follows from our desire for voltage to blow up in finite time in simulating the upstroke of a spike. This can be done so long as f scales faster than linearly. The stronger condition that f scales faster than quadratically ensures that the recovery variable u remains bounded. This is proven in Appendix A. Without this assumption, this model and others may exhibit biologically implausible sensitivity to the voltage cutoff value v_{max} and may be vulnerable to period-doubling bifurcations in this scenario [13].

Since our model is not smooth, we may observe a non-smooth equivalent of a fold-on-invariant-circle bifurcation, providing a model of monostable integrators. In-

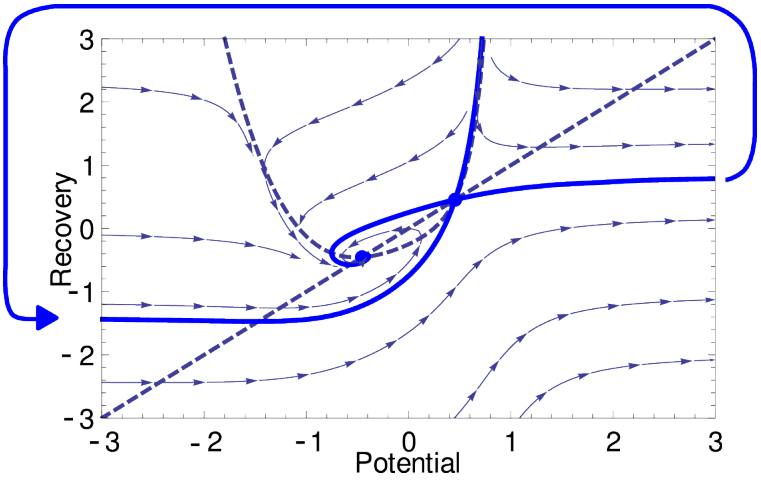

Figure 4.1: The model of choice before a fold-on-invariant-circle bifurcation. We depict the unfolding for $f(x) = x^4 + x$. The saddle point's unstable manifold leading to a spike resets into the stable equilibrium's basin of attraction, forming a heteroclinic invariant circle. Dashed lines represent the nullclines of the system; thick lines represent the stable and unstable manifolds of the saddle point. Image generated using *Mathematica* with parameters $(c, d, E, I) = (-3, -2.19, 1, -0.25)$

deed, so long as the saddle's unstable manifold leading to a spike resets into the basin of attraction of the stable equilibrium, the orbit of any trajectory starting on this unstable manifold will form an invariant heteroclinic loop. Any model in this configuration undergoes a fold-on-invariant-circle bifurcation rather than a fold bifurcation. See Figure (4.1).

We can also observe the nonsmooth equivalent of the "big" saddle-homoclinic-orbit bifurcation discussed in Section 2.4 and illustrated in Figure (4.2). In this instance, the bifurcation causes the model to transition from acting as a monostable resonator to a bistable resonator (or *vice versa*).

Since our model is capable of producing a saddle-homoclinic-orbit bifurcation (following from the existence of a Bogdanov-Takens bifurcation) and a fold-on-invariant-circle bifurcation, a natural question is whether these two bifurcations ever occur together. Such a bifurcation would produce a saddle-node homoclinic orbit bifurcation (as in 4.3). Thanks to our discontinuous reset, the boundary between the saddle-node-

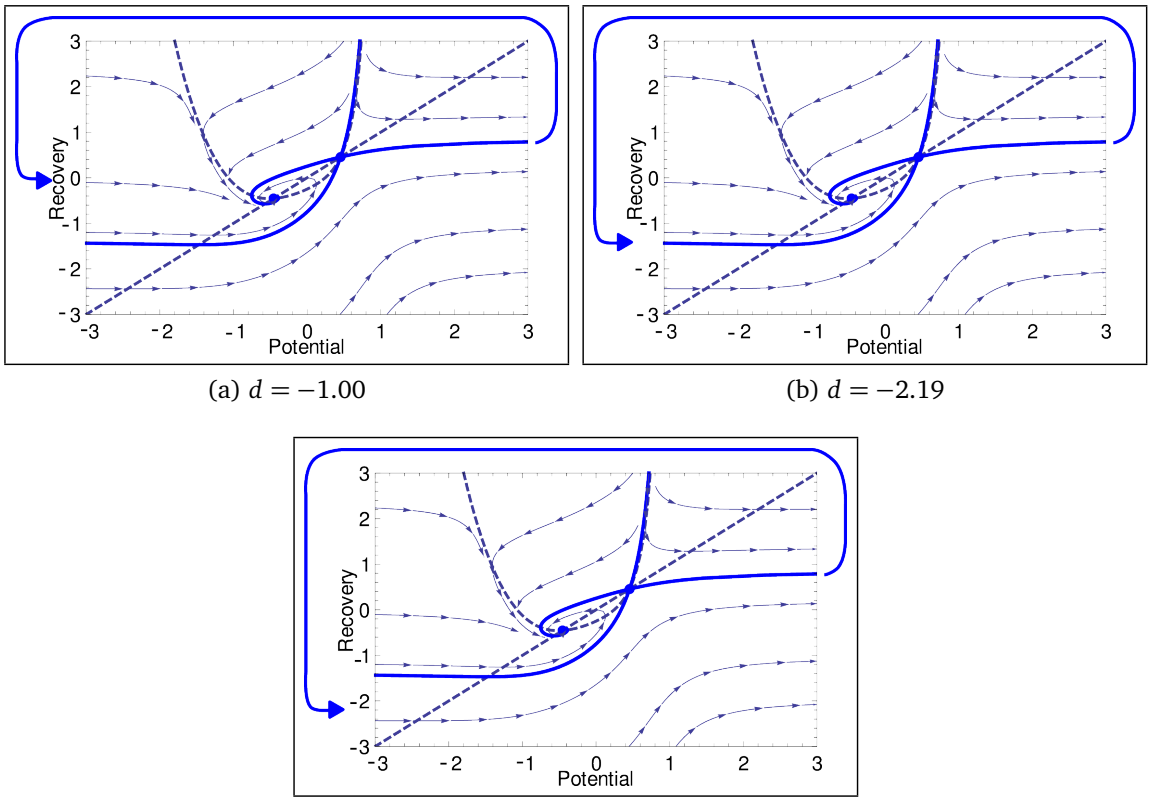

(a) $d = -1.00$

(b) $d = -2.19$

(c) $d = -2.45$

Figure 4.2: The model of choice undergoing "big" saddle-homoclinic-orbit bifurcation. We depict the unfolding with $f(x) = x^4 + x$ undergoing a "big" saddle-homoclinic-orbit bifurcation, transitioning from bistable to monostable as the after-spike recovery variable reset d varies. Dashed lines represent the nullclines of the system; thick lines represent the stable and unstable manifolds of the saddle equilibrium. Phase portraits generated in *Mathematica* with the model of choice using the parameters $(c, d, E, I) = (-3, d, 1, -0.25)$ where d varies as in the captions above.

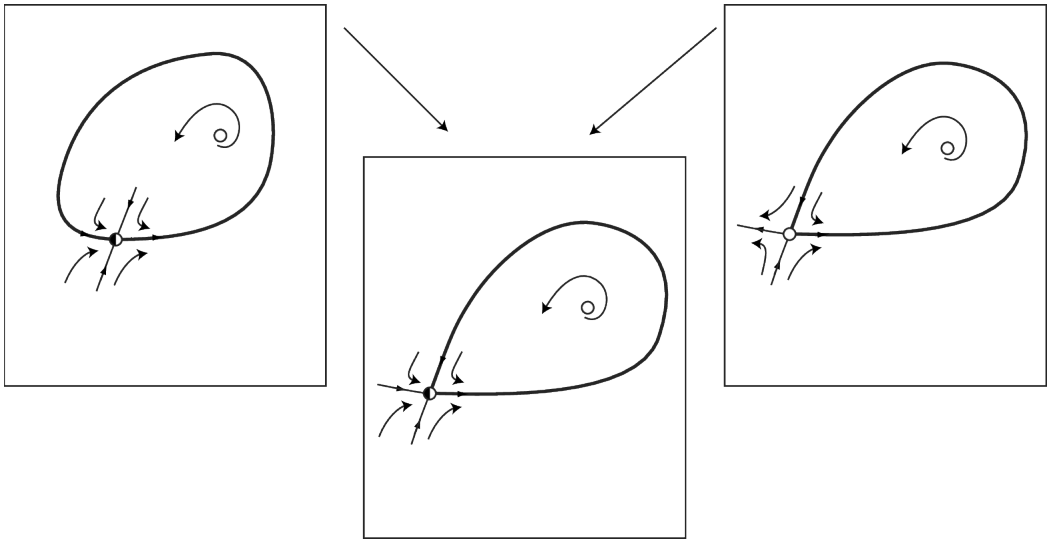

Figure 4.3: The unfolding of a saddle-node-homoclinic-orbit bifurcation. These occur when fold-on-invariant-circle and saddle-homoclinic-orbit bifurcations occur simultaneously. Our model is capable of a hybrid version of this bifurcation with only two, rather than three, equilibria.

homoclinic-orbit, the "big" saddle-homoclinic orbit, and the fold-on-invariant-circle bifurcations is blurry. If a fold-on-invariant-circle bifurcation occurs simultaneously with a "big" saddle-homoclinic bifurcation, then a saddle-node-homoclinic-orbit bifurcation has occurred (illustrated by Figure 4.2 with the stages in opposite order, that is, proceeding from (c) to (a)). Biologically, this bifurcation corresponds to the transition from quiescence to spiking in a monostable resonator. Hence, even though traditional continuous-time models of spiking neurons are only capable of governing this transition in monostable resonators with a super-critical Andronov-Hopf bifurcation, the hybrid nature of our model allows us to generate this transition. That is, our model is capable of two distinct dynamical behaviors, one smooth and one non-smooth, both of which lead to the biological phenomena of monostable resonance.

4.2. Comparison with Biological Neurons

Real neurons are capable of producing tonic, phasic, mixed-mode, rebound, and inhibition induced spiking and bursting, as well as spike frequency adaptation, Hodgkin Class 1 and 2 excitability, spike latency, subthreshold oscillations, threshold variability, bistability, and depolarizing after potentials, and accommodation, among other myriad behaviors. We numerically investigate simulations of the model proposed by Izhikevich [9]

$$\begin{cases} \dot{v} & = f(v) + u(v - E) + I \\ \dot{u} & = bv - u \\ v & \geqslant v_{\max} \Rightarrow v \leftarrow c, u \leftarrow u + d \end{cases} \tag{4.1}$$

in which $f(x) = x^4 + x$, we choose $I, c, d \in \mathbb{R}$ and $b > 0$. We follow Izhikevich's suggestion that we may change coordinates so that conductance reversal energy E may be taken without loss of generality as a member of the set $\{-1, 0, 1\}$. That is, in this section, we diverge from our previous notation and treat I and b as the bifurcation parameters so as to coincide with previous literature more closely.

Note that if the trace of this system at an equilibrium vanishes, then the determinant is $bE - 1$, which can only be positive if $E > \frac{1}{b} > 0$. That is, the model is only capable of an Andronov-Hopf bifurcation if we presume $E = 1$. Hence, in this Chapter we investigate the system

$$\begin{cases} \dot{v} & = v^4 + uv + v - u + I \\ \dot{u} & = bv - u \end{cases} \tag{4.2}$$

Model 4.2 is capable of many of the biological behaviors of interest. In this section, we utilize a Runge-Kutta method implemented in the programming language Python to obtain numerical approximations to solutions to the system of differential

equations in 4.2 to simulate the interspike behavior of a neuron. Due to the non-linearity of the model, detecting the time at which the simulated neuron crosses the maximum voltage cutoff value $v_{\max}$, which corresponds to the firing of a spike, requires a linear interpolation, as described by Izhikevich in [9]. Figure 4.4 depicts the different neurocomputational properties we discovered, and Table 4.1 lists the corresponding parameter values used for the numerical computations. It is an open question whether this example, however, is capable of generating rebound- and inhibition-induced bursts as well as accommodation.

Figure 4.5 (from [8]) illustrates the six most common neocortical firing patterns. We can obtain the behavior of regular spiking, intrinsically bursting, and low-threshold spiking neurons out of our model with no modifications. Figure 4.6 illustrates our model mimicking a regular spiking neuron. Figure 4.7 illustrates our model mimicking an intrinsically bursting neuron, firing a burst of spikes before settling into a tonic spiking pattern. Figure 4.8 illustrates our model mimicking a low-threshold spiking neuron, with a voltage adaptation. Note that our low-threshold simulation can only be loosely described as such, as low-threshold neurons exhibit a fairly low frequency-amplitude sensitivity, whereas our model's spiking frequency is sensitive to amplitude.

It is an open question whether the other three common types (chattering, fast-spiking, and late-spiking interneurons) can be simulated by model 4.2. We discuss this more in Chapter 5.

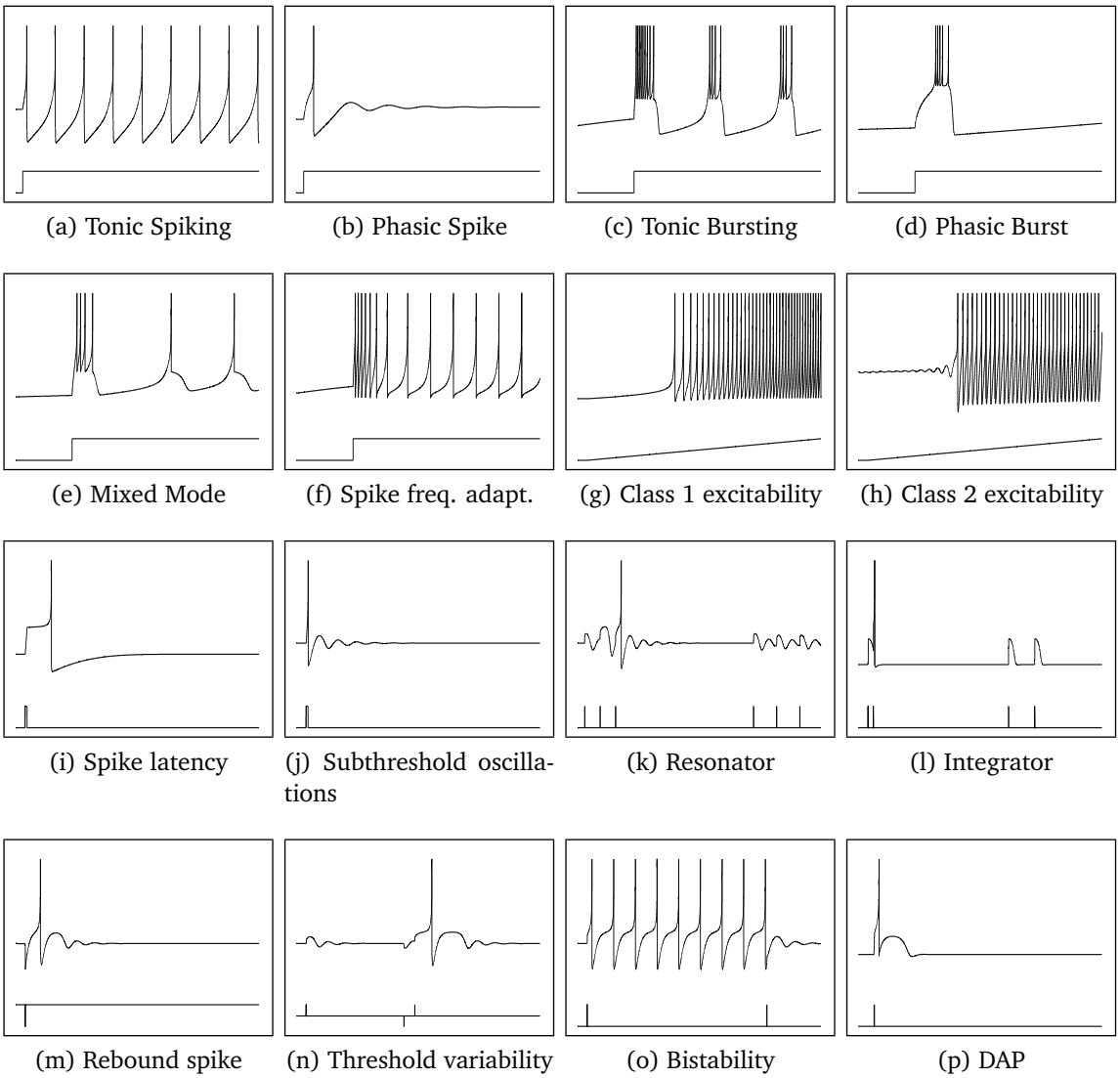

(a) Tonic Spiking (b) Phasic Spike (c) Tonic Bursting (d) Phasic Burst

(e) Mixed Mode (f) Spike freq. adapt. (g) Class 1 excitability (h) Class 2 excitability

(i) Spike latency (j) Subthreshold oscillations (k) Resonator (l) Integrator

(m) Rebound spike (n) Threshold variability (o) Bistability (p) DAP

Figure 4.4: Some neurocomputational properties of which the model is capable. In all cases, the top curve is (dimensionless) membrane voltage, the bottom curve is (dimensionless) input current, and the horizontal axis represents (dimensionless) time. Parameters used to generate each spike train displayed in Table 4.1

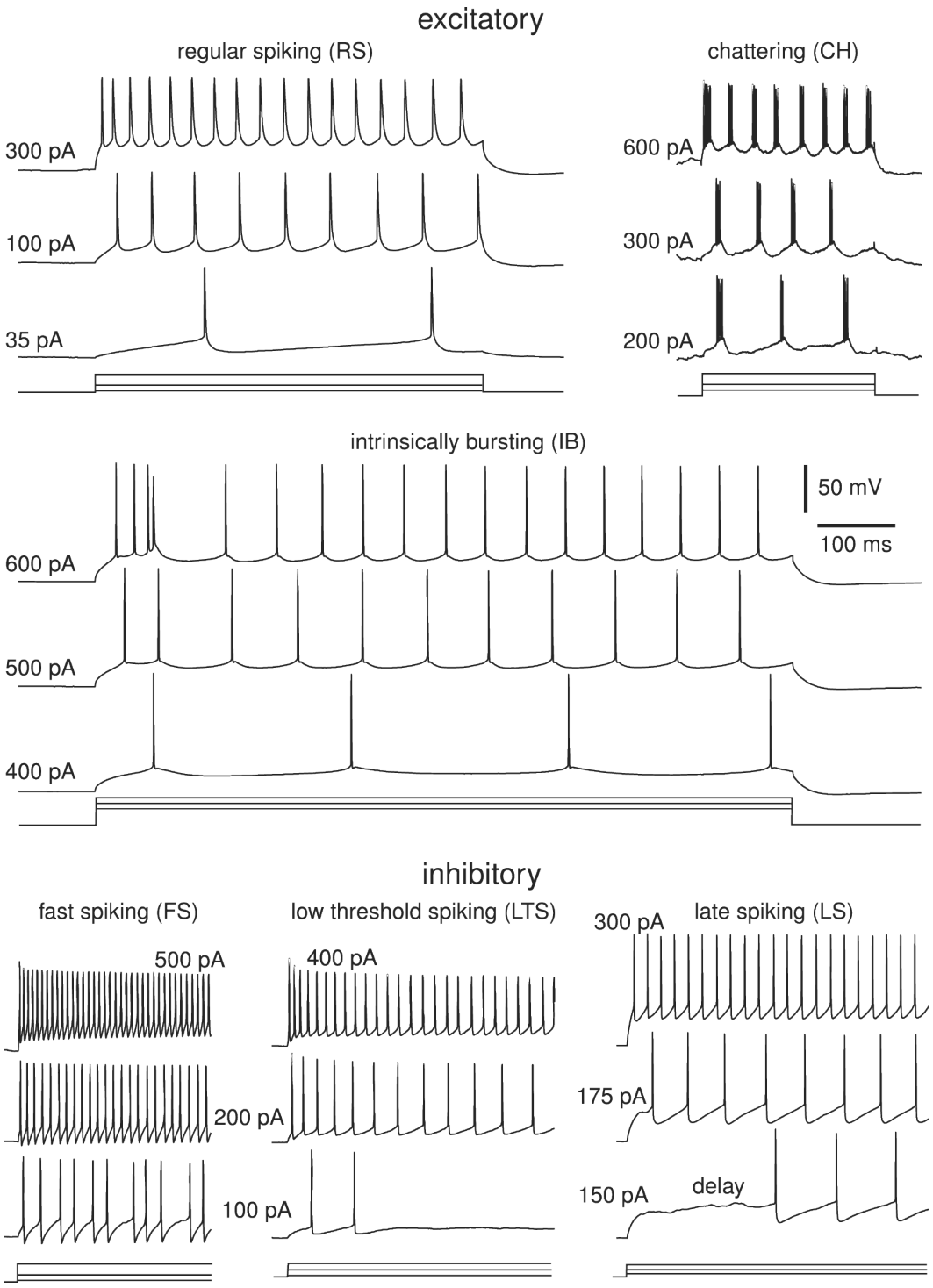

Figure 4.5: Spiking patterns of six common neocortical neurons. All recordings are plotted on the same voltage and time scale, and the data are available at www.izhikevich.com.

Property	b	c	d
Tonic spiking	5	-2.0	0.1
Phasic spiking	50	-1	0.1
Tonic bursting	200	0.2	0.1
Phasic bursting	50	0.7	0.1
Mixed mode	50	0.0	0.1
Spike frequency adaptation	200	-1.0	0.1
Class 1 excitable	0.25	-1.0	0.01
Class 2 excitable	0.47	-1.0	0.5
Spike latency	0.5	-1.0	1.0
Subthreshold oscillations	2.0	-1.0	0.1
Resonator	2.0	-1.0	0.1
Integrator	0.1	-1.0	0.1
Rebound spike	1.0	-0.5	0.1
Threshold variability	1.0	-0.5	0.1
Bistability	1.0	-1.0	0.1
Depolarizing after-potential	0.5	-0.7	-1.1

Table 4.1: Table of parameter values used to generate spike trains in Figure 4.4.

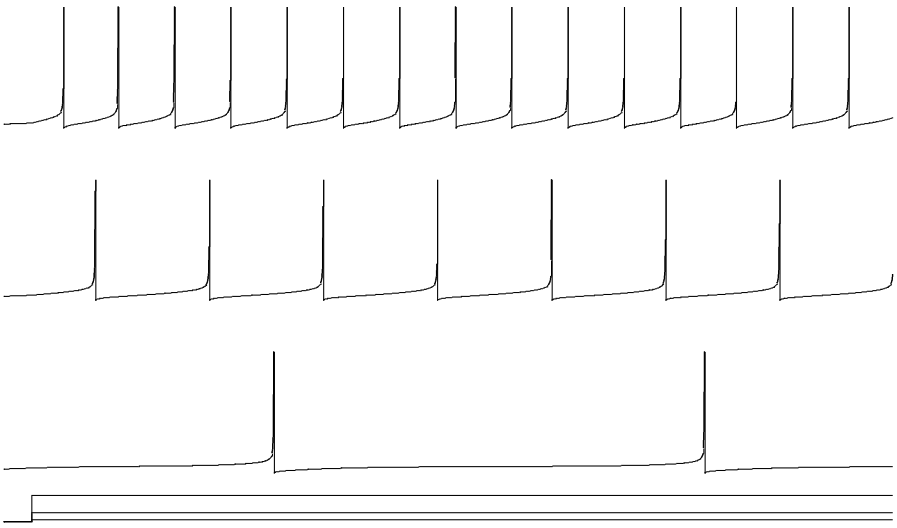

Figure 4.6: The model of choice simulating a regular-spiking neuron. Compare with Figure 4.5. Simulation obtained with parameter values $(b, c, d, E) = (0.5, -2.0, 0.4, 1)$ with $I \in \{0.21, 1, 3\}$

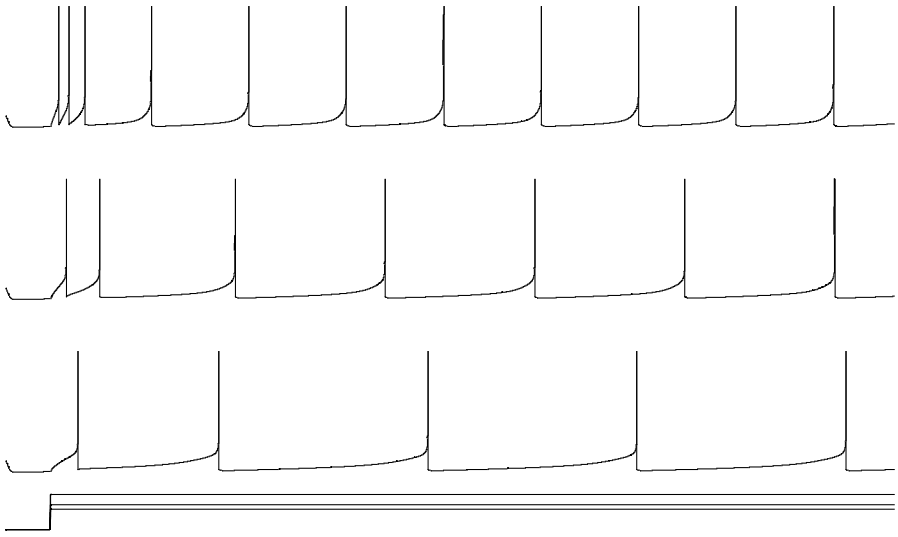

Figure 4.7: The model of choice simulating an intrinsically bursting neuron. Compare with Figure 4.5. Simulation obtained with parameter values $(b, c, d, E) = (10, -0.75, 0.3, 1)$ with $I \in \{0.15, 0.4, 1\}$

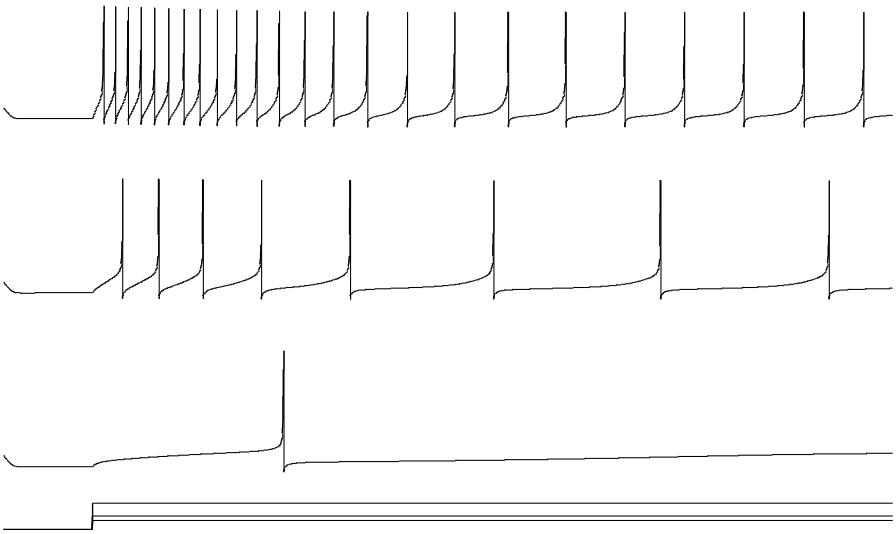

Figure 4.8: The model of choice simulating an low-threshold spiking neuron. Compare with Figure 4.5. Simulation obtained with parameter values $(b, E) = (5, 1)$ with non-constant values for $v_{max} = \max(10 - 0.5u, 1)$ and $c = \max(\min(-1 - 0.25u, 0), -3)$ with $I \in \{0, 0.5, 2\}$

CHAPTER 5. FURTHER QUESTIONS

In this chapter, we address inevitable questions that remain unanswered in our analysis. Certainly the connection between Examples 3.7 and 3.8 may be solidified by considering model 3.1 and taking $f(x) = x^4 + mx$ with $m \in \mathbb{R}$ taken as a new bifurcation parameter. When we choose $m = 1$, as in Example 3.7, the model cannot exhibit a Bautin bifurcation, but for $m = 6$, as in Example 3.8, the model can exhibit a Bautin bifurcation. By treating m as a continuous bifurcation parameter, the model should present a rich bifurcation portrait.

Behaviorally, it is an open question whether our model is capable of simulating a chattering neuron, a fast-spiking neuron, or a late-spiking neuron without a method such as multi-compartment models. Multi-compartment models simulating dendritic spikes can be used to obtain a variety of more complicated behavior. With such a multi-compartment model, we may be able to obtain chattering, fast-spiking, and late-spiking neuron models from our simple model. We may be able to obtain still further complicated behavior by coupling our model of choice in one compartment with other hybrid spiking models in other compartments. To this author's knowledge, no multi-compartment, multiple-model neuron has been studied in the literature.

In [8], Izhikevich classified the four canonical neural behaviors with smooth models alone (see Figure 1.1, Chapter 1). We have demonstrated in our neural model that the discontinuous reset allows us to represent neurons like monostable integrators with a nonsmooth "big" saddle-homoclinic-orbit bifurcation. The existence of a Bogdanov-Takens bifurcation in a model such as ours could possibly be exploited so as to obtain very slowly decaying orbits to resting state when the system is near an SHO curve. With a sufficiently slow decay rate, the system may approximate stable endogeneous subthreshold oscillations without a stable subthreshold limit cycle. Investigating a more thorough expansion of neural classification using smooth and

nonsmooth dynamics both, perhaps utilizing the works in [2], would be a fruitful avenue of further research.

From the dynamical systems perspective, this model is rich in behavior. The intersections of bifurcation curves are interesting, corresponding to bifurcation points of high codimension, and our model has many bifurcation curves. In [2], Coombes, Thul, and Wedgwood demonstrated that the dynamics arising from the nonsmooth cutoff in similar hybrid neuron models may give rise to wide arrays of bifurcation-like behaviors, of which we have only a given a cursory review. We have only partially answered the question of completely classifying both the smooth and nonsmooth behavior of model 3.1; answering the question *in toto* may present an interesting combinatorial challenge.

We may generalize our system further to obtain:

$$\begin{cases} \dot{v} &= f(v) + g(v)u + I \\ \dot{u} &= v - u \end{cases} \tag{5.1}$$

where $I \in \mathbb{R}$ and $f, g \in C^2(\mathbb{R})$ are both convex functions. This generalization is a natural extension of model 3.1. Since Andronov-Hopf bifurcations together with clear numerical evidence of a Bautin bifurcation have been demonstrated when $g(v)$ is taken to be a linear function, it is evident that this generalization will produce at least a similar range of behavior. Hence, further investigation into this very general class of spiking neuron models may be a fruitful area of research, as it may have a yet wider range of behaviors.

Certainly, the bifurcation portrait we have included here is not complete. Among other things, we have only highlighted a few examples of how manipulation of discontinuous reset parameters can give rise to homoclinic and heteroclinic orbit bifurcations like the "big" saddle-homoclinic-orbit bifurcation. Also, we have not rigorously investigated the Bautin bifurcation and we have avoided rigorously addressing the existence

of limit cycles that come about due to the hybrid nature of our model. A complete bifurcation portrait of model 3.1 demands analysis of all limit cycles in the model, including ones that arise due to the discontinuous reset. Such an analysis may follow a similar procedure as that set forth by Coombes, Thul, and Wedgwood in [2]. A general theorem regarding the existence and uniqueness of spiking limit cycles would be helpful toward completing our analysis of model 3.1. A proof of such a theorem regarding the existence of stable limit cycle attractors in the hybrid system may benefit from the use of the lemmata of Appendix A, and will almost certainly benefit from other tools such as the Poincaré map.

Finally, it is worth noting that while we have avoided a rigorous treatment of spiking limit cycle attractors, we have seen strong numerical evidence of spiking limit cycle attractors in the hybrid model (see Figure 4.4). Our demonstrations of the biologically plausible phenomena of tonic spiking, tonic bursting, mixed-mode spiking, spike frequency adaptation, and bistability in Section 4.2 illustrate the existence of these spiking limit cycles (see Figure 4.4).

REFERENCES

[1] R. Brette and W. Gerstner. Adaptive exponential integrate-and-fire model as an effective description of neuronal activity. *Journal of Neurophysiology*, 94:3637–3642, 2005.

[2] S Coombes, R Thul, and K Wedgwood. Nonsmooth dynamics in spiking neuron models. *Physica D*, 2011.

[3] D.M. Grobman. Homeomorphisms of systems of differential equations. *Doclady Akademii Nauk SSSR*, 128:880–881, 1959.

[4] A.L. Hodgkin. The local electric changes associated with repetitive action in a non-medulated axon. *Journal of Physiology*, 107:165–181, 1948.

[5] A.L. Hodgkin and A.F. Huxley. A quantitative description of membrane current and its application to conduction and excitation in nerve. *The Journal of Physiology*, 117:500–544, 1952.

[6] E.M. Izhikevich. Simple model of spiking neurons. *IEEE Transactions on Neural Networks*, 14:1569–1572, 2003.

[7] E.M. Izhikevich. Which model to use for cortical spiking neurons? *Neural Networks, IEEE Transactions on*, 15(5):1063–1070, 2004.

[8] E.M. Izhikevich. *Dynamical Systems in Neuroscience*. The MIT Press, 2010.

[9] E.M. Izhikevich. Hybrid spiking models. *Philosophical Transactions of the Royal Society A: Mathematical, Physical and Engineering Sciences*, 368(1930):5061–5070, 2010.

[10] Yuri Kuznetsov. *Elements of Applied Bifurcation Theory*. Springer, 2010.

[11] V.A. Pliss. A reduction principle in the theory of stability of motion. *Izv. Akad. Nauk SSSR Ser. Mat.*, 28:1297–1324, 1964.

[12] Jonathan Touboul. Bifurcation analysis of a general class of nonlinear integrate-and-fire neurons. *SIAM Journal on Applied Mathematics*, 68(4):1045–1079, 2008.

[13] Jonathan Touboul. Importance of the cutoff value in the quadratic adaptive integrate-and-fire model. *Neural Computation*, 21(8):2114–2122, 2009. PMID: 19409056.

APPENDIX A. JUSTIFICATION FOR ASSUMPTIONS

Herein, we demonstrate why we assume that f must eventually scale faster than quadratically. Indeed, without this assumption, the recovery variable u in our model may blow up in finite time with membrane voltage v in some scenarios; Touboul demonstrated that, in similar hybrid models, such behavior can lead to biologically implausible period-doubling bifurcations [13].

For the purposes of terminology, if $f : \mathbb{R} \to \mathbb{R}$ and there exists some $\alpha, \epsilon > 0$ such that, for any x sufficiently large, $f(x) \geqslant \alpha x^{2+\epsilon}$, we say that f *eventually scales faster than quadratically*, and if there exists some $\alpha, \epsilon > 0$ such that, for any x sufficiently large, $f(x) \geqslant \alpha x^{1+\epsilon}$, we say that f *eventually scales faster than linearly*.

First, observe that, for any $\epsilon, \alpha > 0$, any solution to the differential equation $\frac{dx}{dt} = f(x)$ where $f(x) \geqslant \alpha x^{1+\epsilon}$ with a strictly positive initial condition will blow up in finite time. Indeed, the trajectory passing through $x = x_0 > 0$ when $t = 0$ in the system $\frac{dx}{dt} = \alpha x^{1+\epsilon}$ is

$$x(t) = \left(x_0^{-\epsilon} - \epsilon\alpha t\right)^{-1/\epsilon}$$

and hence any such system will blow up in finite time, in particular when $t = \left(\epsilon\alpha x_0^{\epsilon}\right)^{-1}$. Thus, any system with a strictly positive initial condition whose derivative is bounded below by $\alpha x^{1+\epsilon}$ will also blow up in finite time.

Now let $\alpha, \epsilon > 0$ and let $g(x)$ eventually scale faster than linearly. Then solutions to the differential equation $\frac{dx}{dt} = g(x)$ with sufficiently large initial conditions will also blow up in finite time. In particular, if f scales faster than linearly and $h : \mathbb{R} \to \mathbb{R}$ is defined by $h(x) = \beta x + \gamma$ for any $\beta, \gamma \in \mathbb{R}$, then $f(x) + h(x)$ will also eventually scale

faster than linearly. Indeed, we have the following:

$$f(x) + \beta x + \gamma \geqslant \alpha x^{1+\epsilon} + \beta x + \gamma \tag{A.1}$$

$$\geqslant \alpha x^{1+\epsilon} \left(1 + \frac{\beta}{\alpha x^{\epsilon}} + \frac{\gamma}{\alpha x^{1+\epsilon}}\right) \tag{A.2}$$

Of course, for any $\epsilon_0 > 0$, we can pick a sufficiently large x such that $\left|\frac{\beta}{\alpha x^{\epsilon}}\right| \leqslant \frac{\epsilon_0}{2}$ and $\left|\frac{\gamma}{\alpha x^{1+\epsilon}}\right| < \frac{\epsilon_0}{2}$. Hence, given $\epsilon > 0$, for a sufficiently large x we have that

$$1 + \frac{\beta}{\alpha x^{\epsilon}} + \frac{\gamma}{\alpha x^{1+\epsilon}} > 1 - \epsilon_0$$

Therefore, if $f(x) \geqslant \alpha x^{1+\epsilon}$ for some $\epsilon > 0$ and $\alpha > 0$ given any sufficiently large x, we have that $g(x) \geqslant \hat{\alpha} x^{1+\epsilon}$ where $\hat{\alpha} = \alpha\left(1 - \epsilon_0\right)$.

In particular, if f eventually scales faster than linearly, then for any $I \in \mathbb{R}$, we have that $f(v) + I$ will eventually scale faster than linearly. Using a similar proof method, it is easily shown that if f scales faster than linearly but does not scale faster than quadratically and $g(x)$ scales faster than quadratically, then $f(x) + g(x)$ scales faster than quadratically.

With these facts, we can demonstrate that, if f scales faster than linearly and voltage $v(t)$ in system 3.1 blows up, it does so in finite time. We will also show that if f does not grow sufficiently rapidly, then the corresponding recovery variable $u(t)$ will also blow up in finite time. Finally, we will show that if f scales faster than quadratically, then u will not blow up in finite time.

To this end, we will consider the model of choice in the sequel for $E, I \in \mathbb{R}$ and $f \in C^1(\mathbb{R})$:

$$\begin{cases} \dot{v} &= f(v) + u(v - E) + I \\ \dot{u} &= v - u \end{cases} \tag{A.3}$$

In this system, an equilibrium $(v,u) = (v_0,u_0)$ must satisfy $u_0 = v_0$ and $f\left(v_0\right) + v_0\left(v_0 - E\right) + I = 0$.

We make some observations about the vector field in our model and make some definitions. Assume f eventually scales faster than linearly for some $\alpha, \epsilon > 0$. Since f eventually scales faster than linearly, so does $f(v)+I$, and so there exists some V_∞ and $\beta > 0$ such that $f(v) + I \geqslant \beta v^{1+\epsilon} > 0$ for any $v \geqslant V_\infty$. We can choose $V_\infty > |E|$. Now define $S_\infty := \left\{(v,u) \mid v \geqslant V_\infty, 0 \leqslant u \leqslant v\right\}$.

Lemma A.1. Assume f eventually scales faster than linearly for some $\epsilon, \alpha > 0$ with corresponding set S_∞ as defined above. Any trajectory $(v(t),u(t))$ satisfying $v(t) \to \infty$ as $t \to \infty$ eventually enters and remains in S_∞.

Proof. We first prove that any trajectory that enters S_∞ remains in S_∞ for all time. We then prove that any trajectory satisfying $v(t) \to \infty$ as t increases will eventually enter S_∞.

The vector field on the boundary of S_∞ points inward, and hence any trajectory entering S_∞ will never exit S_∞. Indeed, when $u = v$ and $v \geqslant V_\infty$, we have $\frac{du}{dt} = 0$ and since $v(v-E) > 0$, we also have that $\frac{dv}{dt} = f(v) + v(v-E) + I > \beta v^{1+\epsilon} > 0$. That is, a trajectory with a point starting on this boundary enters S_∞.

On the other hand, when $v = V_\infty$ and $0 < u < V_\infty$, we have that $u(v-E) > 0$, we also have that $\frac{dv}{dt} = f(v) + u(v-E) + I > \beta v^{1+\epsilon} > 0$. Hence, a point with a trajectory starting on this boundary also enters S_∞. Finally, when $u = 0$ and $v \geqslant V_\infty$, we have that $\frac{du}{dt} > 0$ and $\frac{dv}{dt} = f(v) + I \geqslant \beta v^{1+\epsilon} > 0$. All trajectories that enter S_∞ must remain in S_∞.

It remains to be shown that if $v(t) \to \infty$ as t increases, then $(v(t),u(t))$ enters S_∞. Certainly if $v(t) \to \infty$ as t increases, then there exists some $t_0 \in \mathbb{R}$ such that $v(t_0) \geqslant V_\infty$ and $\frac{dv}{dt}(t_0) \geqslant 0$, otherwise $v(t) \not\to \infty$. If this point is already in S_∞, then we

are done. If not, then either $u(t_0) > v(t_0)$ or $0 > u(t_0) \geqslant \frac{f(v(t_0))+I}{E-v(t_0)}$; this latter inequality follows from the fact that $v'(t_0) \geqslant 0$.

Consider trajectories starting from points in the region $\{(v,u) \mid v \geqslant V_\infty, u > v\}$. Notice that for trajectories starting at a point with $v = V_\infty$, we have that $\frac{dv}{dt} > 0$, and hence the trajectory enters the region $v \geqslant V_\infty$. Further, we have that $v - u < 0$ and $u(v-E) > 0$. Hence $\frac{d}{dt}(u-v) = (v-u) - f(v) - u(v-E) - I < -f(v) - I$. But $f(v)+I \geqslant \beta V_\infty^{1+\epsilon}$ in this region, and hence $\frac{d}{dt}(u-v) \leqslant -\beta V_\infty^{1+\epsilon} < 0$. Hence, trajectories starting from points in this region approach $u - v = 0$ in finite time. We have already seen that points on $v = u$ enter S_∞.

On the other hand, consider trajectories starting from points in the region

$$\left\{(v,u) \mid v \geqslant V_\infty, \frac{f(v)+I}{E-v} < u < 0\right\} \tag{A.4}$$

Notice that trajectories starting on the boundary $v = V_\infty$, $-\frac{f(V_\infty)+I}{V_\infty - E} < u < 0$ of region A.4 enter region A.4. Indeed, $\frac{dv}{dt} = (V_\infty - E)(u + \frac{f(V_\infty)+I}{V_\infty - E}) > 0$.

Similarly, trajectories starting on the boundary $u = -\frac{f(v)+I}{v-E}$ with $v \geqslant V_\infty$ have $\frac{dv}{dt} = 0$, $\frac{du}{dt} > 0$. Further, when $v \geqslant V_\infty$, we have that $\frac{d^2v}{dt^2}$ exists since $f \in C^1(\mathbb{R})$ and $\frac{d^2v}{dt^2} = \frac{du}{dt}(v-E) > 0$, so all trajectories crossing this boundary will enter region A.4.

Of course region A.4 shares its only remaining boundary with S_∞, and we have shown any trajectory on that boundary enters and stays in S_∞. But any point within region A.4 will have $\frac{du}{dt} = v - u \geqslant V_\infty > 0$, and since $u < 0$ in this region, we see that u must become positive within finite time. That is, any trajectory with a point starting in region A.4 will enter S_∞. □

With Lemma A.1 in hand, we demonstrate that trajectories $(v(t), u(t))$ that enter S_∞ will have $v(t), u(t) \to \infty$ in finite time whenever f eventually scales faster than

linearly but not sufficiently rapidly, and will have $v(t) \to \infty$ but $u(t)$ converge to a finite value whenever f eventually scales faster than quadratically.

Lemma A.2. Assume that f eventually scales faster than linearly, $f(v)/v^2 \to \infty$ as $v \to \infty$, and that $\int_{x_0}^{\infty} \frac{x}{f(x)} dx$ is divergent for some x_0. If $(v(t), u(t))$ is a trajectory such that $v(t) \to \infty$, then both $v(t)$ and $u(t)$ both blow up in finite time.

Proof. Notice that any function that scales faster than quadratically will be excluded from this Lemma; for these functions, the stated integral converges. An example of a function that satisfies the hypothesis of the Lemma is $f(v) = v^2 \ln(v)$.

If $f(v) \geqslant \alpha v^{1+\epsilon}$ for sufficiently large v, let $\beta > 0$, $V_\infty > |E|$ as above so that $f(v) + I \geqslant \beta v^{1+\epsilon}$ for any $v \geqslant V_\infty$. Notice that any trajectory $(v(t), u(t))$ with $v(t) \to \infty$ certainly enters S_∞ following Lemma A.1. Furthermore, for any point in S_∞, we have $\frac{dv}{dt} = f(v) + u(v-E) + I \geqslant \beta v^{1+\epsilon}$ since $u(v-E) \geqslant 0$. By our observation at the beginning of this appendix, this must blow up in finite time since it starts with a positive initial condition; further notice that this is true even if $\epsilon > 1$.

We will demonstrate that u blows up in finite time by bounding du/dv from below. Within S_∞, we have that $\frac{dv}{dt} = f(v) + u(v-E) + I \leqslant f(v) + v^2 + vV_\infty + I$ since $V_\infty > |E|$ and $0 \leqslant u \leqslant v$. Therefore, $vg(v) - ug(v) \leqslant \frac{du}{dv}$ where $g(v) := \left(f(v) + v^2 + vV_\infty + I\right)^{-1}$.

We pause to make some observations about the function $g(v)$ and the related function $vg(v)$. Observe that $g(v)$ is a positive function. Further, notice that $f(v) + I > 0$ eventually implies that $f(v) + v^2 + vV_\infty + I \geqslant v^2$ eventually. Hence, $\int_{v_1}^{\infty} g(s) ds$ is finite for any sufficiently large $v_1 \geqslant V_\infty$. The property $f(v)/v^2 \to \infty$ provides that

$$\begin{aligned} f(v) + v^2 + vV_\infty + I &= f(v)\left(1 + \frac{v^2 + vV_\infty + I}{f(v)}\right) \\ &< 2f(v) \end{aligned}$$

for sufficiently large v. Hence, $g(v) > \frac{1}{2f(v)}$ for sufficiently large v. Now since $\int_{x_0}^{\infty} \frac{x}{f(x)} dx$ diverges for some x_0, for a sufficiently large v_2, we then have that $\int_{v_2}^{\infty} sg(s)ds$ diverges.

Now, we have $\frac{du}{dv} + ug(v) \geqslant vg(v) > 0$, which has an integrating factor $e^{\int_{v_1}^{v} g(s)ds}$. The integrating factor is bounded since $\int_{v_1}^{\infty} g(s)ds$ is finite. In fact, there exists some $M \in \mathbb{R}$ such that for all $v \geqslant v_1$, $1 \leqslant e^{\int_{v_1}^{v} g(s)ds} \leqslant M$. We obtain

$$\begin{aligned}
\frac{d}{dv}\left(ue^{\int_{v_1}^{v} g(s)ds}\right) &\geqslant vg(v)e^{\int_{v_1}^{v} g(t)dt} \\
ue^{\int_{v_1}^{v} g(s)ds} &\geqslant \int_{v_1}^{v} sg(s)e^{\int_{v_1}^{s} g(t)dt} ds + u_1 \\
u &\geqslant e^{-\int_{v_1}^{v} g(s)ds} \int_{v_1}^{v} sg(s)e^{\int_{v_1}^{s} g(t)dt} ds + u_1 e^{-\int_{v_1}^{v} g(s)ds}
\end{aligned}$$

Since $e^{\int_{v_1}^{v} g(s)ds} \geqslant 1$ for any v, we have $sg(s)e^{\int_{v_1}^{s} g(t)dt} \geqslant sg(s) > 0$. In particular, $\int_{v_1}^{v} sg(s)e^{\int_{v_1}^{s} g(t)dt} ds \geqslant \int_{v_1}^{v} sg(s)ds$. Furthermore, $e^{-M} \leqslant e^{-\int_{v_1}^{v} g(s)ds} \leqslant 1$ and hence $u \geqslant e^{-M} \int_{v_1}^{v} sg(s)ds$. That is, u is unbounded as $v \to \infty$ and u also blows up. □

Lemma A.3. Assume that f eventually scales faster than quadratically. That is, assume there exists some $\alpha > 0$ and $\epsilon > 0$ such that $f(v) \geqslant \alpha v^{2+\epsilon}$ for any sufficiently large v. If $(v(t), u(t))$ is a trajectory such that $v(t) \to \infty$, then $v(t)$ blows up in finite time, but $u(t)$ converges to a finite value.

Proof. We certainly have that v will blow up in finite time, since if f scales faster than quadratically, then it scales faster than linearly; our argument from Lemma A.2 applies. It is sufficient to show that u does not blow up in finite time. Let $\beta > 0, V_\infty > |E| \geqslant 0$ such that $f(v) + I \geqslant \beta v^{2+\epsilon}$, and notice that our trajectory enters S_∞.

For any $(v,u) \in S_\infty$, we have $0 \leqslant v - u \leqslant v$ and $u(v-E) \geqslant 0$. In particular, $f(v) + u(v-E) + I \geqslant f(v) + I \geqslant \beta v^{2+\epsilon}$, and so $\frac{du}{dv}$ is bounded between two integrable

functions, completing the proof:

$$0 \leqslant \frac{du}{dv} = \frac{v-u}{f(v)+u(v-E)+I} \leqslant \frac{v}{f(v)+I} \leqslant \frac{1}{\beta v^{1+\epsilon}}$$

□

APPENDIX B. SIMULATION CODE

This section describes the *Mathematica* code (presented at the end of this section) used to generate phase portraits in Section 3.6. The code must be modified if a unique equilibrium exists or if no equilibria exist. We present the code in parts.

In this first section, input current I from model 3.1 is coded as `p`, conductance reversal energy E is coded as `n`, and the functions $V^*(E)$ and $I^*(E)$ from Section 3.1 are coded as `vstar` and `istar`, respectively.

The code plots the nullclines of model 3.1 with spike activation function `f[x]` with ordered pairs in `vnull1` (with points to the left of the singularity in the v-nullcline), `vnull2` (with points to the right of the singularity). We use the function `ListLinePlot` to plot these nullclines, and we store this plot in `Pnull`.

```
Clear[p, n, f, vnull1, vnull2, unull, x]
Clear[pr]
(* pr = plot range *)
pr = {{-3, 2}, {-2, 2}};


Clear[n, p];
(* n = conductance reversal energy, E *)
(* p = input current, I *)
n = 6.44176;
p = -2.44434;


Clear[f]
f[x_] := x^4 + 6 x;


Clear[vstar, istar]
```

```
vstar = v /. NSolve[f'[v] + 2*v - n == 0, v, Reals][[1]];
istar = vstar^2*(3*vstar^2 + 1);

Clear[xm, vnull1, vnull2, unull]
xm = 10;
vnull1 = Table[{x, -(f[x] + p)/(x - n)}, {x, -xm, n - 1/20, 1/20}];
vnull2 = Table[{x, -(f[x] + p)/(x - n)}, {x, n + 1/20, xm, 1/20}];
unull = Table[{x, x}, {x, -xm, xm, 1/20}];

Clear[ps, Pnull]
ps = {{Blue, Dashed}};
Pnull = ListLinePlot[{vnull1, vnull2, unull}, PlotRange -> pr,
   PlotStyle -> ps];
```

The code next plots the direction field of model 3.1 for spike activation function `f[x]` by defining $\dot{v}$ and $\dot{u}$ as `vdot[v_,u_]` and `vdot[v_,u_]`, respectively. Here we have clipped the vector fields to our plotrange so that they are zero outside of our plotrange; due to the nonlinearity of our system, failing to do so can lead to numerical blowups (see Appendix A). We use the function `StreamPlot` to plot the direction fields, and we store this plot in `Pstream`.

```
Clear[vdot, udot, Pstream]
vdot[v_, u_] :=
  If[v >= xm, 0,
   If[v <= -xm, 0,
    If[u >= xm, 0, If[u <= -xm, 0, f[v] + u*(v - n) + p]]]];
udot[v_, u_] :=
  If[v >= xm, 0,
```

```
   If[v <= -xm, 0, If[u >= xm, 0, If[u <= -xm, 0, v - u]]]];
Pstream =
  StreamPlot[{vdot[v, u], udot[v, u]}, {v, -xm, xm}, {u, -xm, xm},
   PlotRange -> pr];
```

The code next plots the ordered pairs corresponding to equilibria, if any exist, using the `Graphics` function, storing these plots in the `Psaddle` and `Prest`, corresponding to the saddle equilibrium and the resting state equilibrium, respectively (which is not necessarily a stable resting state).

```
Clear[vstar, istar, equilibria, saddle, rest]
vstar = v /. NSolve[f'[v] + 2*v - n == 0, v, Reals][[1]];
istar = vstar^2*(3*vstar^2 + 1);
If[p >= istar, 0,
  equilibria = v /. NSolve[f[v] + v^2 - n*v + p == 0, v, Reals]];
saddle = Max[equilibria];
rest = Min[equilibria];
Psaddle =
  Graphics[{Blue, PointSize[Large], Point[{saddle, saddle}]}];
Prest = Graphics[{Blue, PointSize[Large], Point[{rest, rest}]}];
```

The code next generates some initial conditions associated with the stable and unstable mandfolds of a saddle equilibrium, allows the user to enter the user's own initial conditions, and plots the trajectories for these initial conditions into two different plots to distinguish them. By perturbing the saddle equilibrium ordered pair in the direction of the eigenvectors scaled by a small factor, we obtain initial conditions that have orbits "very near" the stable and unstable manifolds of the saddle equilibrium. The variable `vects` stores the eigenvectors of the saddle equilibrium scaled by a factor of `scale`.

We store the ordered pairs corresponding to the initial conditions of orbits "very near" the stable and unstable manifolds of the saddle equilibrium in `startingPoints1`. The user then may uncomment the code to perturb the resting point according to its eigenvectors similarly and store that information in `startingPoints2` to investigate phenomena like heteroclinic loops induced by the discontinuous reset.

Now that initial conditions associated with the stable and unstable manifolds of the saddle equilibrium are stored, the stores initial conditions associated with specific trajectories of interest in `startingPoints` by hand; these are usually inserted to demonstrate the existence of limit cycles, and so on. We use the `Graphics` function to plot all initial conditions in `startingPoints` desired by the user, and we store this plot in `Pstart`. We use `NDSolve` to find solutions to the system of equations with initial conditions in `startingPoints` on a time interval from `t=0` to `t=tmax`, and store this solution in `sols`. We plot `sols` with `ParametricPlot` and store the plot in `Ptraj`. We then plot the manifold-related trajectories similarly using the initial conditions from `startingPoints1`, storing that plot in `Pmanis`. We usually have the plots in `Ptraj` a distinctly different color than the plots in `Pmanis` so as to indicate a difference between the stable/unstable manifolds.

```
Clear[vects, scale, startingPoints1, startingPoints]
scale = 1/1000;
vects = Re[
   scale* Eigenvectors[{{f'[saddle] + saddle,
       saddle - n}, {1, -1}}]];
(*startingPoints1 = {{saddle,saddle} + vects[[1]], {saddle,saddle} + \
vects[[2]], {saddle,saddle} - vects[[1]], {saddle,saddle} - \
vects[[2]]};*)
```

```
startingPoints1 = {{saddle, saddle} - vects[[1]], {saddle, saddle} -
    vects[[2]]};
Clear[vects, startingPoints2]
scale = 1/5;
vects = Re[scale*Eigenvectors[{{f'[rest] + rest, rest - n}, {1, -1}}]];
startingPoints2 = {{rest, rest} - vects[[2]]};
(*startingPoints = Union[startingPoints1, startingPoints2];*)

Clear[startingPoints]
(*startingPoints=Union[startingPoints1,startingPoints2];*)
\
(*startingPoints=Union[startingPoints1,{{-0.6615,-0.6429},{-0.2769,-0.\
2695}}];*)
startingPoints = {{-0.8729, -0.8773}, {-0.6985, -0.6783}};
(*startingPoints=startingPoints2*)

Pstart = Graphics[{Red, PointSize[Medium], Point[startingPoints]}];

Clear[sols, Ptraj, tmax]
tmax = 200;
sols = Table[
   NDSolve[{v'[t] == vdot[v[t], u[t]], u'[t] == udot[v[t], u[t]],
     v[0] == startingPoints[[k]][[1]],
     u[0] == startingPoints[[k]][[2]]},
    {v, u}, {t, 0, tmax}, MaxSteps -> Infinity], {k, 1,
    Length[startingPoints]}];
```

```
Ptraj = ParametricPlot[Evaluate[{v[t], u[t]} /. sols], {t, 0, tmax},
   PlotRange -> Automatic, PlotStyle -> {{Blue, Thick}}];

Clear[startingPoints, manis, Pmanis, tmax]
tmax = 30
startingPoints = startingPoints1;
manis = Table[
   NDSolve[{v'[t] == vdot[v[t], u[t]], u'[t] == udot[v[t], u[t]],
     v[0] == startingPoints[[k]][[1]],
     u[0] == startingPoints[[k]][[2]]},
    {v, u}, {t, -tmax, tmax}, MaxSteps -> Infinity], {k, 1,
    Length[startingPoints]}];
Pmanis = ParametricPlot[
   Evaluate[{v[t], u[t]} /. manis], {t, -tmax, tmax},
   PlotRange -> Automatic, PlotStyle -> {{Purple, Thick}}];
```

Finally, we allow the user to reset the plot range pr and then use the Show command to illustrate Pnull, Pstream, Ptraj, Pmanis, and Pstart.

```
Clear[pr]
pr = {{rest - 1.5, saddle + 0.2}, {rest - 0.2, saddle + 0.2}};

(*Show[Pnull,Pstream,Psaddle,Prest,Ptraj,Pstart,PlotRange->pr,Frame->\
True]*)
Show[Pnull, Pstream, Ptraj, Pmanis, Pstart, PlotRange -> pr,
 Frame -> True]
(*Show[Pnull,Pstream,Pmanis,PlotRange->pr,Frame->True]*)
```